Principles and Theory of Radar Interferometry

Paul A Rosen

Jet Propulsion Laboratory

August 4, 2014
UNAVCO Short Course

Acknowledgments

- Materials compiled and modified from presentations shared among a number of colleagues over the years
  - Scott Hensley
  - Tony Freeman
  - Jakob van Zyl
  - Piyush Agram
  - Howard Zebker

Motivation – Understanding the processes and phenomenology of radar interferometry

Satellite Observation

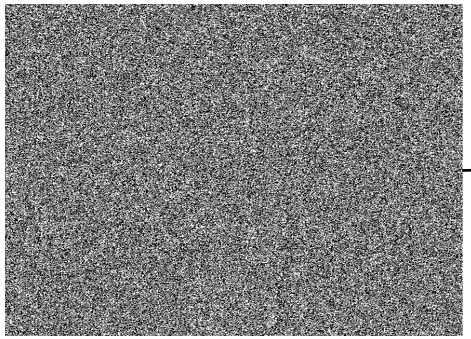

First Time

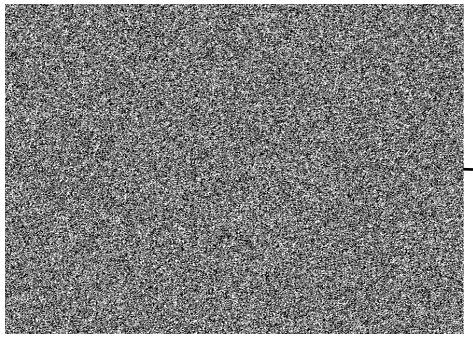

Next Time

Magic of imaging

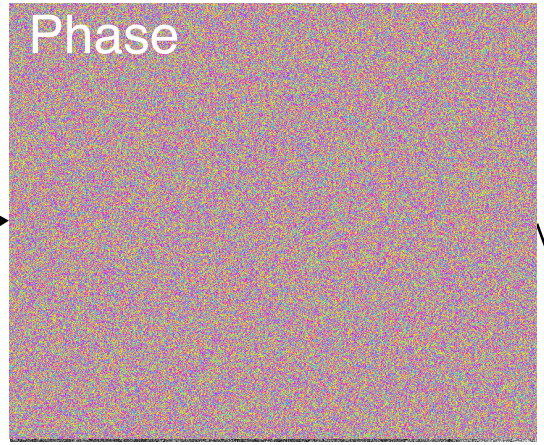

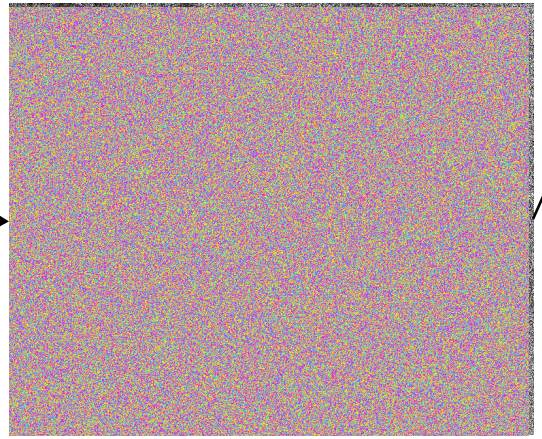

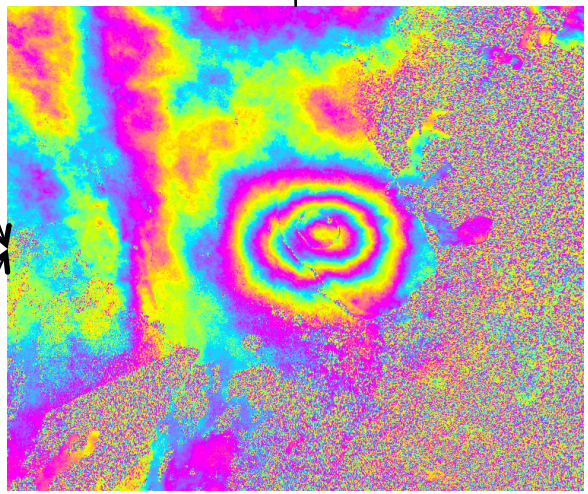

Magic of interferometry

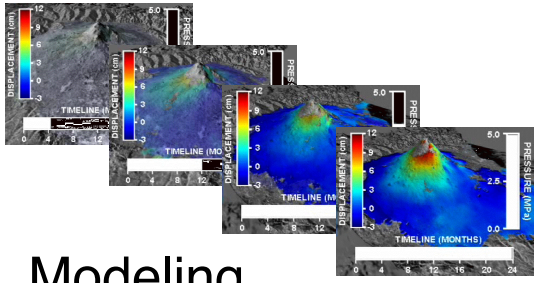

Modeling

Wave Properties of Light

- Radar waves, like lightwaves, are electromagnetic energy that propagates

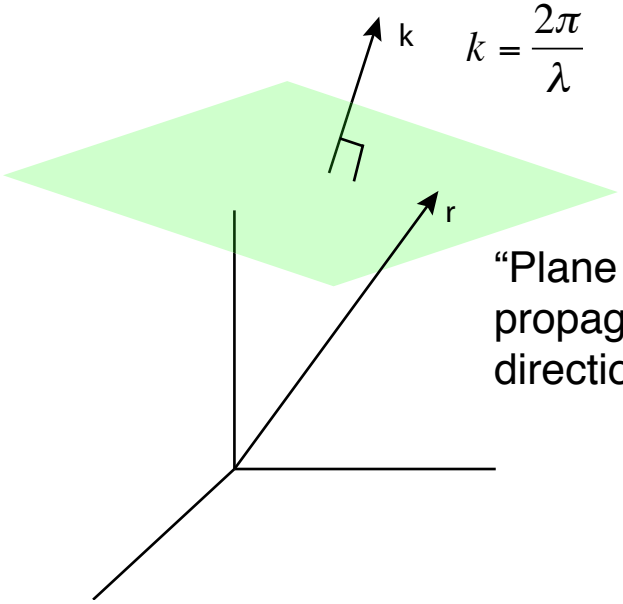

$$k = \frac{2\pi}{\lambda}$$

"Plane wave" propagating in direction k

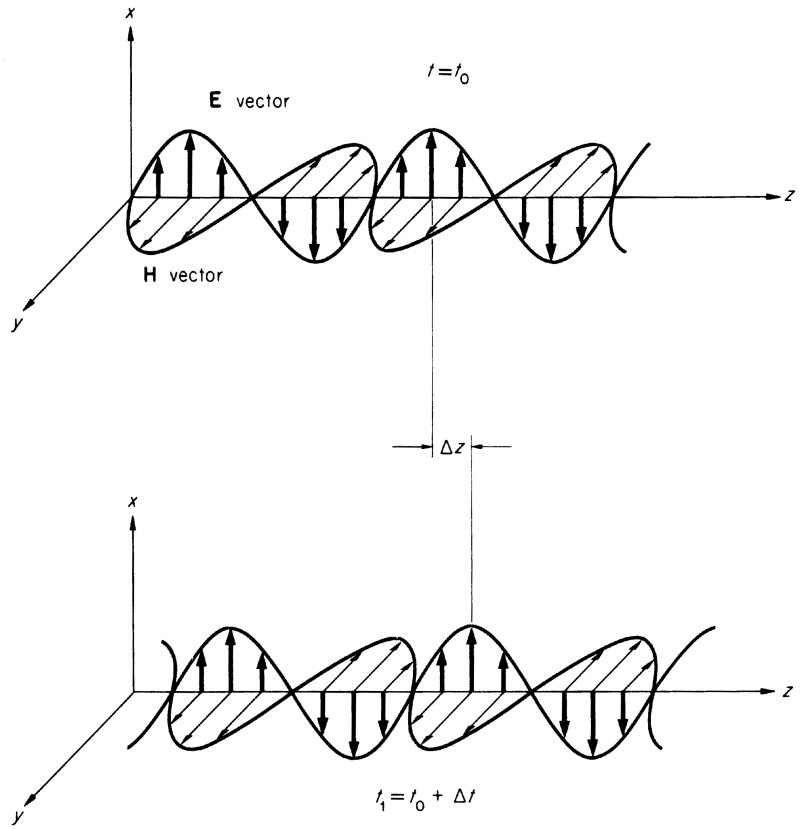

Energy propagates →

"Phase" ↘ frequency ↘

$$E(x,y,z,t) = E_0 e^{j\phi(x,y,z,t)} = E_0 e^{j(\omega t - \vec{k}\cdot\vec{r})}$$

Outline of Theory Sessions

Morning

I. Radar Imaging Fundamentals

A. Basic Principles of Radar and SAR

B. Properties of Radar Images

Afternoon

II. Geometric Aspects of Interferometry and Interferometric Phase

A. Topographic Mapping

B. Deformation Mapping

C. Phase Unwrapping and Atmosphere

III. Interferometric Correlation

A. SNR and Interferometric Correlation

B. Geometric, Temporal, Volumetric Decorrelation

Radar and Light Waves

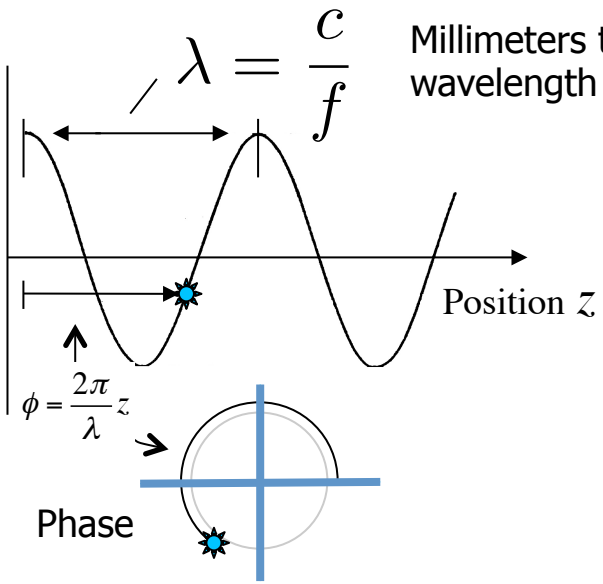

Millimeters to meters wavelength

- Radars operate at microwave frequencies, an invisible part of the electromagnetic spectrum
- Microwaves have wavelengths in the millimeter to meter range
- Like lasers, radars are coherent; we can determine the signal's phase

Common Radar Frequency Bands

Band	Ka	Ku	X	C	S	L	P
Wavelength (cm)	1	2	3	6	12	24	75
Frequency (G-cycles/s)	30	15	10	5	2.5	1.2	0.4

The Electromagnetic Spectrum

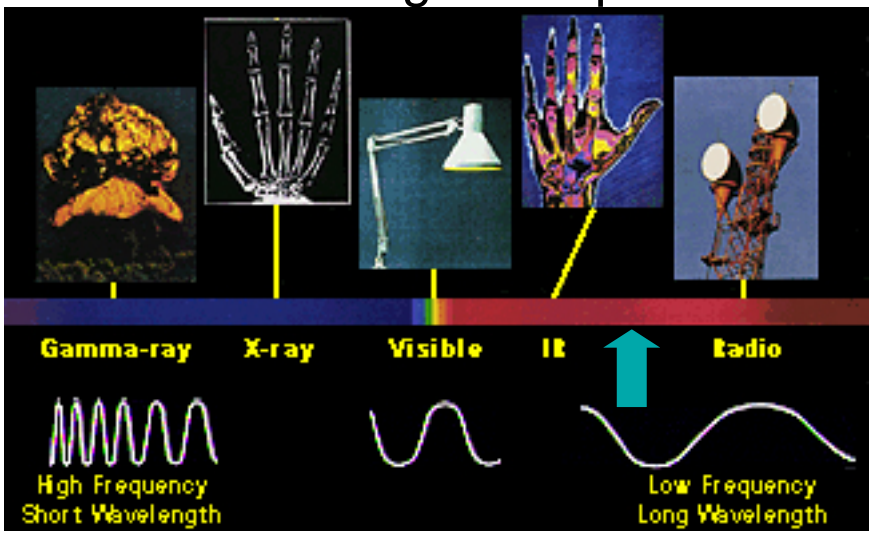

tiny 100's μm mm's to m's

The Radar Concept

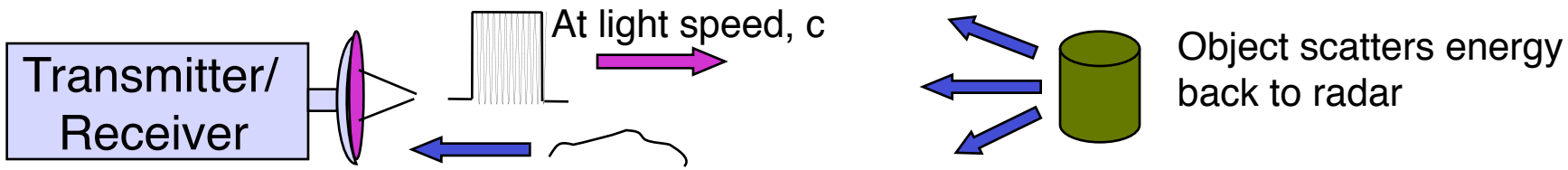

- Much like sound waves, radar waves carry information that echoes from distant objects
- The time delay of the echo measures the distance to the object
- The changes of the message in the echo determines the object characteristics

Achieving resolution in range

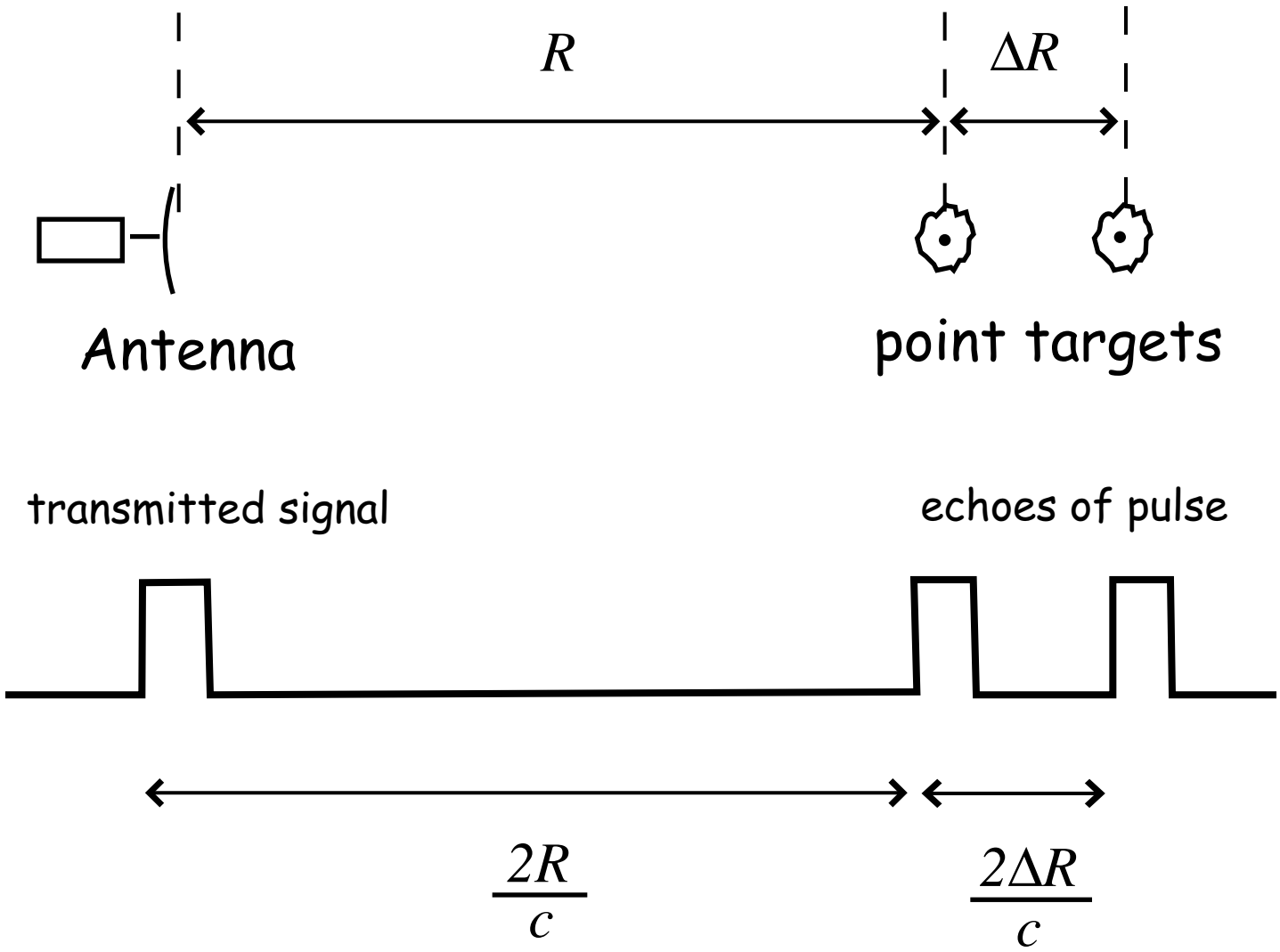

If possible, use a narrow pulse to resolve close targets

Achieving resolution in range

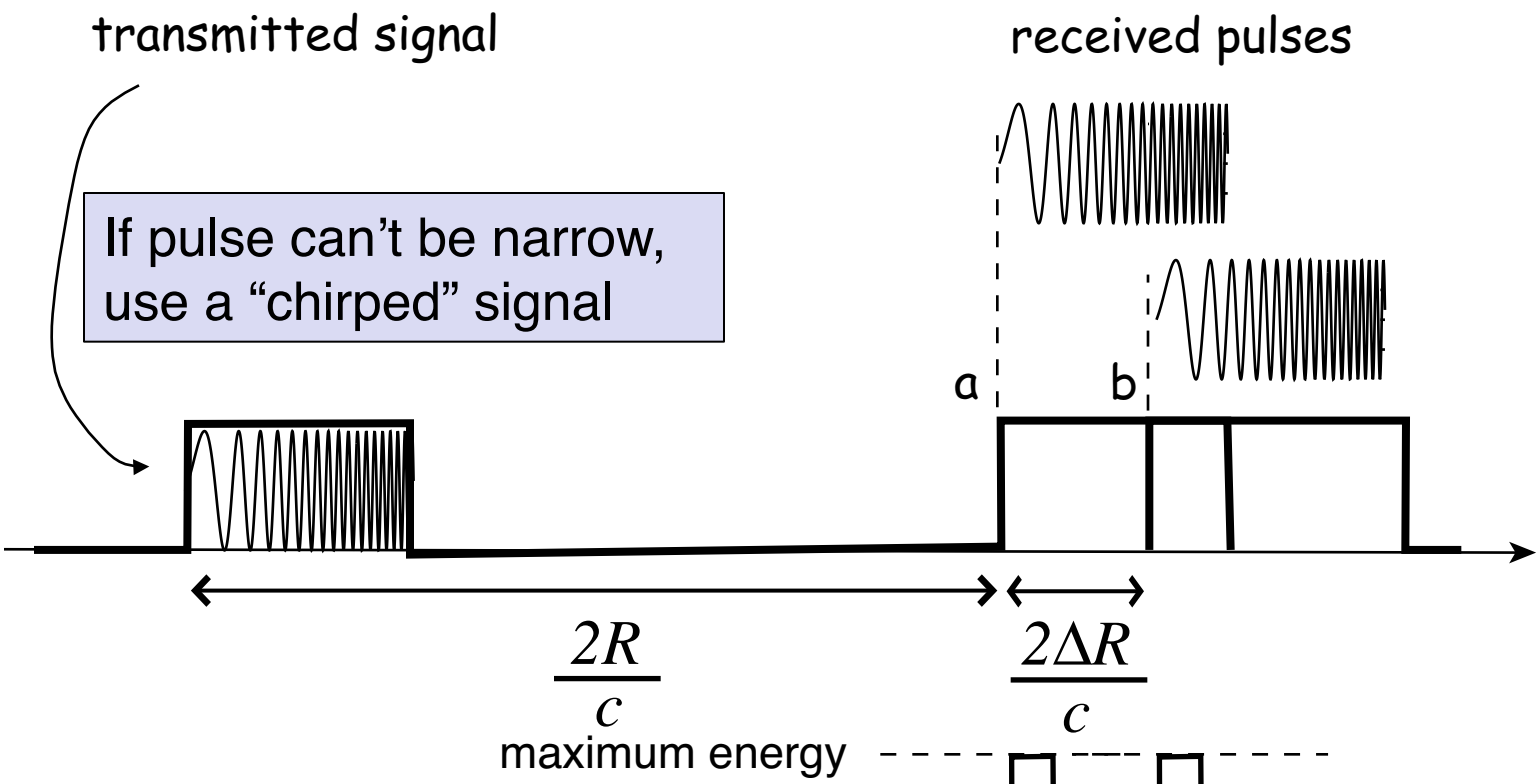

If pulse can't be narrow, use a "chirped" signal

Matched filtering can recover smeared targets

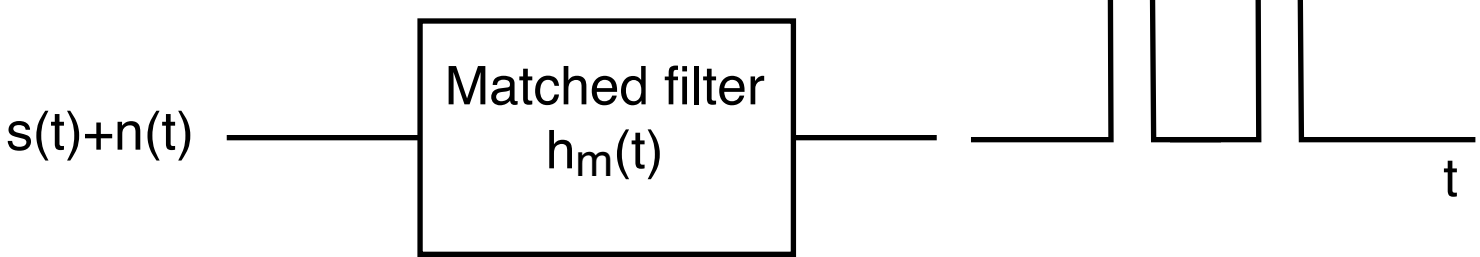

Radar on a Moving Platform

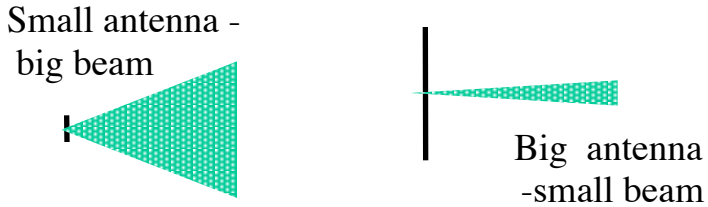

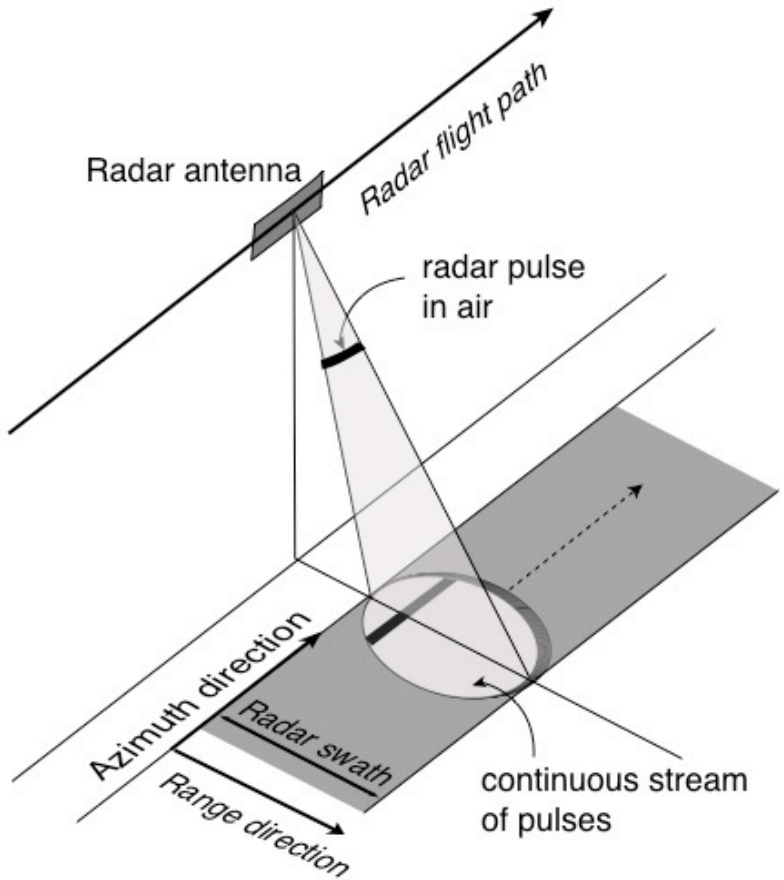

- Pulses are transmitted from the radar platform as it moves along its flight path
- Each pulse has finite extent in time, illuminating a narrow strip of ground as it sweeps through the antenna beam
- Some of the energy from the ground is scattered back to the radar instrument

Antenna Beamwidth

$$\theta_{3dB} = \frac{\lambda}{L}$$

Footprint Size on Ground

$$\Delta X_{az} \approx \rho\theta_{3dB_{az}} = \frac{\rho\lambda}{L_{az}}$$

$$\Delta X_{\rho} \approx \rho\theta_{3dB_{\rho}} = \frac{\rho\lambda}{L_{\rho}}$$

Matched Filtering of Received Echo

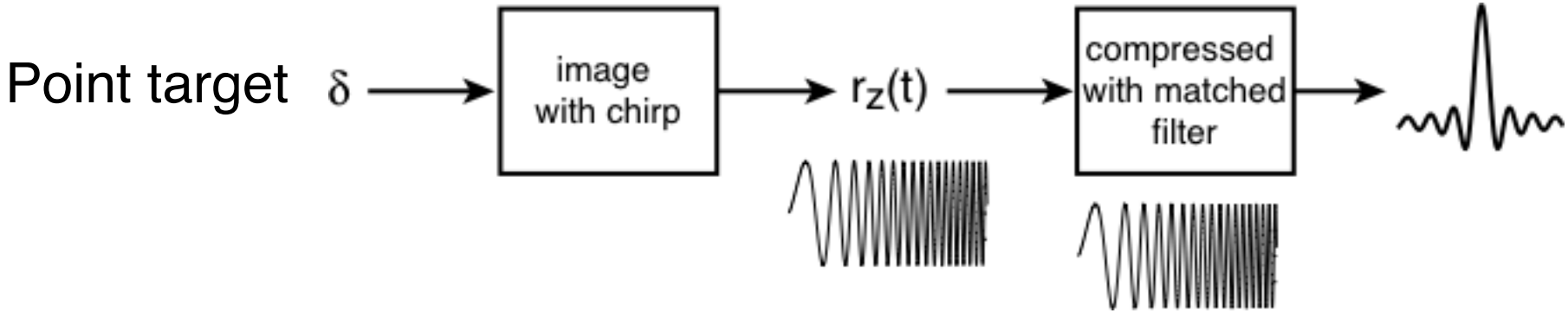

In general, the ground surface can be though of as a distribution of point targets, so the received echo, r(t), is a convolution of ground and chirp signal

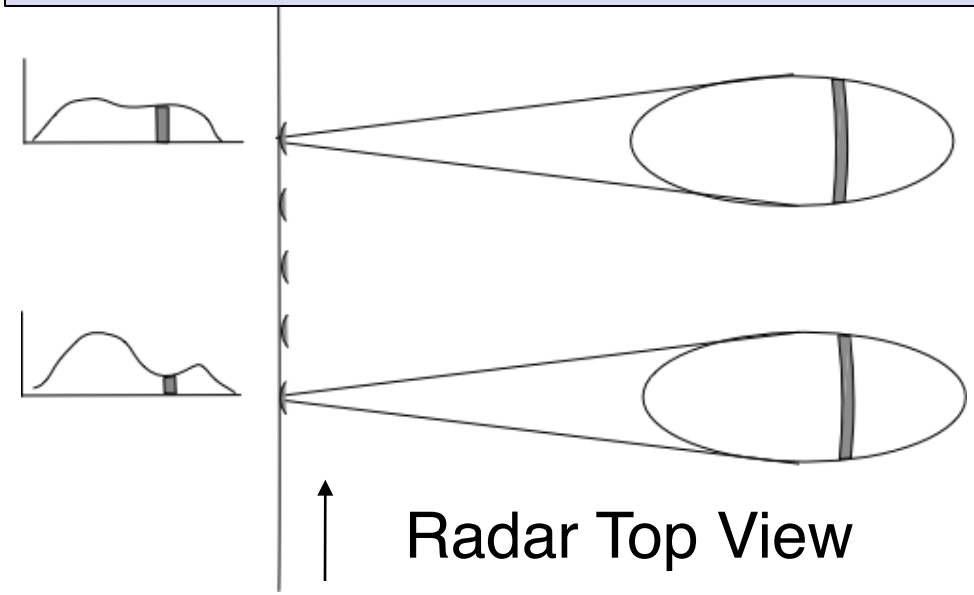

- Transmitted pulses are usually coded waveforms with significant bandwidth
- Matched filtering allows recovery of fine resolution features with a low peak-power pulse train

Radar Geometric Terminology

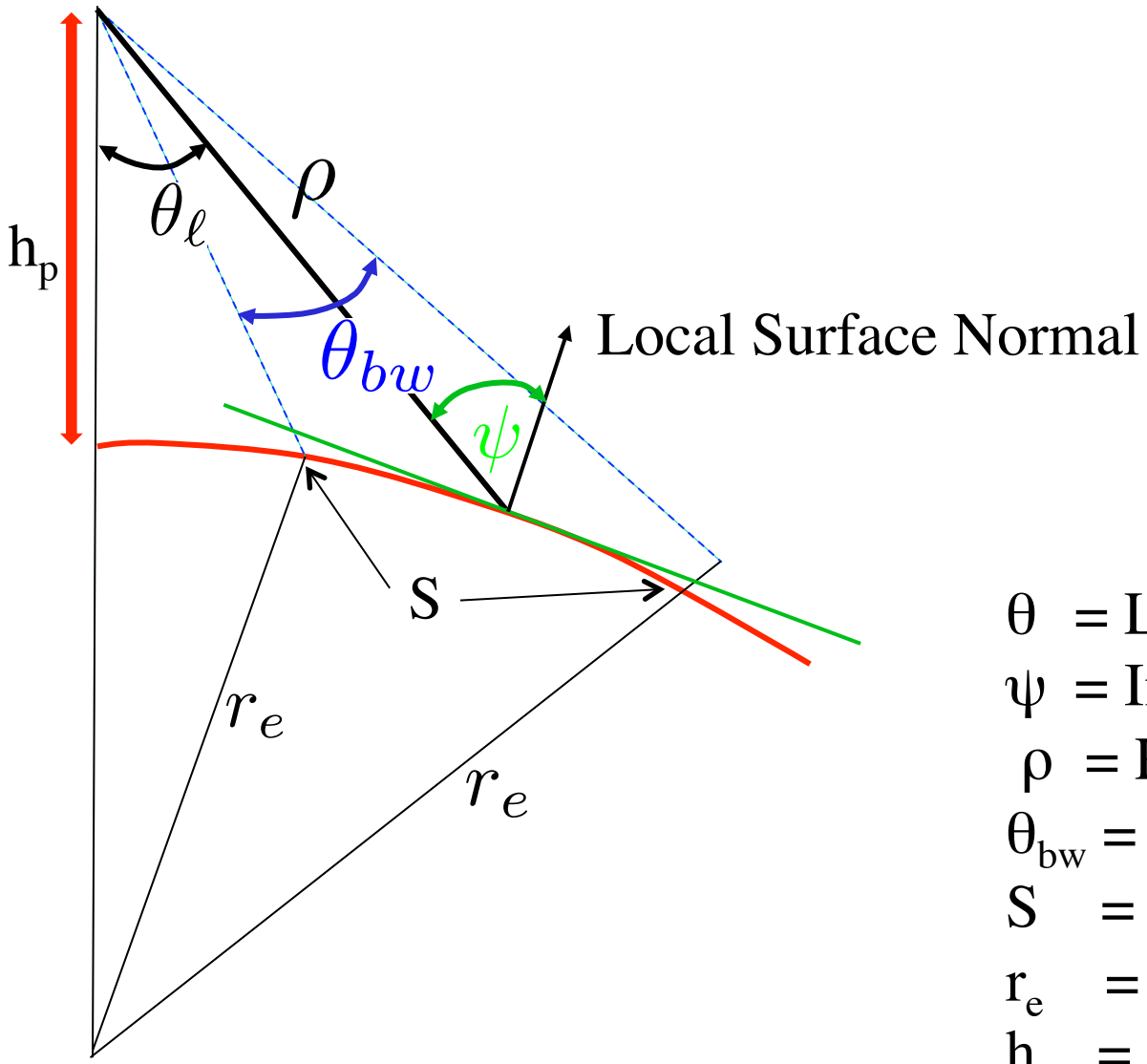

θ = Look Angle
ψ = Incidence Angle
ρ = Range
θ_{bw} = beamwidth
S = Swath width
r_e = Radius of Earth
h_p = Height of platform

Ground Resolution

- The ground resolution, Δg, depends on the range resolution and incidence angle, θ_i.
- Incidence angle is the angle between the wave propagation direction or line-of-sight and the normal to the surface.

$$\Delta g = \frac{\Delta\rho}{\sin\theta_i} = \frac{\Delta\rho}{\sin(\theta_\ell - \tau_\rho)}$$

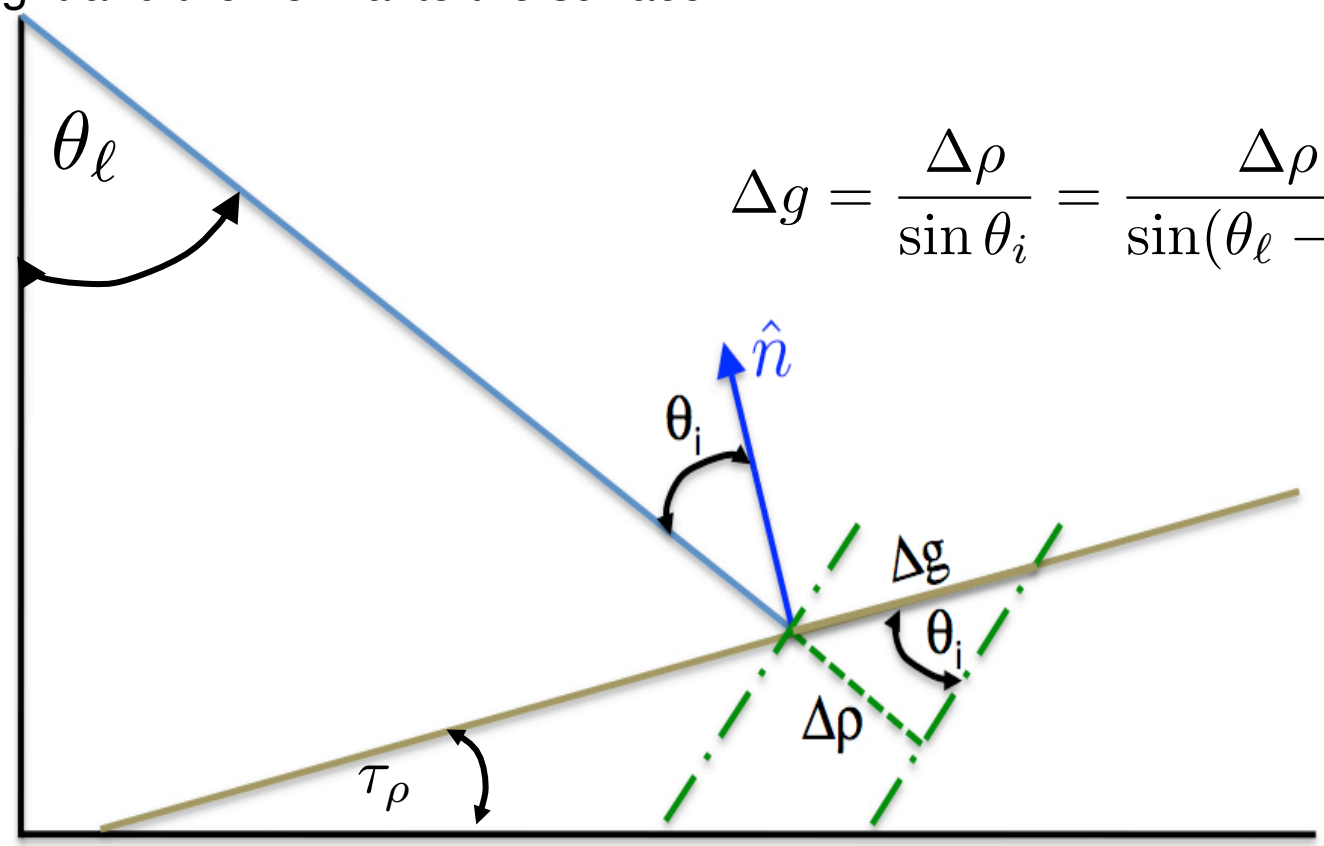

Raw Signal of a Point Target

Range →

Pulse Number →

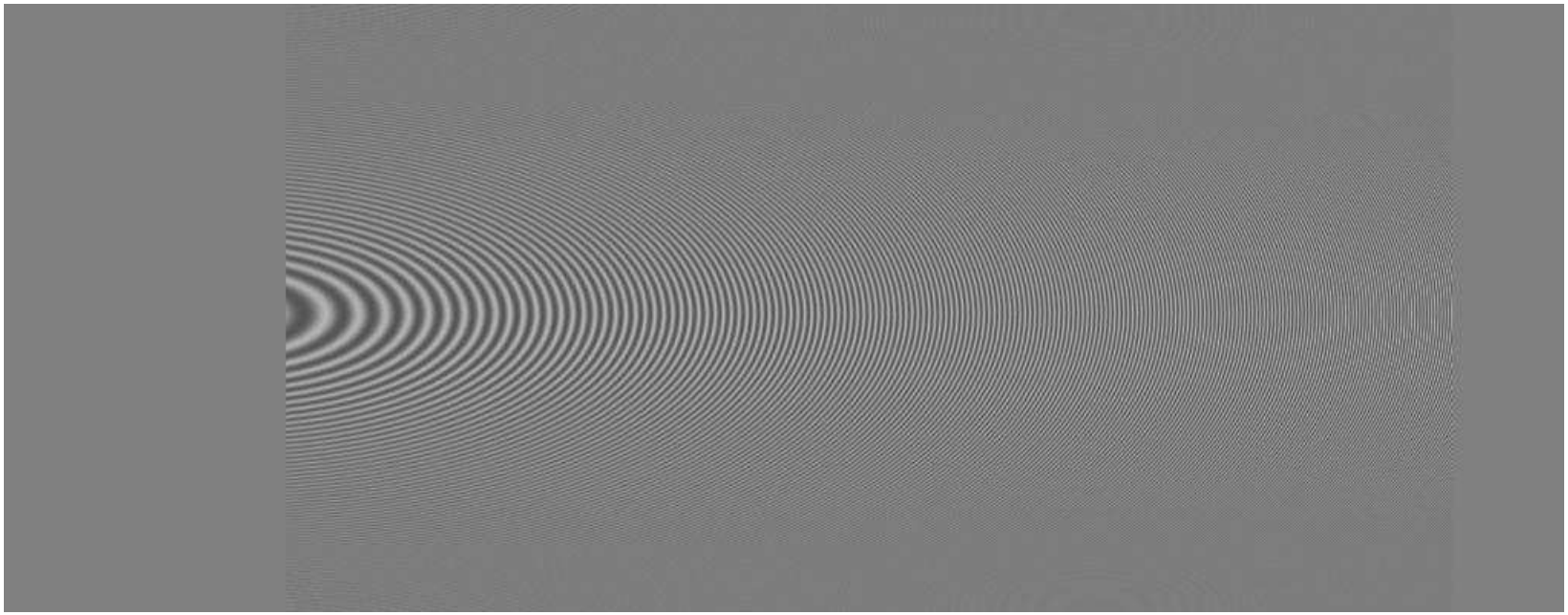

This “image” shows a sequence of simulated pulse echoes from a single point target

Range Compression of a Point Target; after Matched filtering

Range →

Pulse Number →

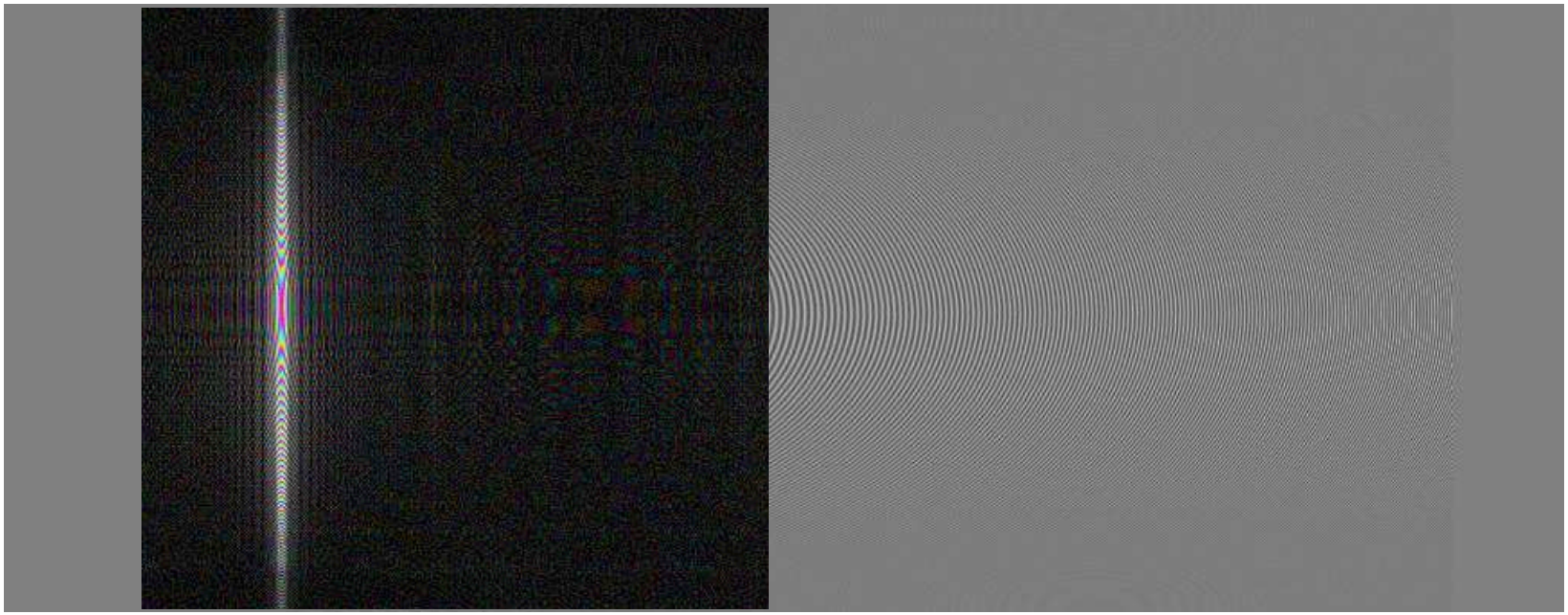

This “image” shows the simulated pulse echoes after range compression matched filtering

Doppler Shift

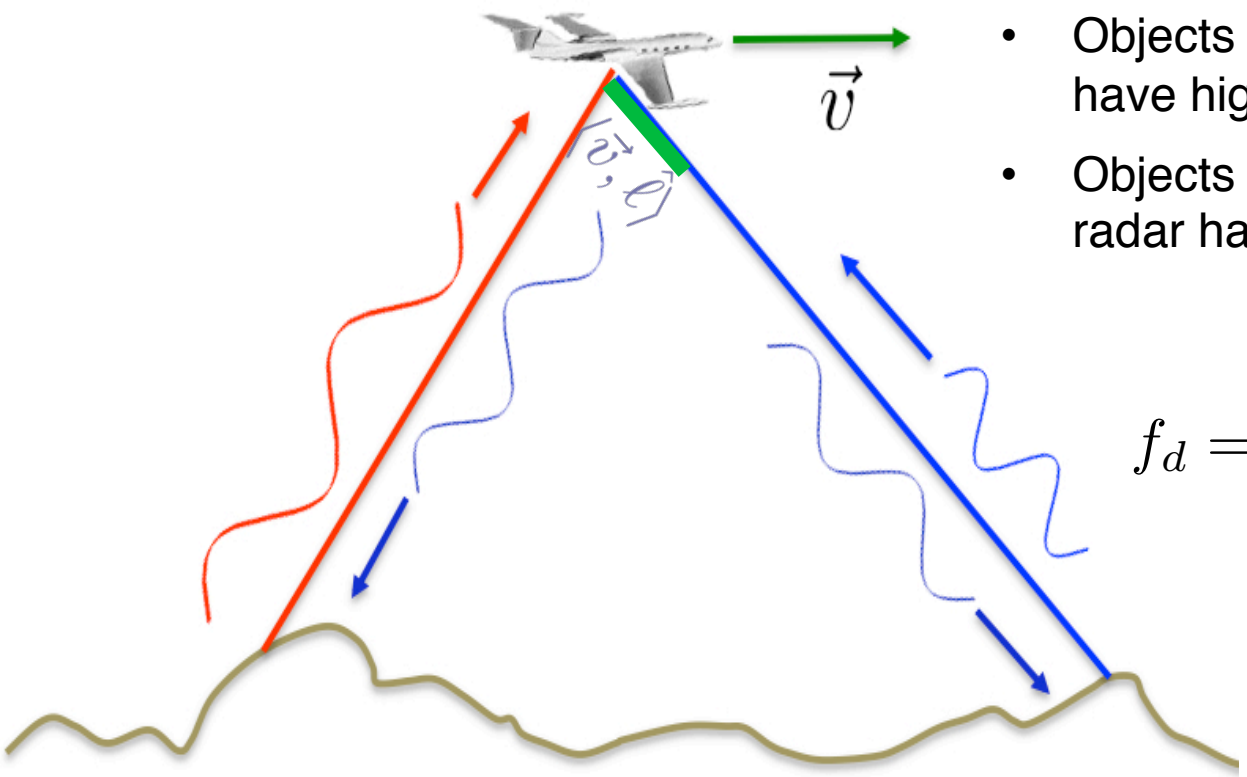

- Objects moving relative to a radar experience a frequency shift called the Doppler shift.
- Objects moving toward the radar have higher frequencies
- Objects moving away from the radar have lower frequencies.

$$f_d = \frac{2\langle \vec{v}, \hat{\ell} \rangle}{\lambda} = \frac{2v\cos\theta_{sq}}{\lambda}$$

SAR Imaging Concept

Real Aperture Imaging

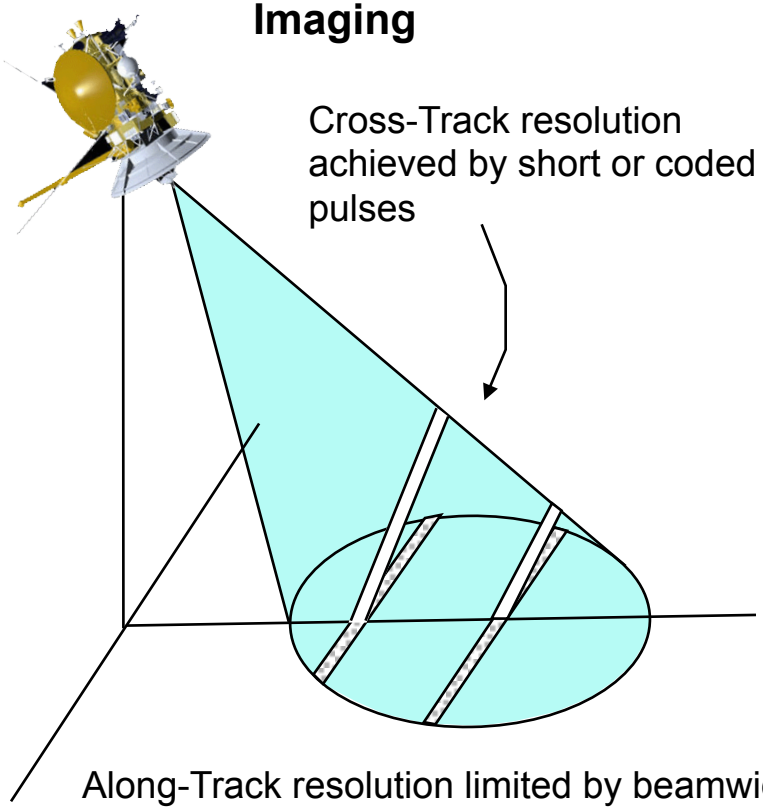

Synthetic Aperture Imaging

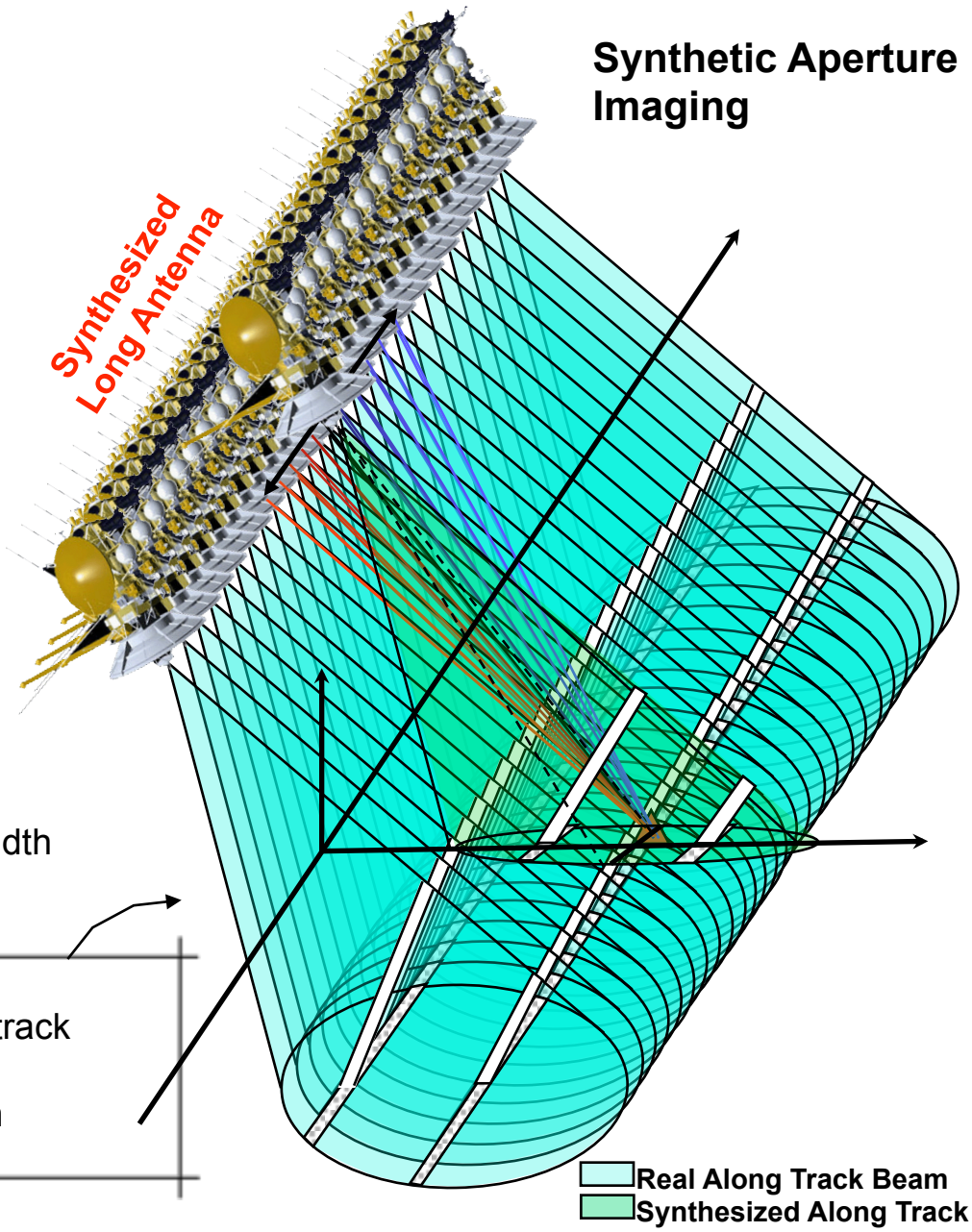

Along-Track resolution achieved by coherently combining echoes from multiple pulses along-track

- Resolution proportional to antenna length
- Independent of Range/Frequency

Doppler in SAR Imaging

$$
\begin{aligned}
R(x) &= \sqrt{R_0^2 + (x - x_0)^2} \\
&\approx R_0 \left(1 + \frac{(x - x_0)^2}{2R_0^2}\right) \\
&\approx R_0 + \frac{(x - x_0)^2}{2R_0}
\end{aligned}
$$

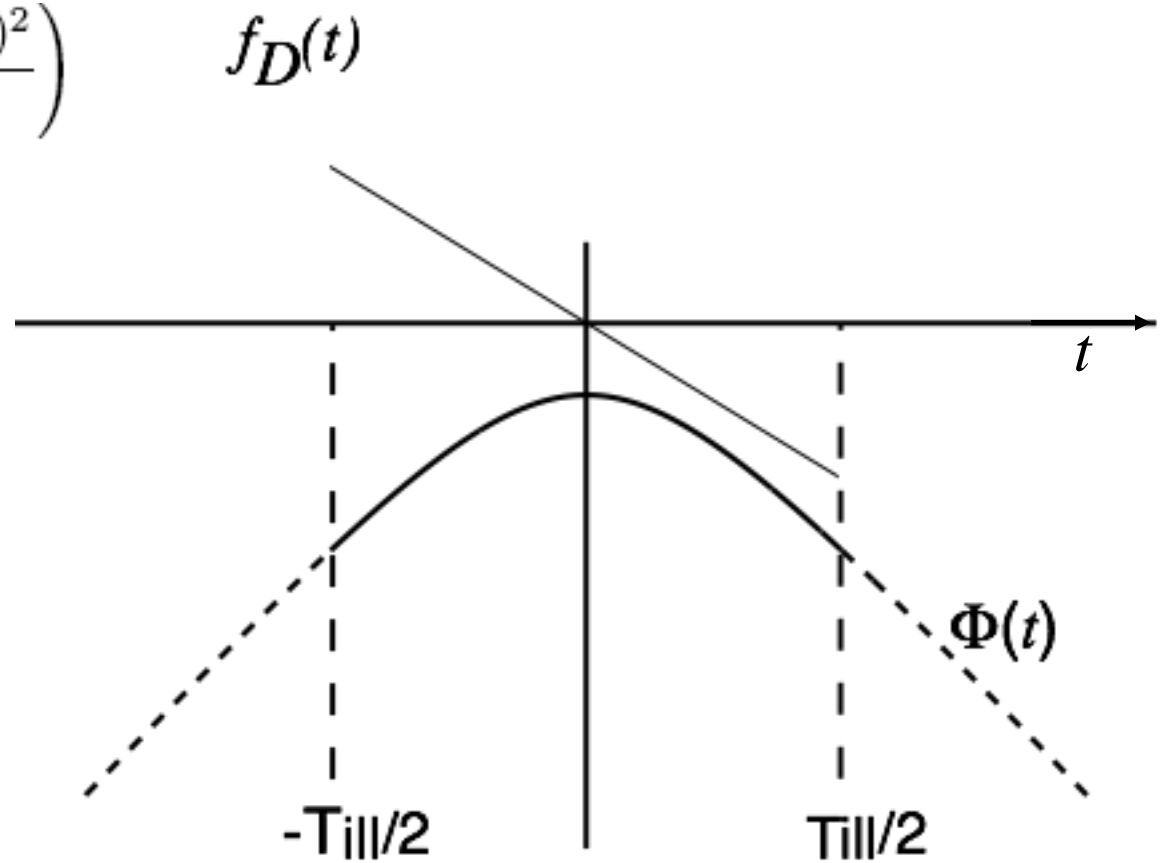

Dropping the constant term

$$
\begin{aligned}
\phi(t) &= -\frac{\pi}{F^2} v^2 (t - t_0)^2 \\
\omega(t) &= -2\pi \frac{v^2}{F^2} (t - t_0) \\
f_D(t) &= -\frac{v^2}{F^2} (t - t_0)
\end{aligned}
$$

$$F^2 = \lambda R_0 / 2.$$

Frequency Domain View of SAR

- Instantaneous frequency spread within an echo in azimuth is a function of the azimuth beamwidth.

$$\Delta f = \frac{2v}{\lambda} \sin\theta_\ell \cos\theta_{az} \Delta\theta_{az}$$

$$\rho\theta_{bw} \approx \Delta a \approx \rho \sin\theta_\ell \theta_{gbw}$$

$$\theta_{gbw} = \frac{\theta_{bw}}{\sin\theta_\ell}$$

$$\begin{aligned} \Delta f &= \frac{2v}{\lambda} \sin\theta_\ell \cos\theta_{az} \frac{\lambda}{\sin\theta_\ell L_{az}} \\ &= \frac{2v}{L_{az}} \cos\theta_{az} \end{aligned}$$

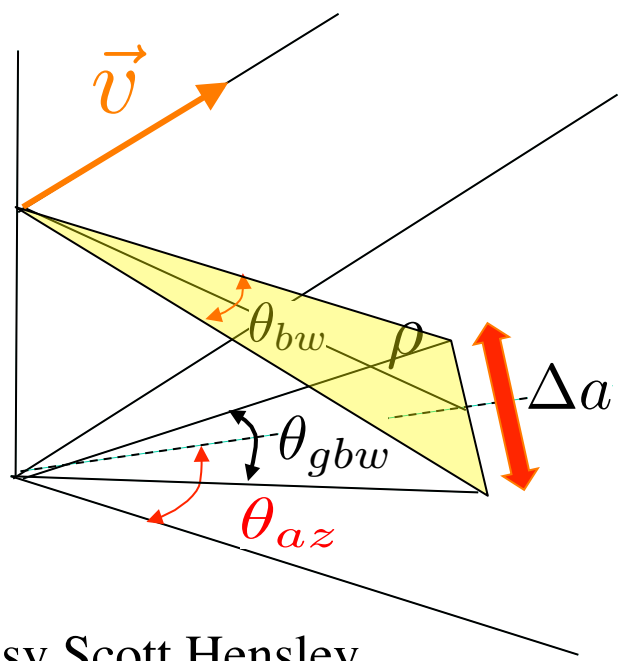

FREQUENCY DOMAIN

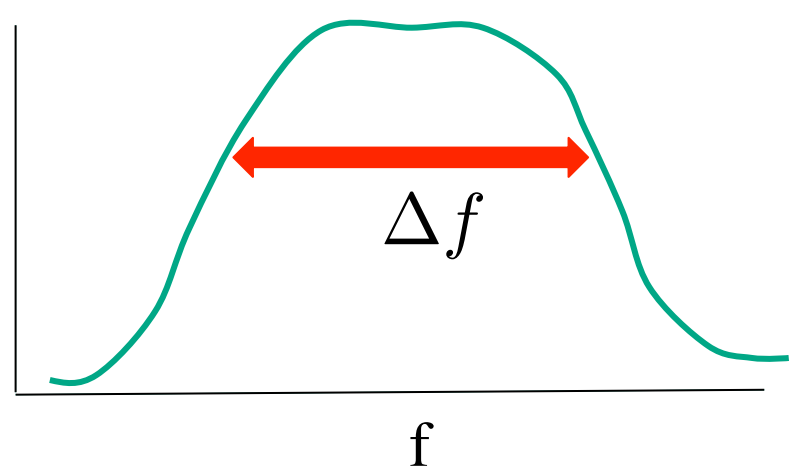

Courtesy Scott Hensley

Nyquist Sampling Theorem

- A consequence of the Nyquist Sampling Theorem is that the radar Pulse Repetition Frequency (PRF) must be twice the bandwidth of the received signal in order to avoid spectral aliasing of the signal.
- Using the expression from the previous viewgraph for the azimuth bandwidth we have that

$$PRF \geq \frac{2v}{L_{az}} \cos\theta_{az}$$

which for small squint angles, θ_{az} smaller than 25°, is often simplified to

$$PRF \geq \frac{2v}{L_{az}}$$

- Note that the required PRF is independent of wavelength and range and only depends on the platform velocity and the azimuth antenna dimension.

Courtesy Scott Hensley

Range-Doppler Coordinates

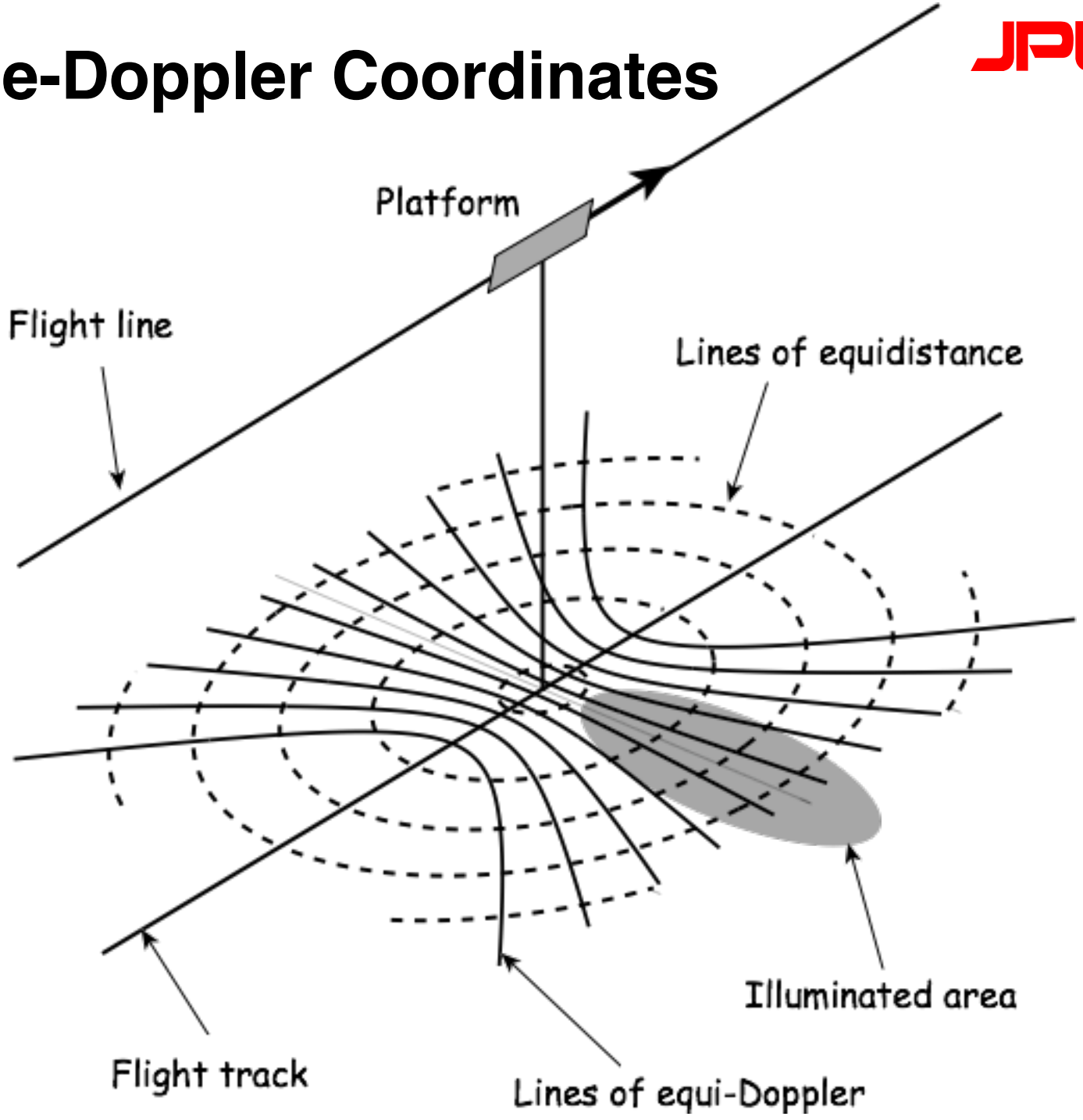

Doppler and Squint

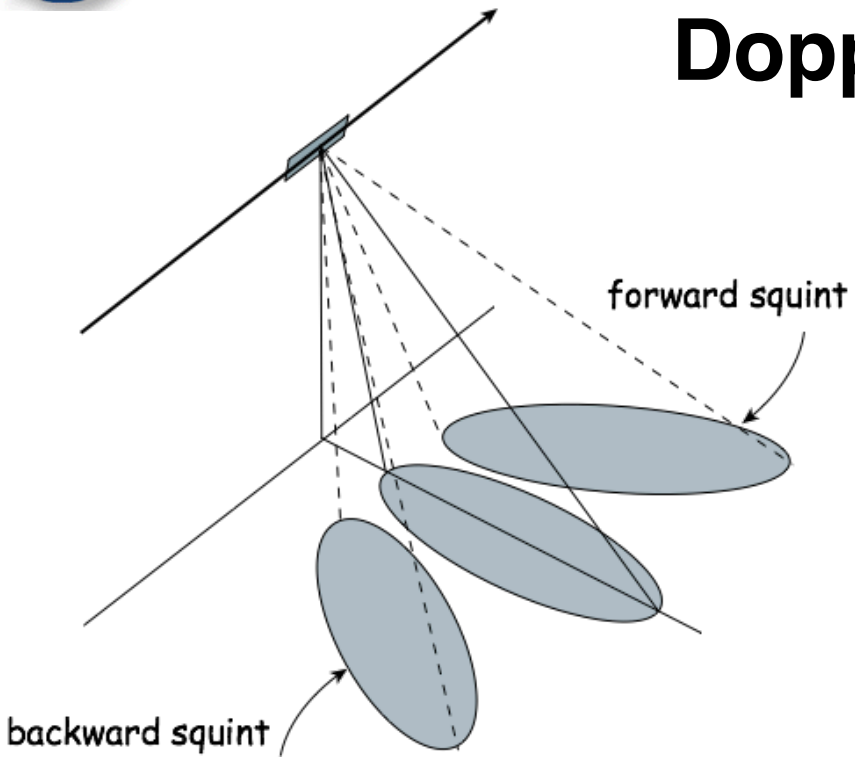

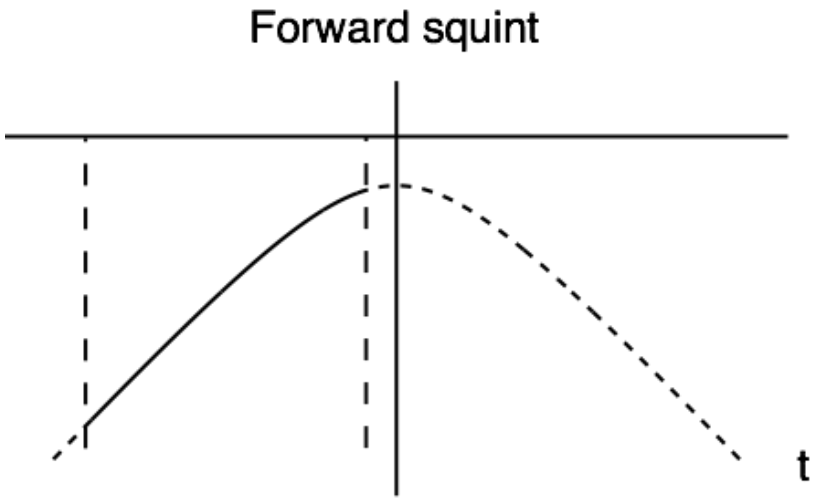

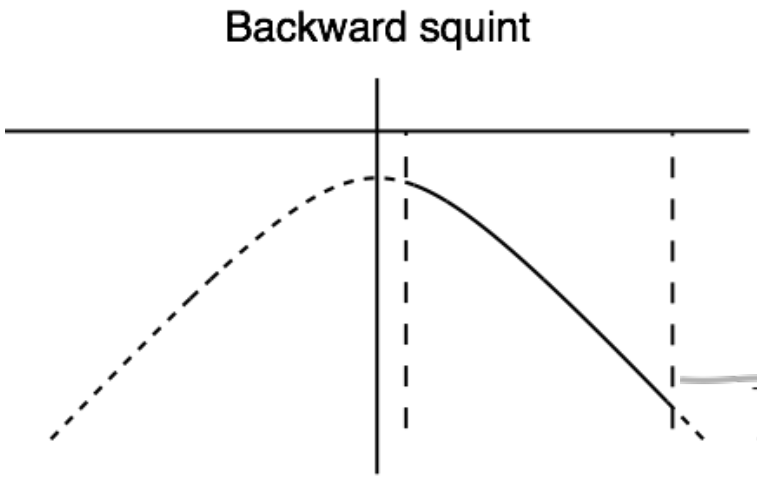

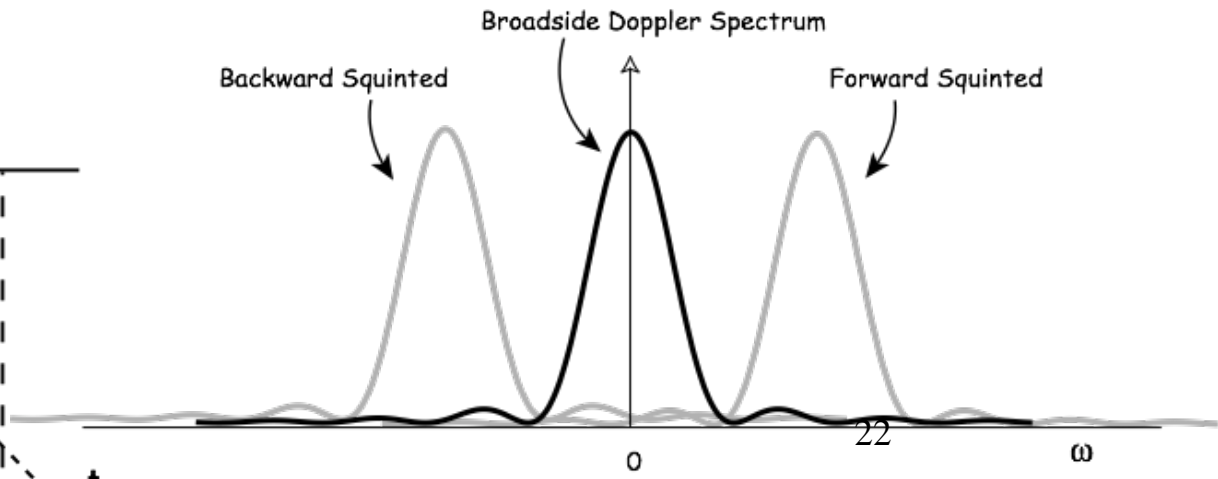

Azimuth Resolution from Aperture Synthesis

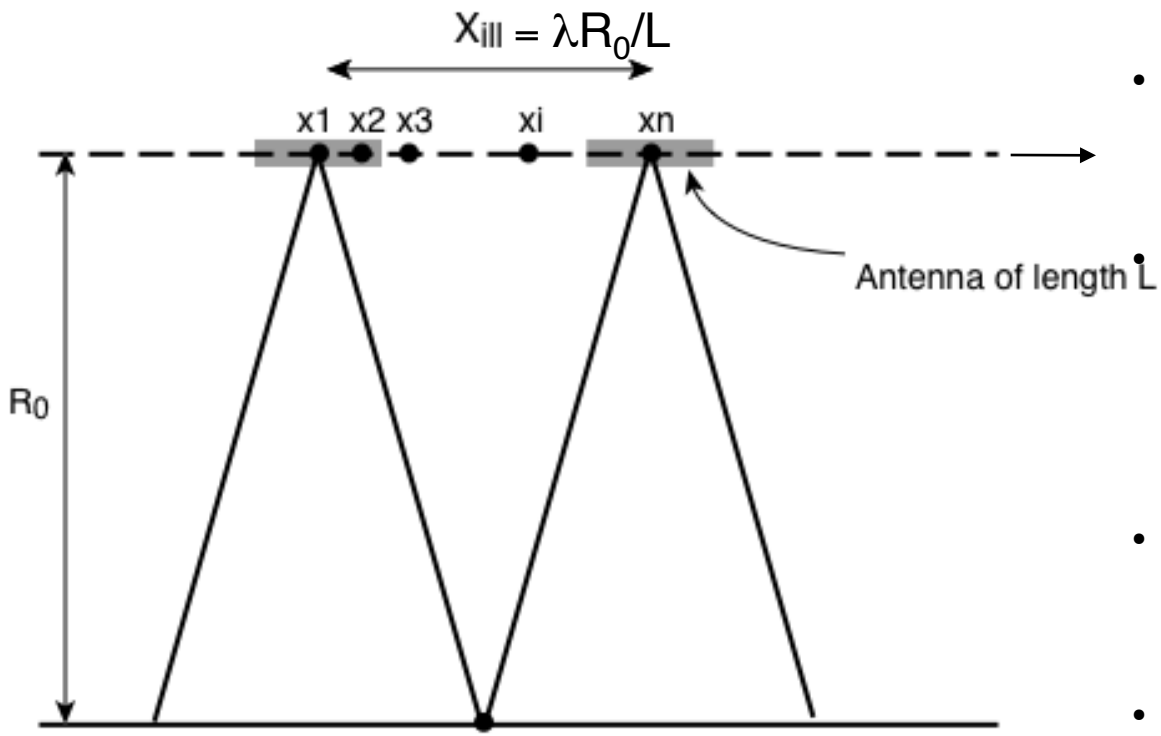

- The illuminated extent of the ground is $\lambda R_0/L$
- The synthetic aperture is $2*X_{ill}$ lengthens as R_0 increases…
- …which decreases the azimuth synthetic aperture's angular beamwidth $\lambda/(2*X_{ill})$ in proportion…
- …but the spatial resolution on the ground ($\lambda R_0/(2*X_{ill})= L/2$) is constant
- Aperture synthesis processing is very similar to matched filtering in range

Raw Signal of a Point Target

Range →

Pulse Number →

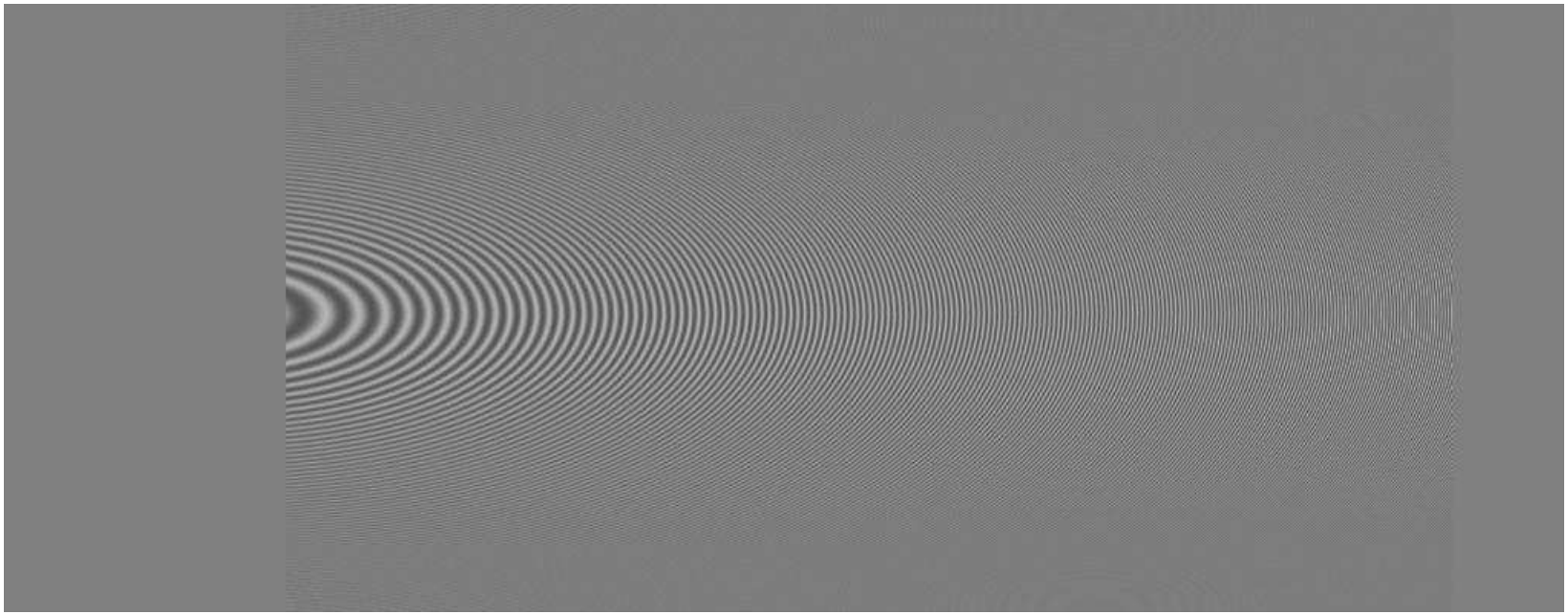

This “image” shows a sequence of simulated pulse echoes from a single point target

Range Compression of a Point Target; after Matched filtering

Range →

Pulse Number →

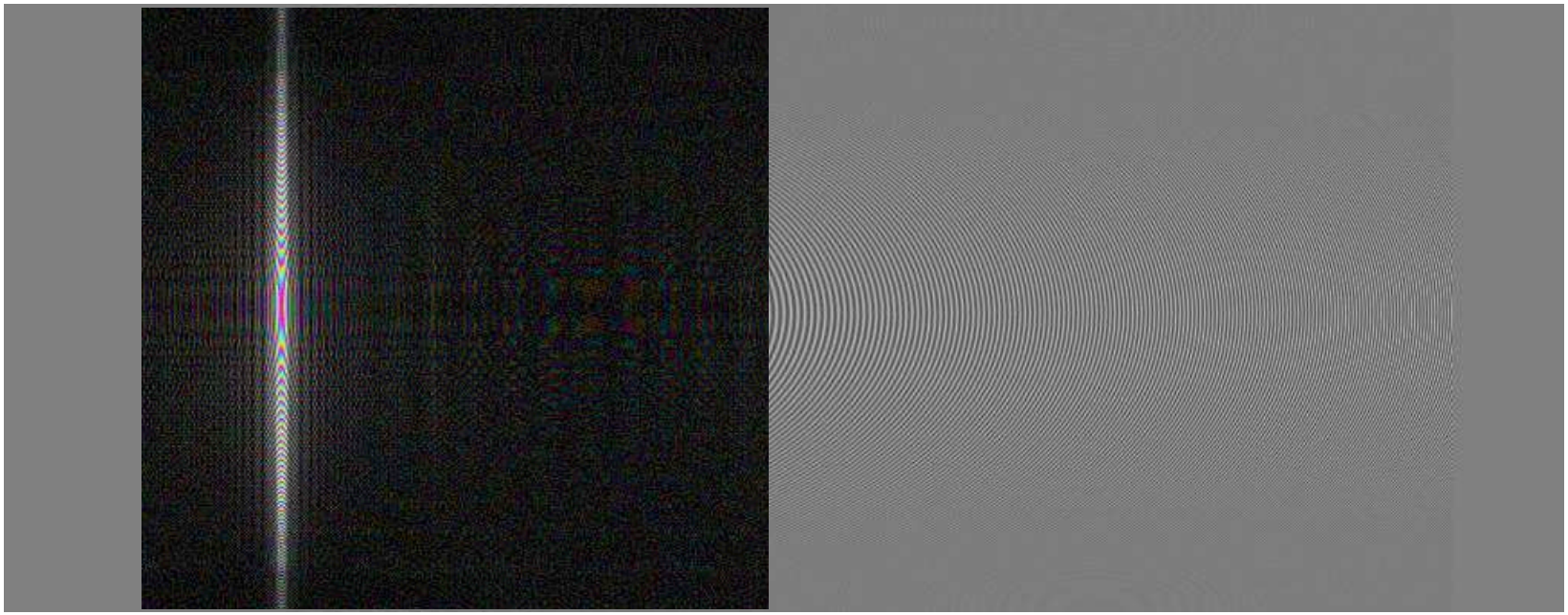

This “image” shows the simulated pulse echoes after range compression matched filtering

Point Target after Azimuth Compression Matched filtering

Range →

Pulse Number →

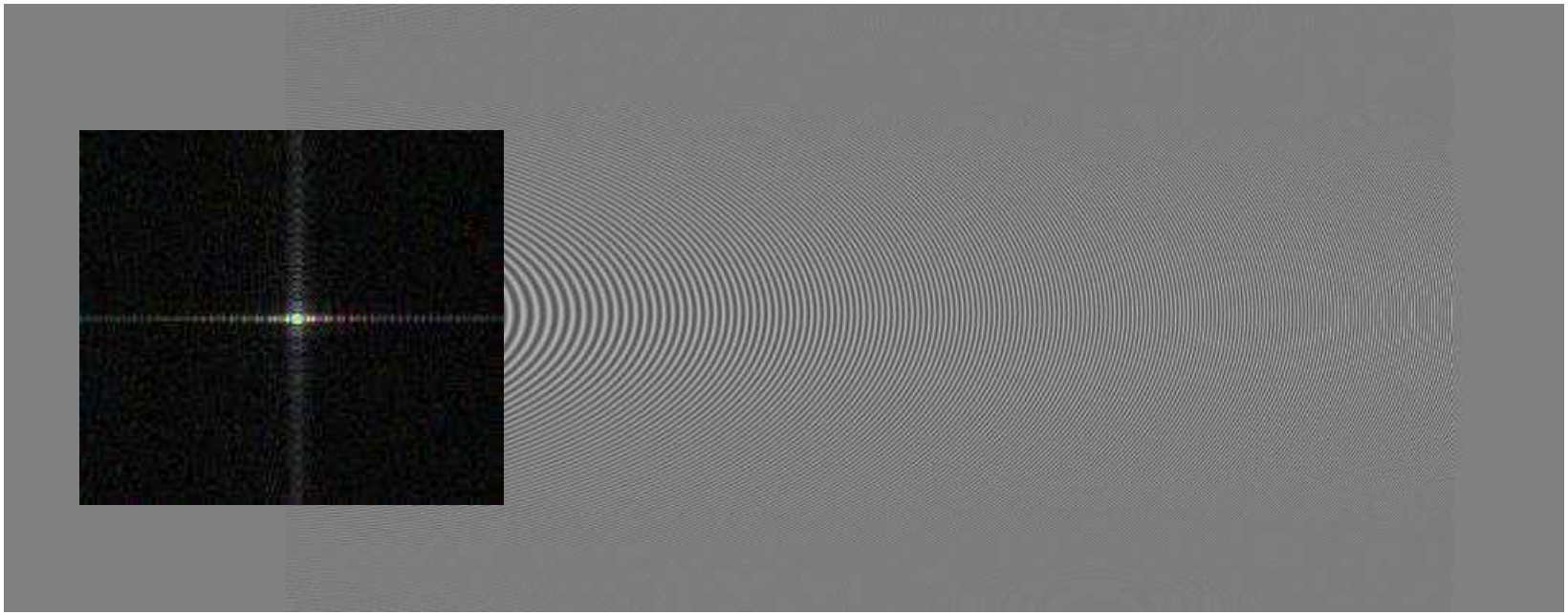

This “image” shows the simulated pulse echoes after range and azimuth compression matched filtering

SEASAT – SAR in Space in 1978

SEASAT SAR image of Death Valley

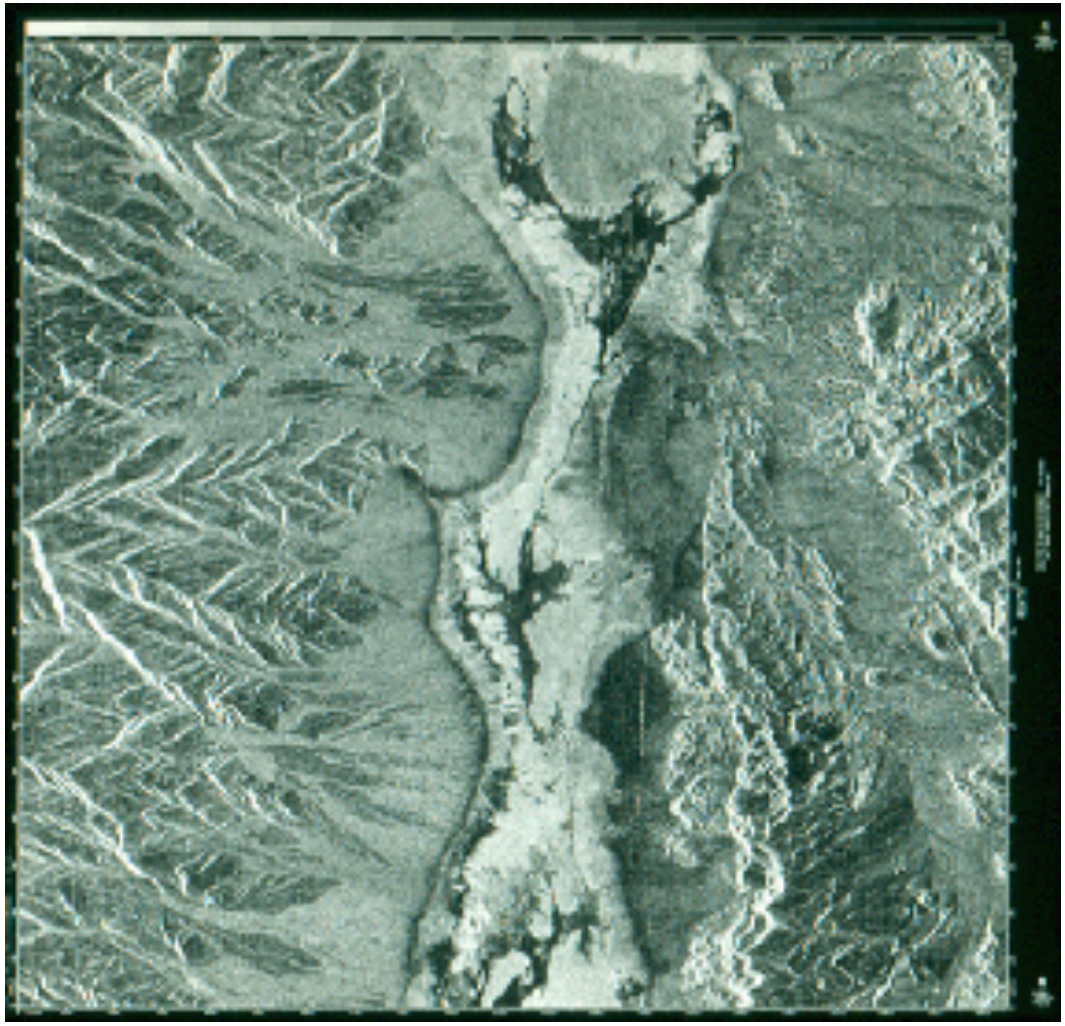

Conventional SAR modes

- Strip-mode SAR
  - Standard SAR mode
  - Send a pulse of energy; receive echo; repeat
  - One pulse transmit and receive at a time
  - Swath width limited by radar ambiguities
- ScanSAR
  - Wider swath low resolution SAR mode
  - Execute sequence as follows:
    - Send a pulse of energy; receive echo; repeat 50-100 times
    - Repoint the beam across-track to position 2 electrically (almost instantaneous)
    - Send a pulse of energy; receive echo; repeat 50-100 times
    - Repoint the beam across-track to position 3 electrically (almost instantaneous)
    - Send a pulse of energy; receive echo; repeat 50-100 times
  - Again, one pulse transmit and receive at a time
  - ScanSAR trades resolution (in along-track dimension) for swath: low impact on data rate
  - Generally poorer ambiguity and radiometric performance than Strip SAR

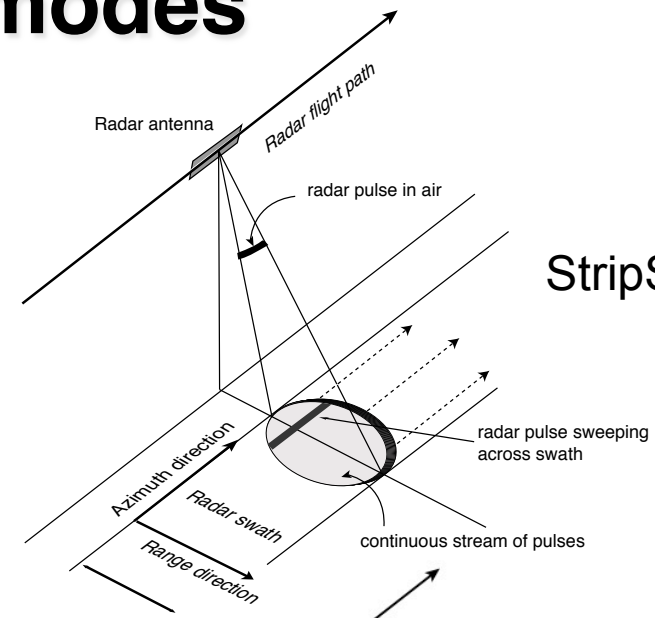

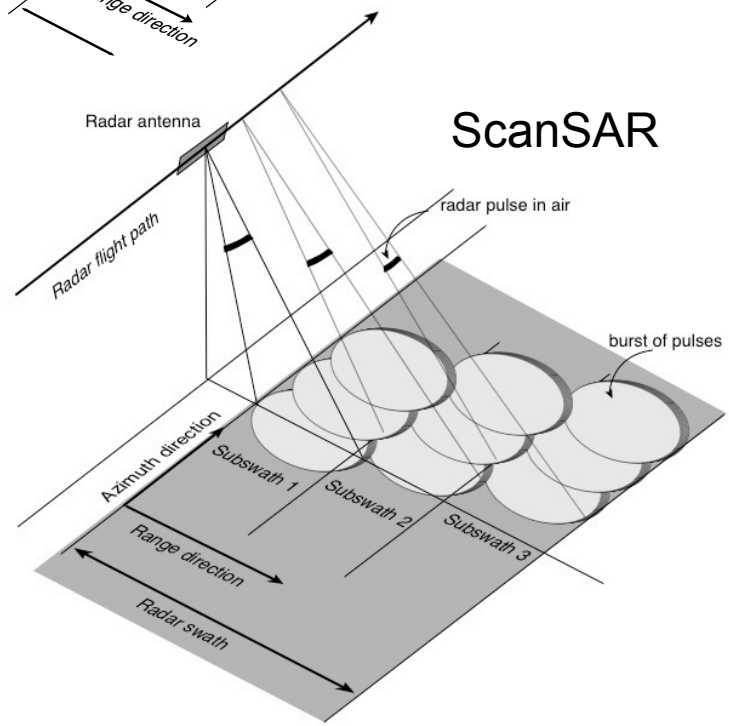

What Radar Can Tell Us

- Transmitted radar signals have known characteristics
  - Amplitude
  - Polarization
  - Phase and Time Reference
  - Wavelength, or Frequency
- A distant object that scatters the radar signal back toward the receiver alters the amplitude, polarization, and phase, differently for different wavelengths
- Comparison of the received signal characteristics to the transmitted signal allows us to understand the properties of the object.

Surface and Volume Scattering Models for Radar

We can model simple scattering from particles or surfaces…

Cross section of a large sphere is its projected area

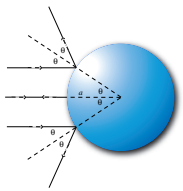

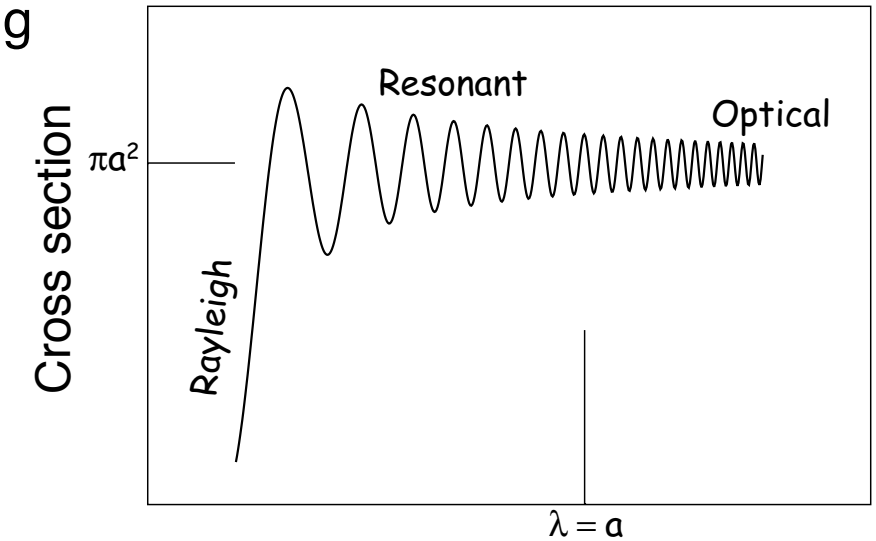

Cross section of a large flat facet goes as area squared

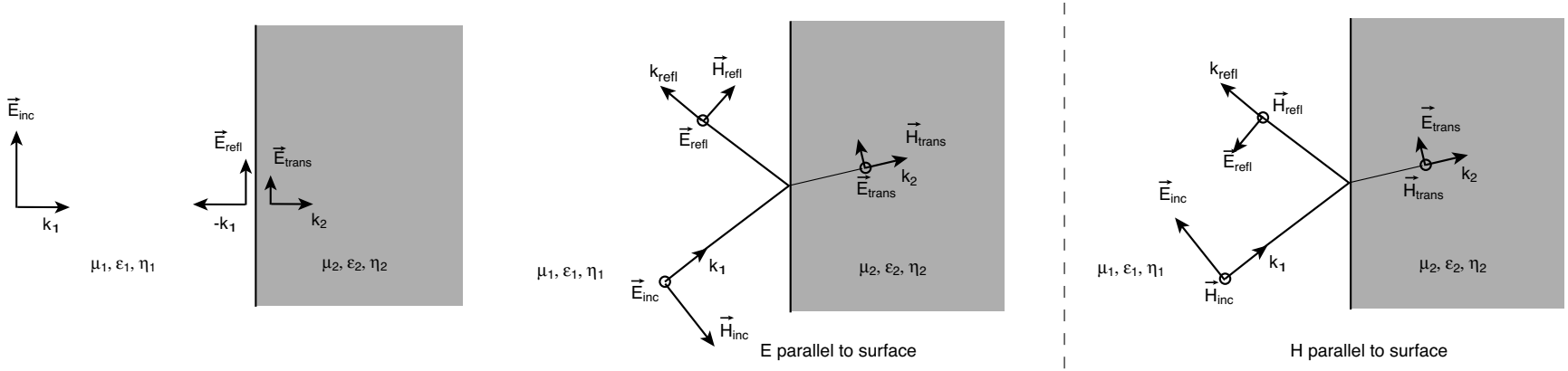

Surface and Volume Scattering Models for Radar

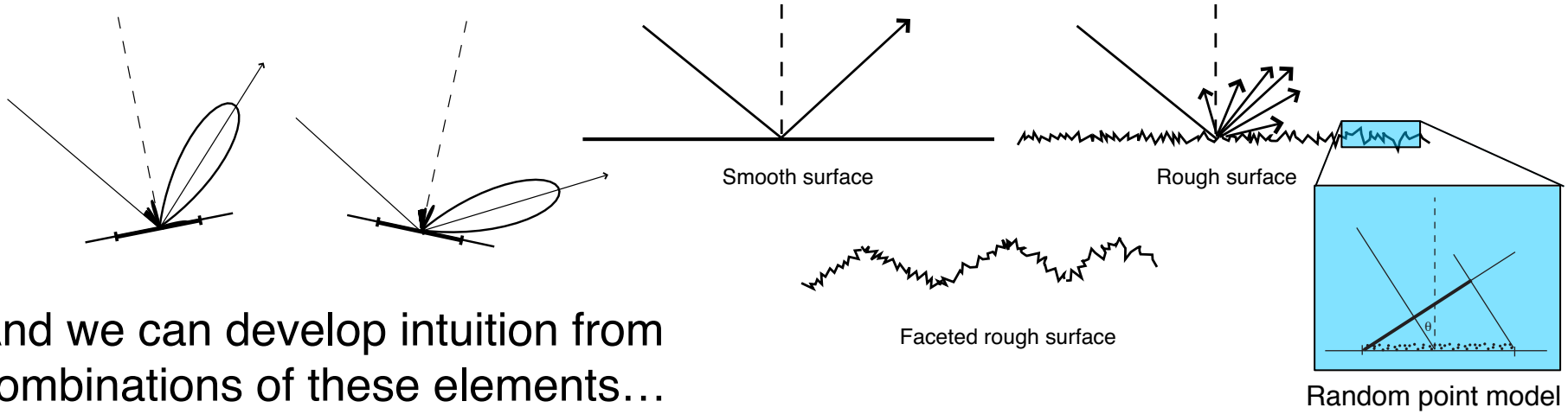

And we can develop intuition from combinations of these elements…

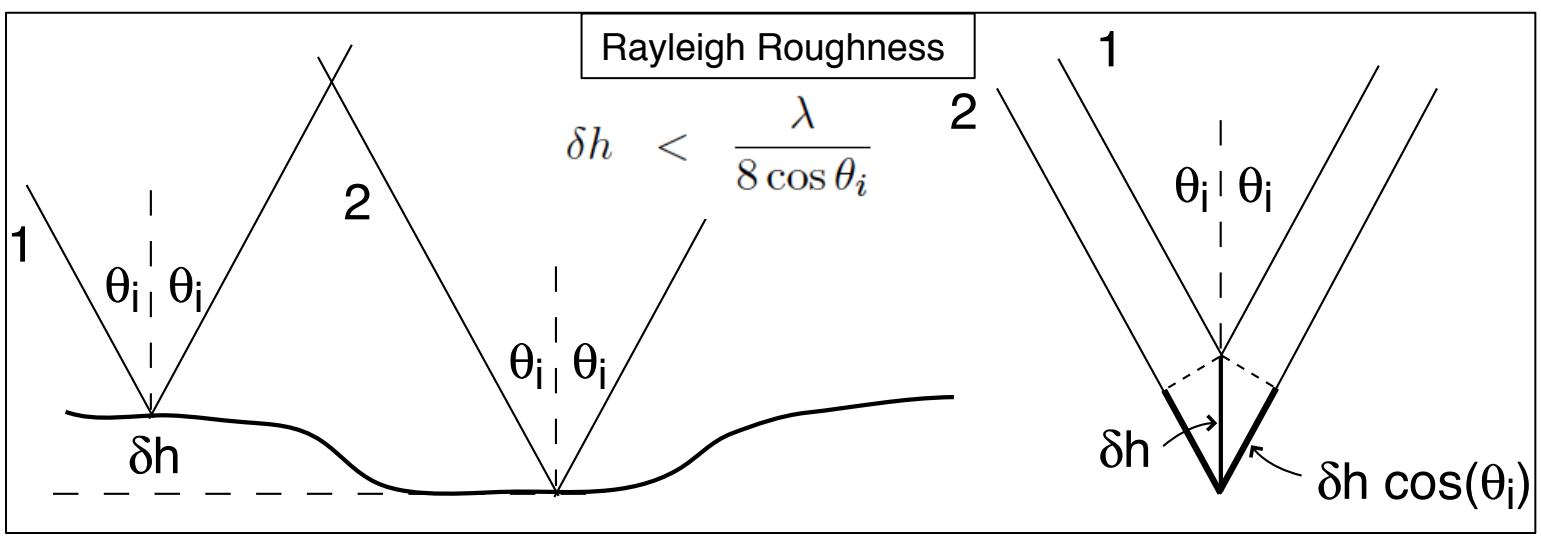

Surface and Volume Scattering Models for Radar

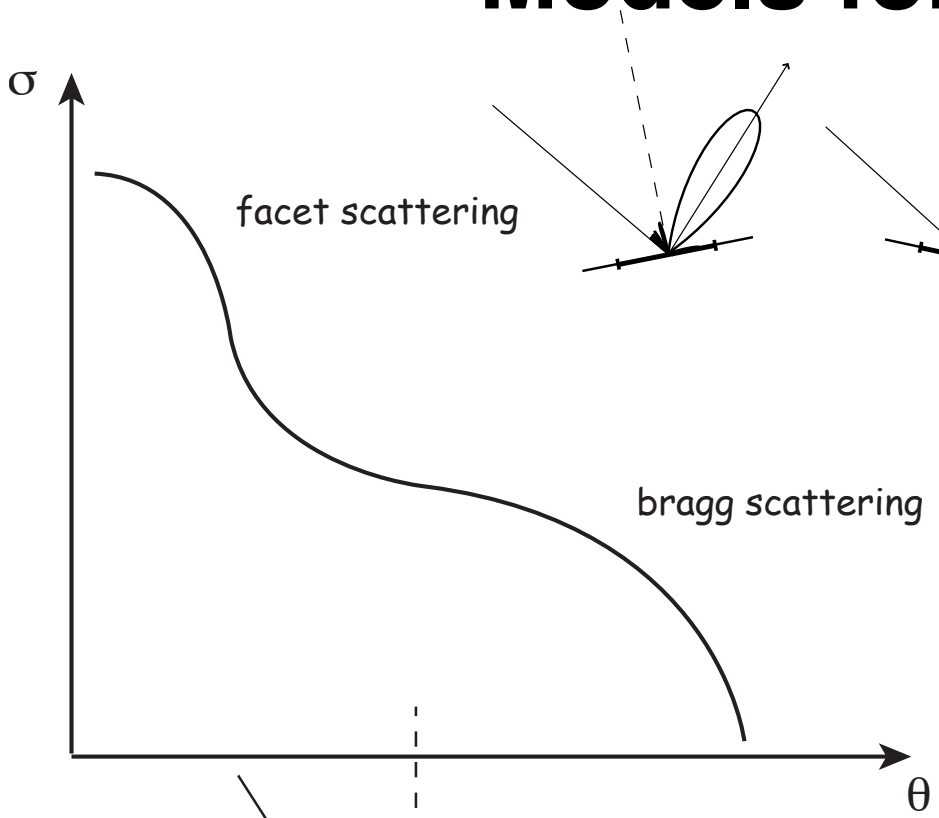

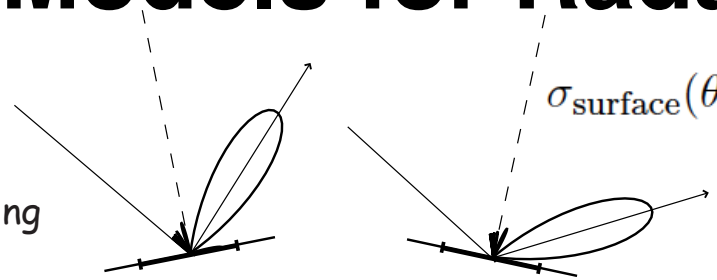

$$\sigma_{\text{surface}}(\theta) = \Gamma^2_{\text{Refl}} \sum_j p^2(\theta, \theta_{\text{inc}} - \alpha_j)$$

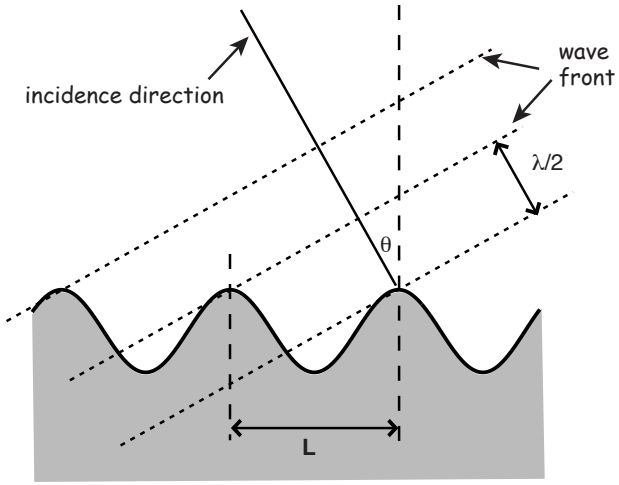

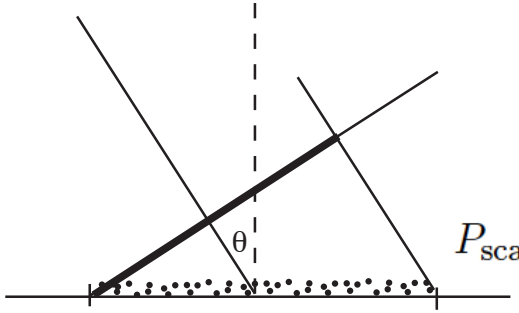

$$P_{\text{scat,d}} = \frac{P_{\text{inc,d}}}{4\pi r^2} \sigma_{\text{point}} \cos\theta_i N$$

Radar Imaging Properties

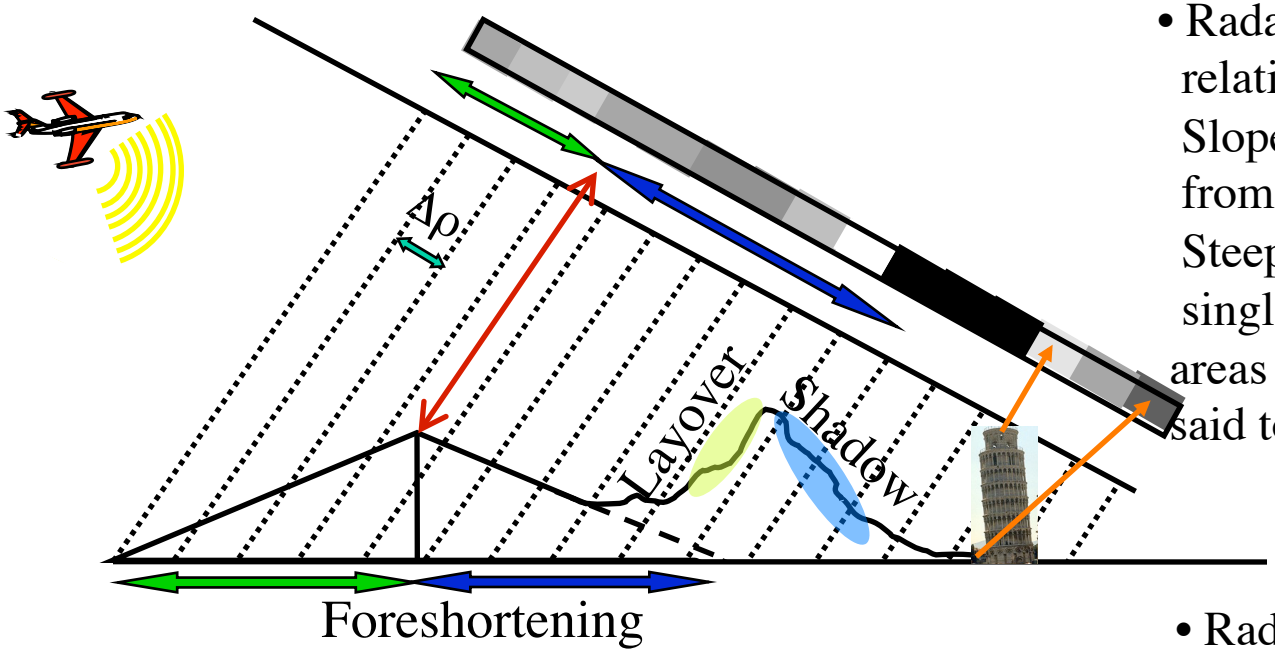

- Radar images are distorted relative to a planimetric view. Slopes facing toward or away from the radar appear foreshortened. Steep slopes are collapsed into a single range cell called layover and areas occulted by other areas are said to be shadowed.

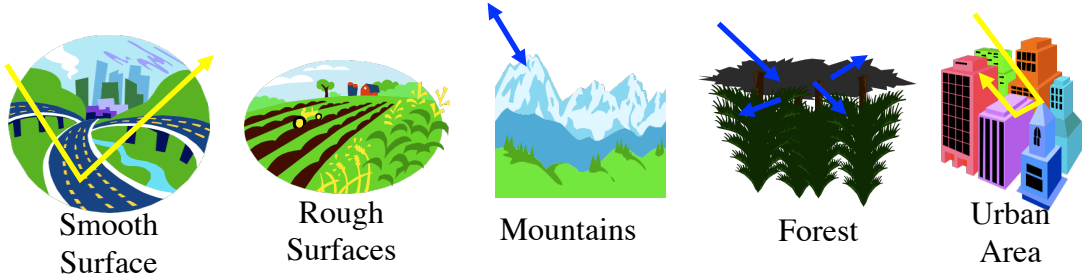

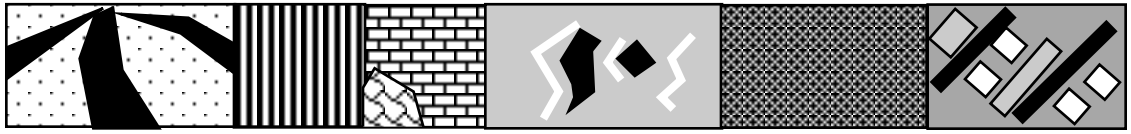

- Radar is primarily sensitive to the structure of objects being imaged whereas optical images are primarily sensitive to chemistry.
- The scale of objects relative to the radar wavelength determines how smooth an object appears to the radar and how bright or dark it is in the imagery.

Wavelength - A Measure of Surface Scale

Light interacts most strongly with objects on the size of the wavelength

Forest: Leaves reflect X-band wavelengths but not L-band

Dry soils: Surface looks rough to X-band but not L-band

Ice: Surface and layering look rough to X-band but not L-band

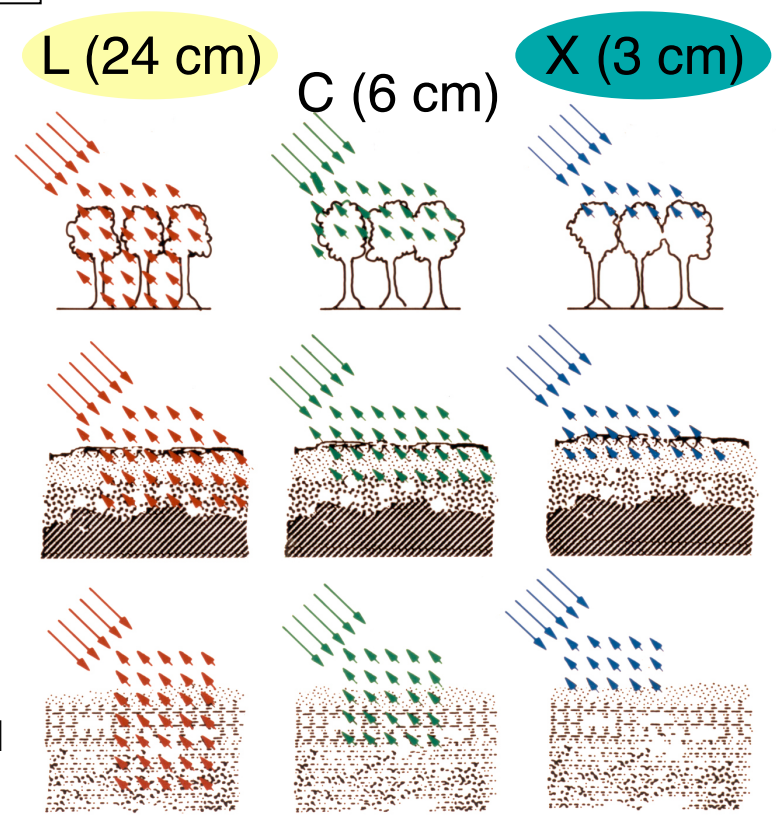

Polarization - A Measure of Surface Orientations and Properties

Wave Polarization

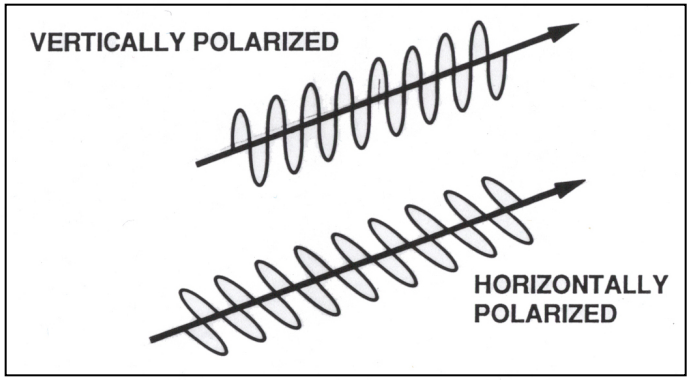

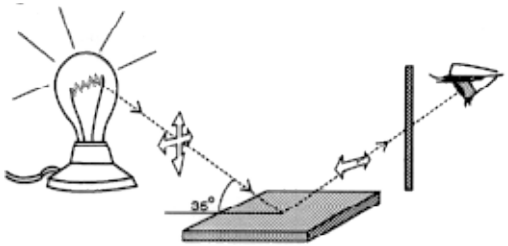

Mostly horizontal polarization is reflected from a flat surface.

Polarization Filters

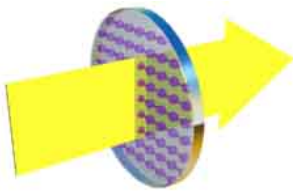

Vertical polarization passes through horizontally arranged absorbers.

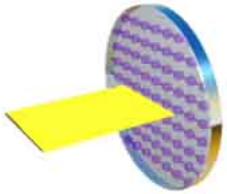

Horizontal polarization does not pass through horizontally arranged absorbers.

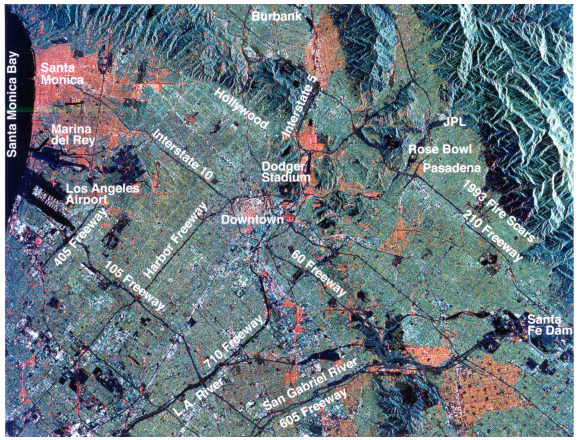

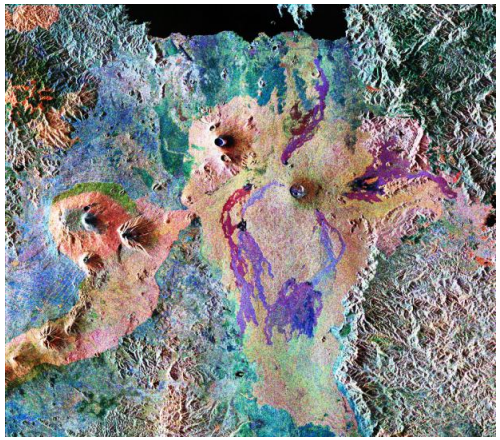

Color figures from www.colorado.edu/physics/2000

Radar Equation in Remote Sensing

- Backscatter can be used to interpret surface properties
  - Often using wavelength and polarization to probe characteristics
- Other radar instrument characteristics affect the science performance
  - Wavelength and antenna size determine illuminated area and real-aperture resolution
  - Antenna size in flight direction determines resolution for a synthetic aperture radar
  - Antenna area determines ambiguity, or aliasing, performance and swath extent
- Sensitivity of the measurement determined by "radar equation"

$$\mathrm{SNR} = P_T \cdot G_T(\lambda) \cdot \frac{1}{4\pi R^2} \cdot \sigma(\lambda) \cdot \frac{1}{4\pi R^2} \cdot A_R \cdot \epsilon(\lambda) \cdot \frac{1}{kTB}$$

Signal-to-Noise Ratio

Transmit Power

Transmit Antenna Gain

Range (distance)

Radar cross-section or "Reflectivity"

Receive Antenna Area

System Efficiency/Losses

Receiver Temperature

Receiver Bandwidth

SAR Imagery and Speckle

- Full resolution SAR imagery has a grainy appearance called speckle, which is a phenomena due to the coherent nature of SAR imaging.
- The total signal return from a resolution cell is the coherent sum of the returns from all the individual scatterers within it that are generally randomly distributed.

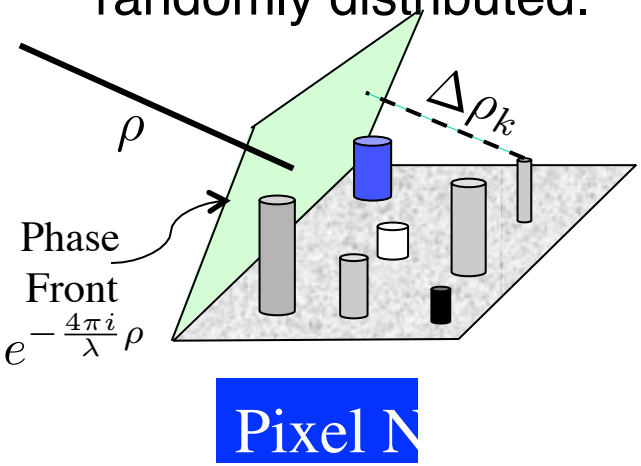

Number and arrangement of scattering elements within resolution cell varies from pixel to pixel.

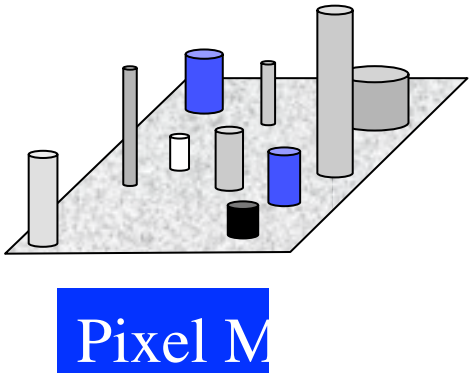

Returned signal is a coherent combination of the returns from the scattering elements.

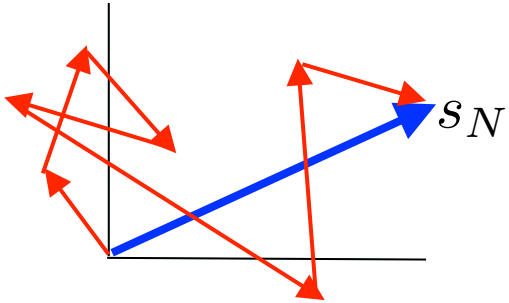

$$s = A \underbrace{e^{-\frac{4\pi i}{\lambda}\rho}}_{\text{Range Phase}} \underbrace{\sum_{k=1}^{N} a_k e^{-\frac{4\pi i}{\lambda}\Delta\rho_k}}_{\text{Scatterer Contribution}}$$

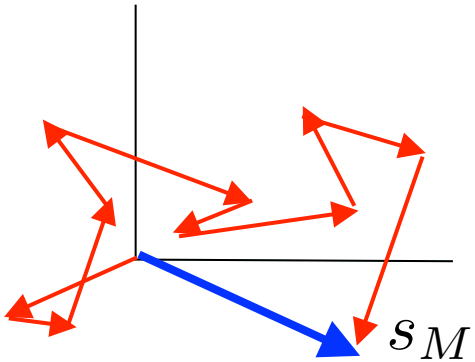

Speckle and Radiometric Accuracy

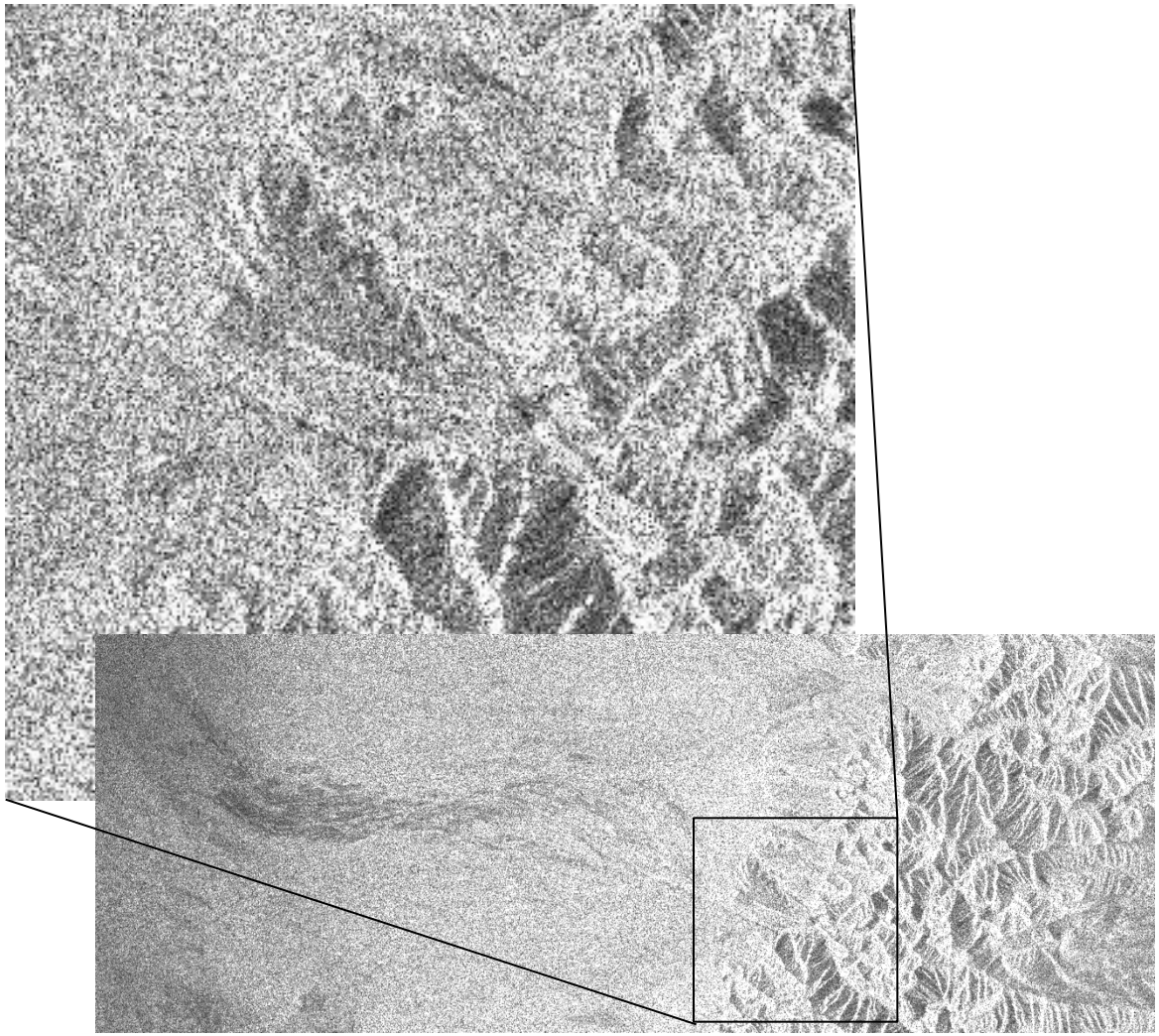

Natural “laser” speckle masks intrinsic radar backscatter which contains surface information, independent of SNR!

Spatial averaging (looks) reduces the speckle and draws out the natural backscatter reflectivity

Spatial Averaging or Looks

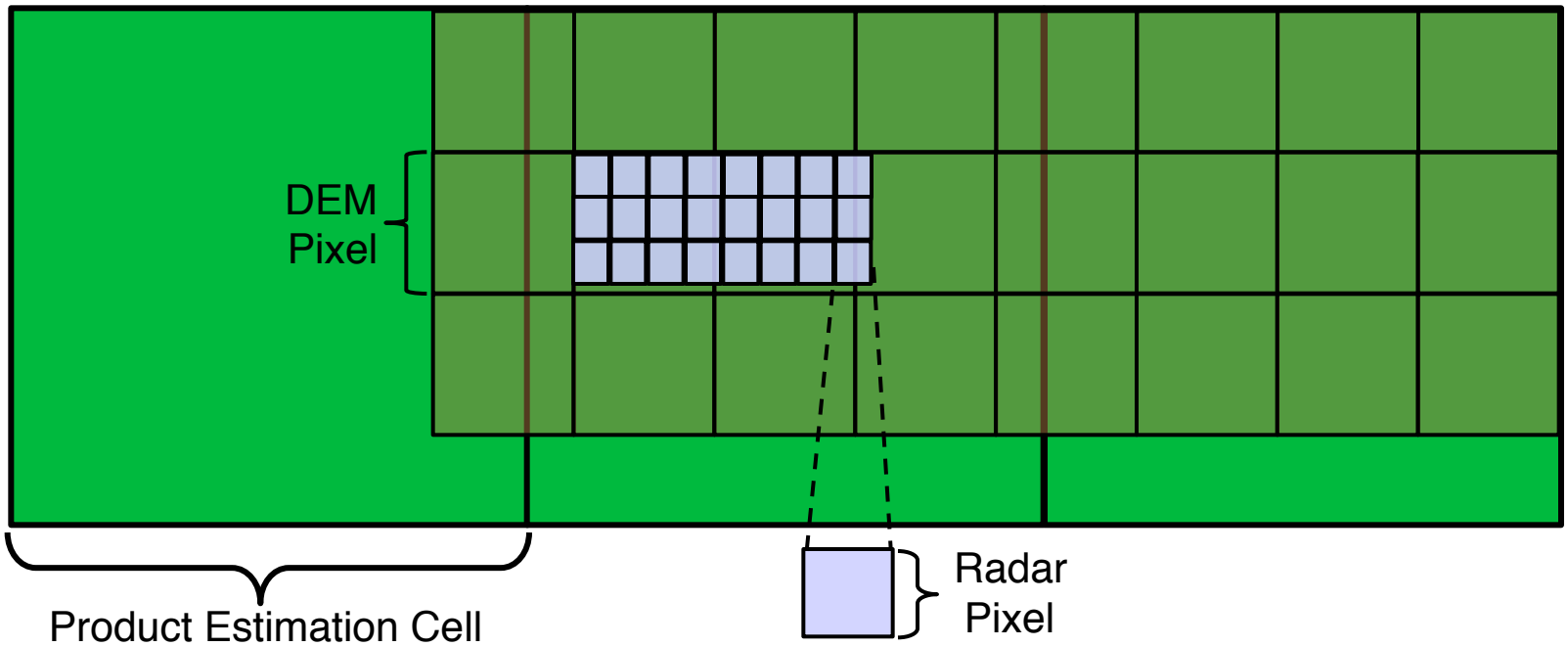

Outline of Theory Sessions

Morning

I. Radar Imaging Fundamentals

A. Basic Principles of Radar and SAR

B. Properties of Radar Images

Afternoon

II. Geometric Aspects of Interferometry and Interferometric Phase

A. Topographic Mapping

B. Deformation Mapping

C. Phase Unwrapping and Atmosphere

III. Interferometric Correlation

A. SNR and Interferometric Correlation

B. Geometric, Temporal, Volumetric Decorrelation

What is Radar Interferometry?

- Radar interferometry can be broadly defined by use of phase measurements to precisely measure the relative distance to an object when imaged by synthetic aperture radar from two or more observations separated either in time or space.
  - Interferometric phase is simply another means of measuring (relative) distance.

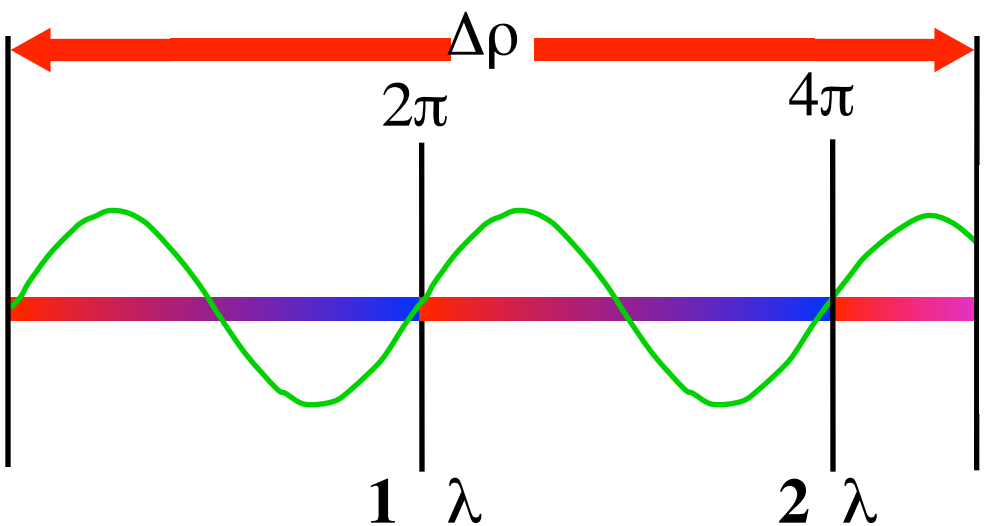

- Phase measurements in interferometric systems can be made with degree level accuracy, and with typical radar wavelengths in 3-80 cm range this corresponds to relative range measurements having millimeter accuracy.

$$\phi = \underbrace{2\pi}_{\text{Radians per wavelength}} \underbrace{\frac{\Delta\rho}{\lambda}}_{\text{Number of wavelengths}}$$

Interference Concept

- Interference occurs when the phase of two different waves is not aligned. The observed intensity, I, is the time average of the sum of the wave fields

$$E(z,t)=E_0 \cos(2\pi(f\,t - z / \lambda))$$

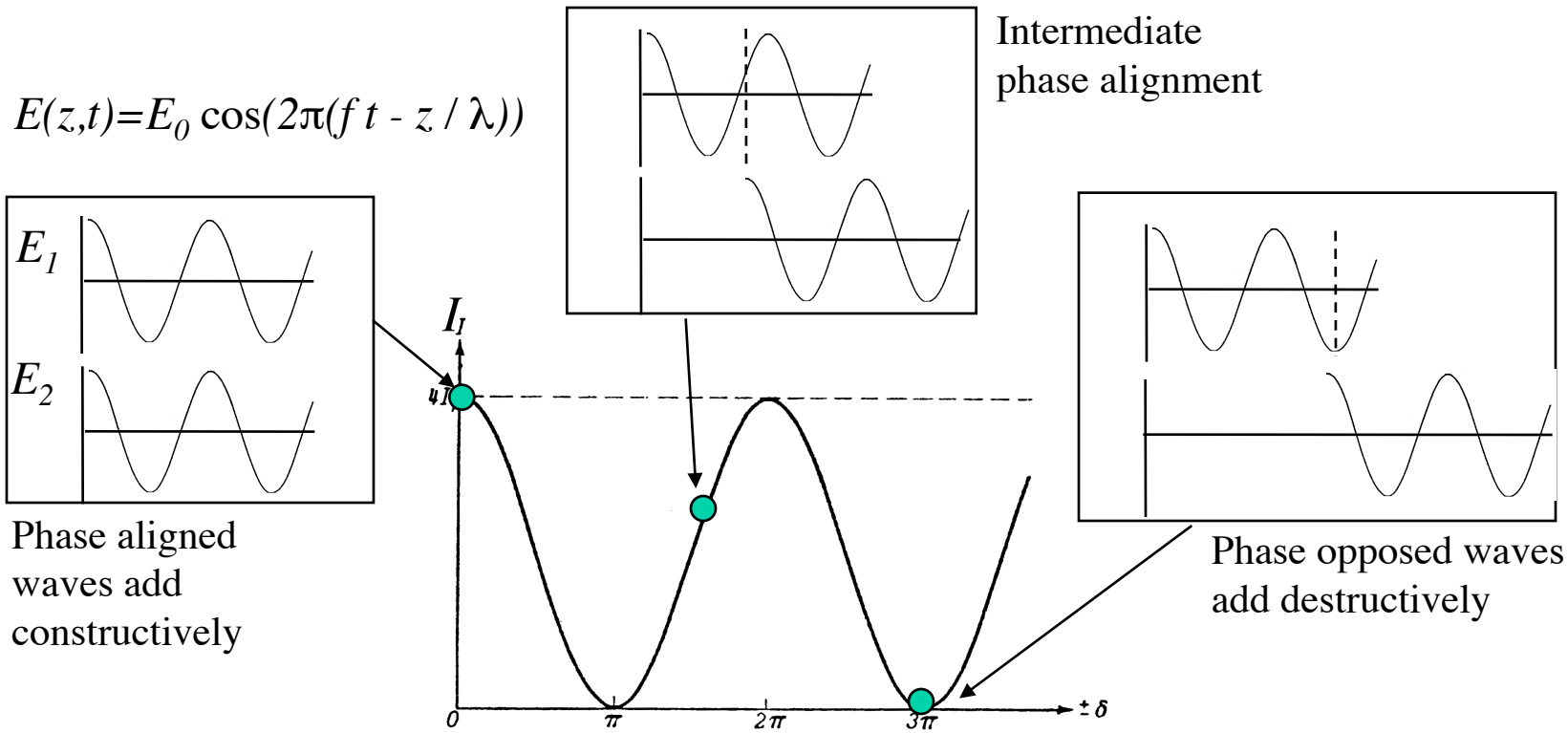

Fig. 7.1. Interference of two beams of equal intensity; variation of intensity with phase difference.

Young's Interferometer

- In Young's experiment, a point source illuminates two separated vertical slits in an opaque screen. The slits are very narrow and act as line sources. For this case, the pattern of intensity variations on the observing screen is bright/dark banding.

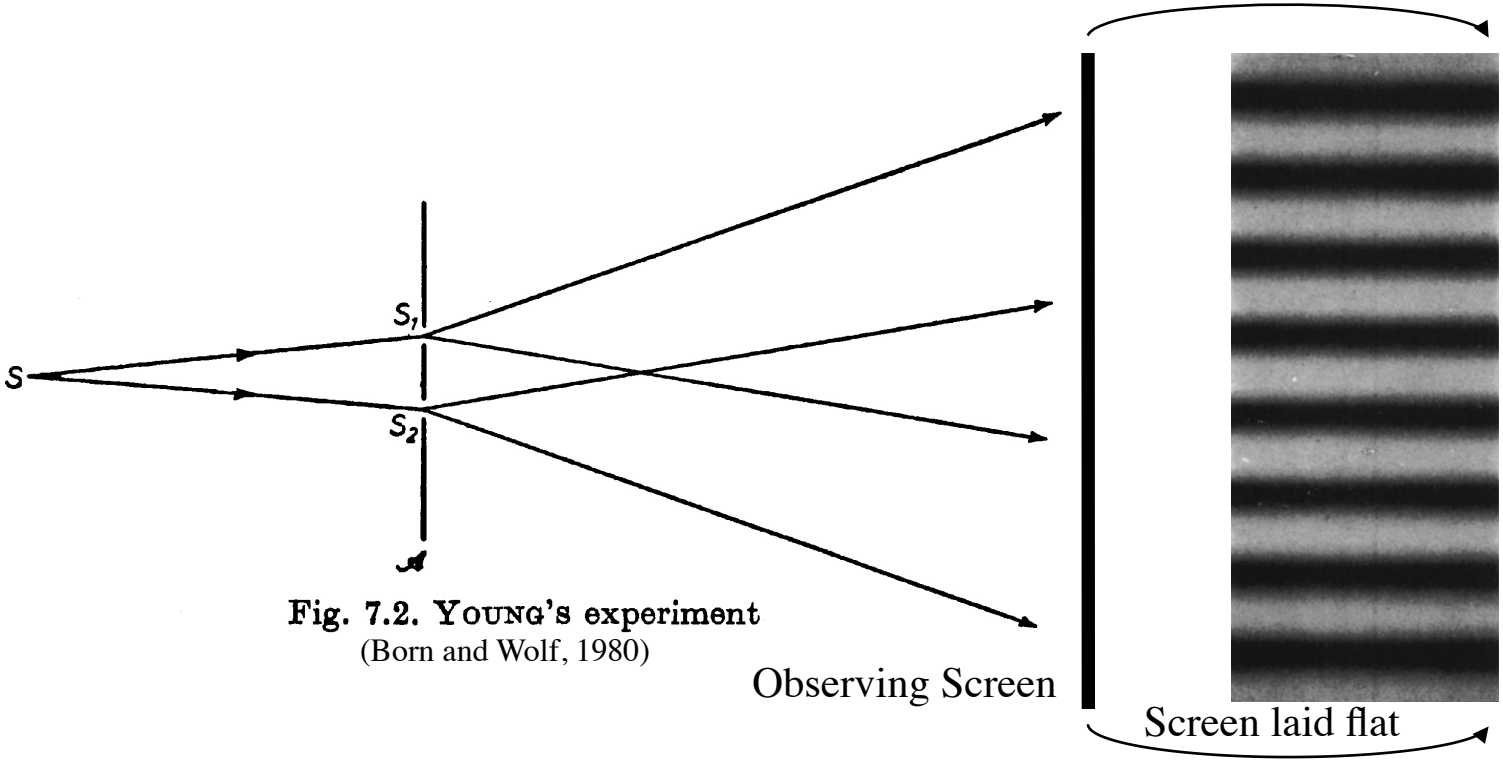

Fig. 7.2. Young's experiment
(Born and Wolf, 1980)

Wave Interference

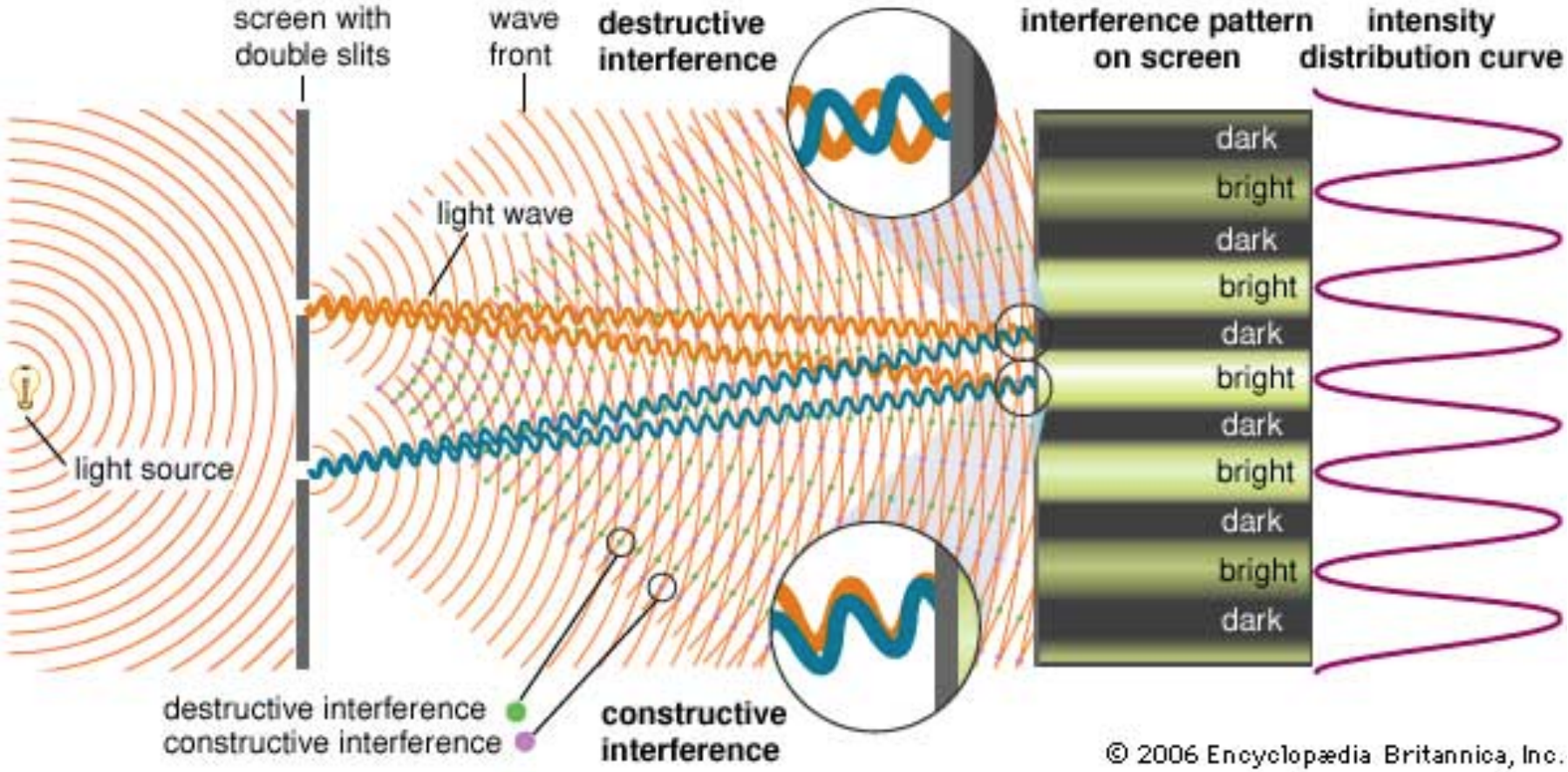

Young's Interferometer with a phase detector

- If the relative phase of the signals could be observed on the screen, it could be represented

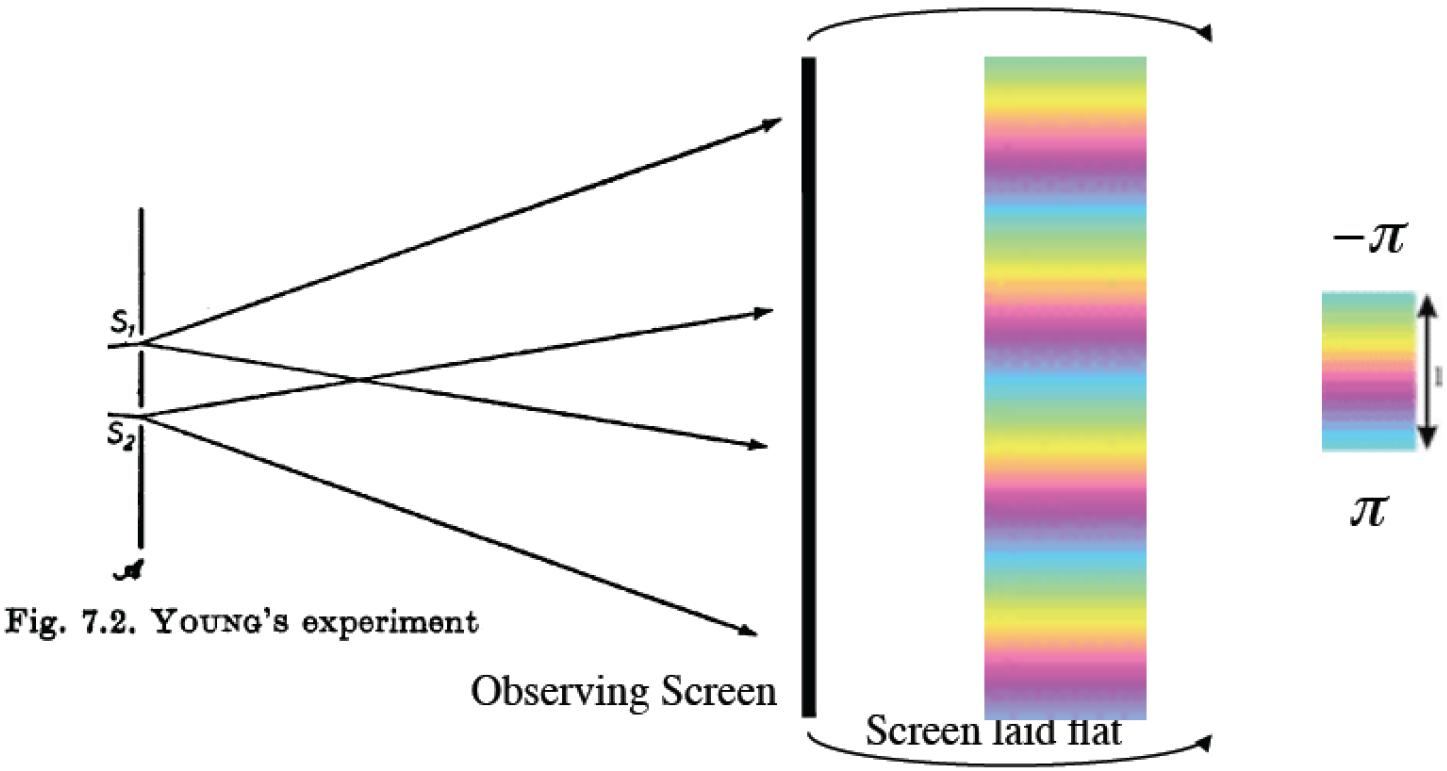

Fig. 7.2. YOUNG's experiment

Radar Interferometry

- Radar Interferometry is a simple extension of the Young's interferometry concept
- Radar has a coherent source much like a laser
- The two radar (SAR) antennas act as coherent point sources

- SAR images are acquired independently, and act as amplitude and phase detector of the surface

- Two SAR images can be combined to observe the interference pattern of the surface.

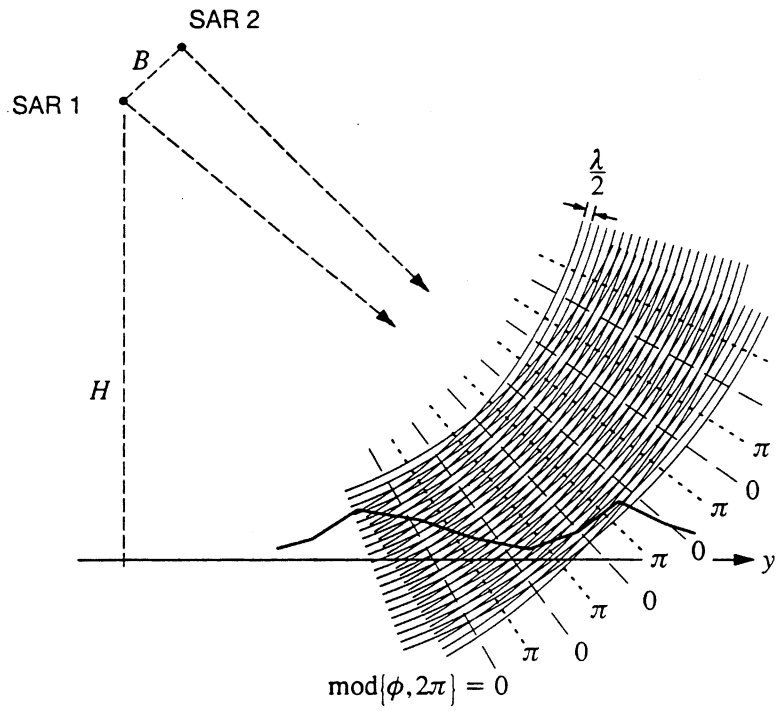

Radar Interferometry Example

Standard Radar Image

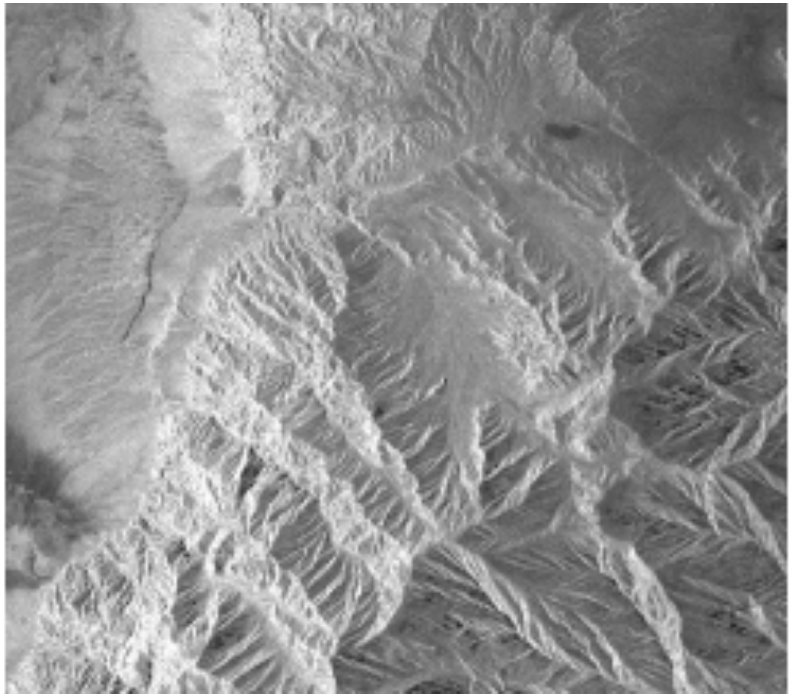

"Interferogram"

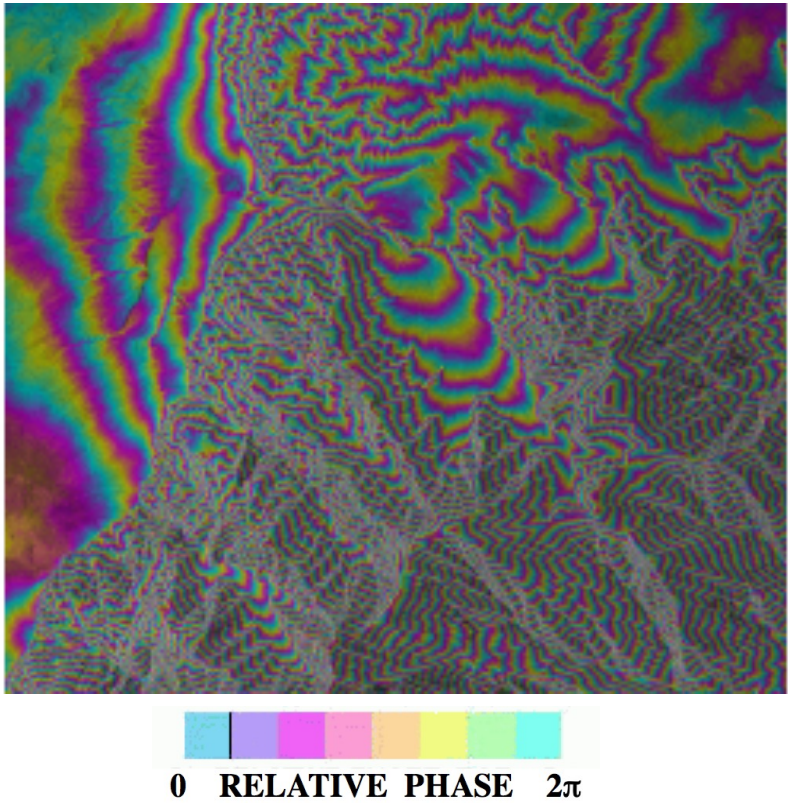

An "interferogram" is a complex image:

- Its magnitude is related to correlation
- Its phase is related to geometry differences

- One cycle of color represents one cycle of relative phase
- Once cycle of relative phase represents $1/p$ wavelengths of path difference, p=1 or 2

Types of Radar Interferometry

- Two main classes of interferometric radars are separated based on the geometric configuration of the baseline vector, i.e. the vector separating the antenna locations in the interferometric pair. These are:
  - Interferometers are used for topographic measurements when the antennas are separated in the cross-track direction.
  - Interferometers are used to measure line-of-sight motion when the antennas are separated in the along-track direction.
  - A single antenna repeating its path can form an interferometer to measure long-term deformation

Cross-Track Interferometer

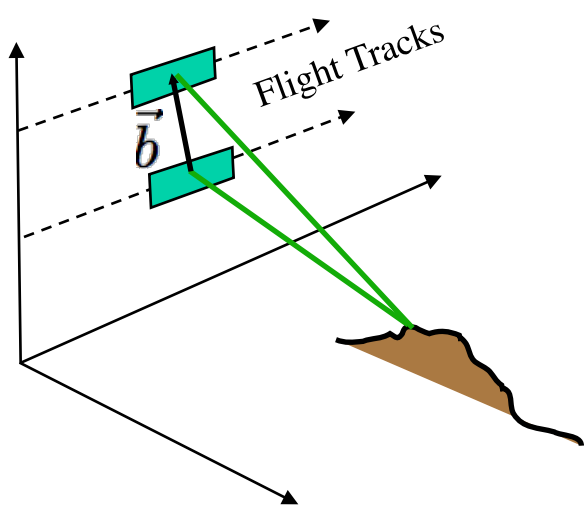

- Dual antenna single pass interferometers
- Single antenna repeat pass interferometers

  ==> Topography and Deformation

Along-Track Interferometer

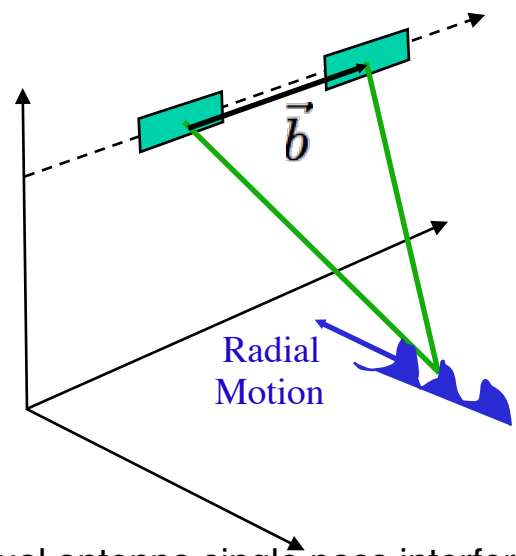

- Dual antenna single pass interferometer
- Along-track separation

  ==> Radial velocity

Interferometry Applications

- Mapping/Cartography
  - Radar Interferometry from airborne platforms is routinely used to produce topographic maps as digital elevation models (DEMs).
  - Shuttle Radar Topography Mission produced near-global 30 m DEM in 2000
  - Tandem-X soon to produce global 12 m DEM
  - Radar imagery is automatically geocoded, easily combined with other (multispectral) data sets.
  - Applications of topography enabled by interferometric rapid mapping
    - Land use management, classification, hazard assessment, intelligence, urban planning, short and long time scale geology, hydrology
- Deformation Mapping and Change Detection
  - Repeat Pass Radar Interferometry from spaceborne platforms is routinely used to produce topographic *change* maps as digital displacement models (DDMs).
    - Sub-centimeter relative displacement accuracy
    - 10-100 m post spacing and resolution
    - 100 km by 100 km DDMs produced rapidly once data is available
  - Applications include
    - Earthquake and volcano monitoring and modeling, landslides and subsidence
    - Glacier and ice sheet dynamics
    - Deforestation, change detection, disaster monitoring

Interferometry for Topography

Measured phase difference:

$$\Delta\phi = -\frac{2\pi}{\lambda}\delta\rho$$

Triangulation:

$$\sin(\theta - \alpha) = \frac{(\rho + \delta\rho)^2 - \rho^2 - B^2}{2\rho B}$$

$$z = h - \rho\cos\theta$$

Critical Interferometer Knowledge:
- Baseline, (B,α), to mm's
- System phase differences, to deg's

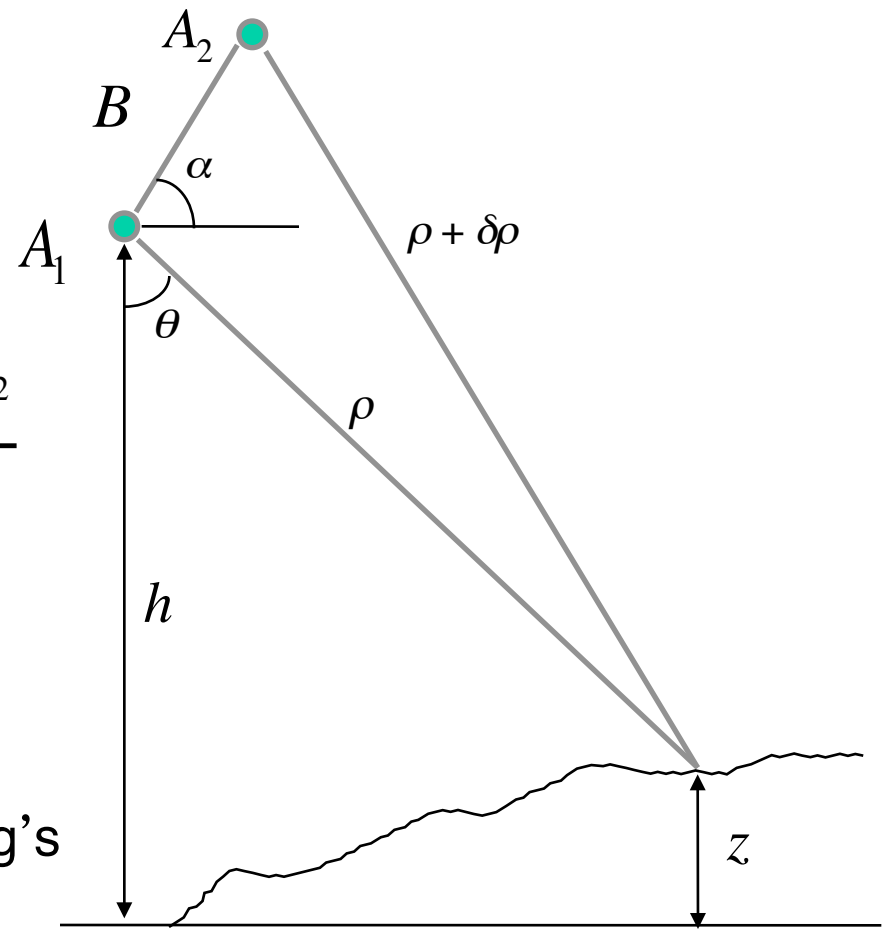

Data Collection Options

For single pass interferometry (SPI) both antennas are located on the same platform. Two modes of data collection are common:

- *single-antenna-transmit mode* - one antenna transmits and both receive
- *ping-pong mode* - each antenna transmits and receives its own echoes effectively doubling the physical baseline.

Classic

$$\Delta\phi = \frac{2\pi}{\lambda}(\rho_2 + \rho_1) - \frac{2\pi}{\lambda}(\rho_1 + \rho_1)$$

$$= \frac{2\pi}{\lambda}(\rho_2 - \rho_1)$$

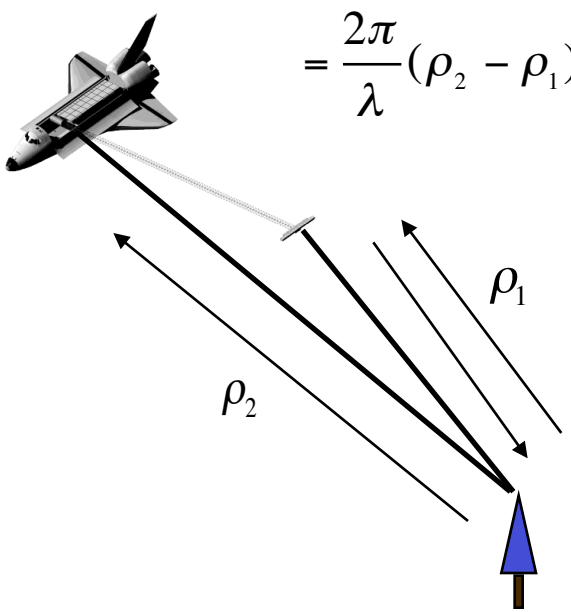

$$\Delta\phi = \frac{2\pi p}{\lambda}\delta\rho,$$

$$p = 1$$

Ping-Pong

$$\Delta\phi = \frac{2\pi}{\lambda}(\rho_2 + \rho_2) - \frac{2\pi}{\lambda}(\rho_1 + \rho_1)$$

$$= \frac{4\pi}{\lambda}(\rho_2 - \rho_1)$$

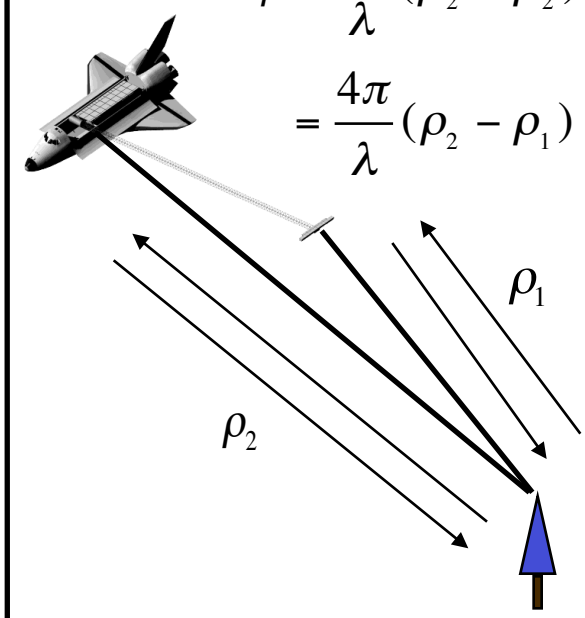

$$\Delta\phi = \frac{2\pi p}{\lambda}\delta\rho,$$

$$p = 2$$

Height Reconstruction

- Interferometric height reconstruction is the determination of a target's position vector from known platform ephemeris information, baseline information, and the interferometric phase.

$\vec{P} =$ platform position vector

$\rho =$ range to target

$\hat{\ell} =$ unit vector pointing from platform to target

$\vec{T} =$ target location vector

BASIC EQUATION

$$\vec{T} = \vec{P} + \rho \hat{\ell}$$

- Interferometry provides a means of determining $\hat{\ell}$

Interferometric Geometry

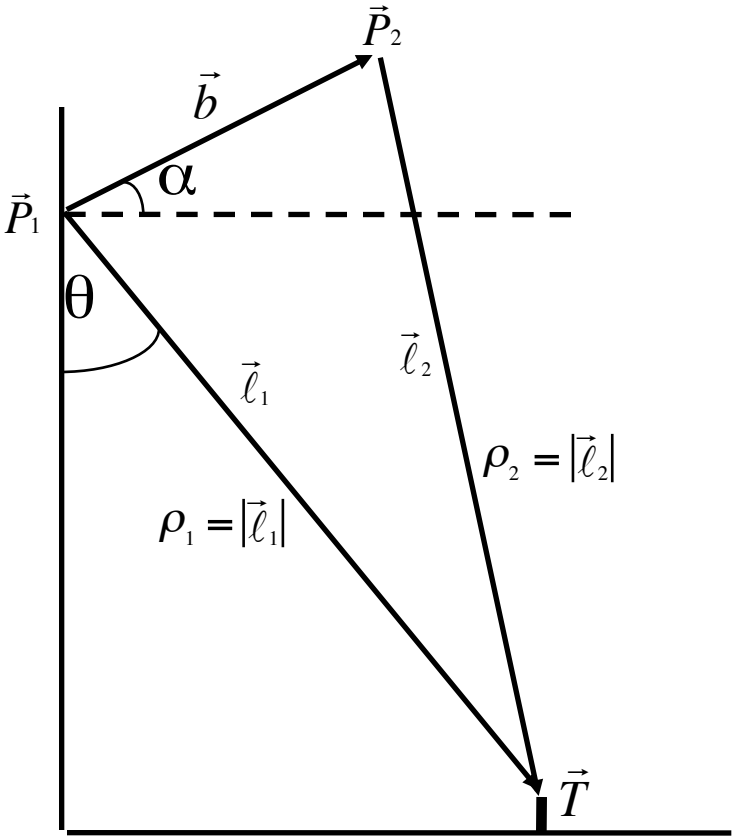

$$\vec{b} = \vec{P}_2 - \vec{P}_1 = \vec{\ell}_1 - \vec{\ell}_2$$

$$\vec{\ell}_2 = \vec{\ell}_1 - \vec{b}$$

$$b = |\vec{b}| = \langle \vec{b}, \vec{b} \rangle^{\frac{1}{2}} \ , \quad \hat{\ell}_1 = \frac{\vec{\ell}_1}{|\vec{\ell}_1|} = \frac{\vec{\ell}_1}{\rho_1}$$

$$\Delta\phi = \frac{2\pi p}{\lambda}(\rho_2 - \rho_1) = \frac{2\pi p}{\lambda}\left(|\vec{\ell}_2| - |\vec{\ell}_1|\right)$$

$$= \frac{2\pi p}{\lambda}\left(\langle \vec{\ell}_2, \vec{\ell}_2 \rangle^{\frac{1}{2}} - \rho_1\right)$$

$$= \frac{2\pi p}{\lambda}\left(\langle \vec{\ell}_1 - \vec{b}, \vec{\ell}_1 - \vec{b} \rangle^{\frac{1}{2}} - \rho_1\right)$$

$$= \frac{2\pi p}{\lambda}\left(\left(\rho^2{}_1 - 2\langle \vec{\ell}_1, \vec{b} \rangle + b^2\right)^{\frac{1}{2}} - \rho_1\right)$$

$$= \frac{2\pi p}{\lambda}\rho_1\left(\left(1 - \frac{2\langle \hat{\ell}_1, \vec{b} \rangle}{\rho_1} + \left(\frac{b}{\rho_1}\right)^2\right)^{\frac{1}{2}} - 1\right)$$

- p equals 1 or 2 depending on system

2-D Height Reconstruction - Flat Earth

Assume that b << ρ and let $\hat{\ell}_1 = \frac{\vec{\ell}_1}{|\vec{\ell}_1|} = \frac{\vec{\ell}_1}{\rho}$. Taking a first order Taylor's expansion of

$$\Delta\phi = \frac{2\pi p}{\lambda}\rho_1\left(\left(1 - \frac{2\langle\hat{\ell}_1, \vec{b}\rangle}{\rho_1} + \left(\frac{b}{\rho_1}\right)^2\right)^{\frac{1}{2}} - 1\right)$$

the interferometric phase can be approximated as

$$\Delta\phi \approx -\frac{2\pi p}{\lambda}\langle\hat{\ell}_1, \vec{b}\rangle$$

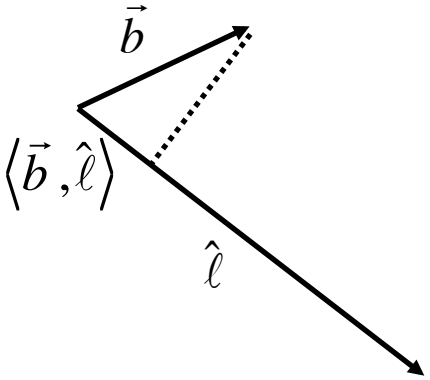

With $\vec{b} = (b\cos(\alpha), b\sin(\alpha))$ and $\hat{\ell} = (\sin(\theta), -\cos(\theta))$ then

$$\Delta\phi = -\frac{2\pi p}{\lambda} b\sin(\theta - \alpha)$$

2-D Height Reconstruction - Flat Earth II

- Let $\vec{P}$ = (y_o , h) be the platform position vector, then

$$\vec{T} = \vec{P} + \rho\,\hat{\ell}$$
$$= (y_o, h) + \rho\,(\sin(\theta), -\cos(\theta))$$
$$= (y_o + \rho\,\sin(\theta), h - \rho\,\cos(\theta))$$

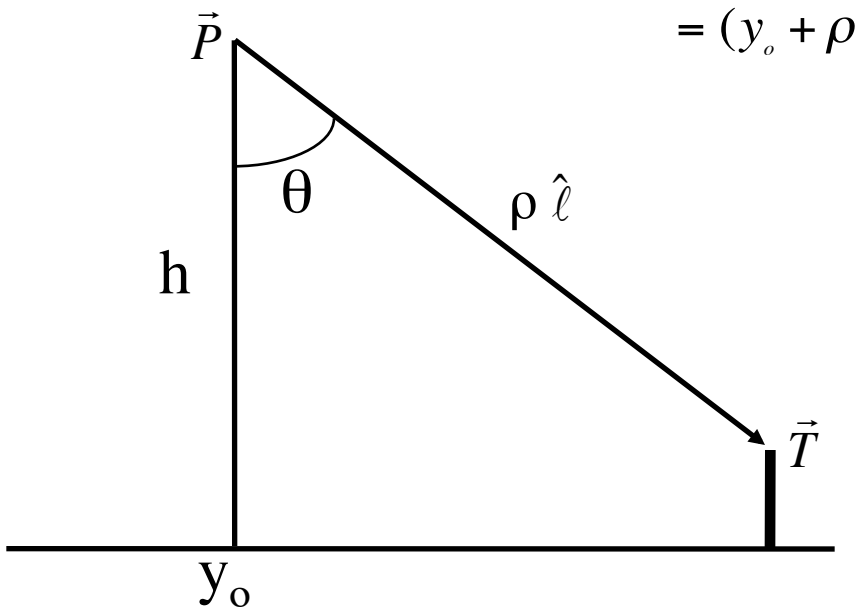

- Solving for θ in terms of the interferometric phase, $\Delta\phi$, yields

$$\theta = \sin^{-1}\left(\frac{-\lambda\Delta\phi}{2\pi p b}\right) + \alpha$$

Phase Gradient

- For a number of applications including flight planning and unwrapping studies it is desirable to be able to compute the interferometric phase gradient for an arbitrarily sloped surface, look geometry and baseline.
- The interferometric phase is well approximated for most applications by

$$\phi \approx -\frac{2\pi p}{\lambda}\left\langle \vec{b}, \hat{l} \right\rangle \qquad (\phi \Leftrightarrow \Delta\phi)$$

where $\vec{b}$ is the baseline vector, $\hat{l}$ a unit vector pointing to the target and λ is the wavelength.

- The phase gradient is

$$\nabla\phi = \begin{bmatrix} \dfrac{\partial\phi}{\partial s} \\ \dfrac{\partial\phi}{\partial\rho} \end{bmatrix} = -\frac{2\pi p}{\lambda}\begin{bmatrix} \left\langle \vec{b}, \dfrac{\partial\hat{l}}{\partial s} \right\rangle \\ \left\langle \vec{b}, \dfrac{\partial\hat{l}}{\partial\rho} \right\rangle \end{bmatrix}$$

where s is the along track coordinate and ρ is the range.

Phase Gradient Observations

- There in a change in phase with respect to range regardless of whether the terrain is sloped in the range direction or not. The phase rate, or fringe rate, with respect to a flat surface is called the flat surface (or spherical earth) fringe frequency.

$$\frac{\partial \phi}{\partial \rho} = \frac{2\pi p}{\lambda} \frac{b\cos(\theta - \alpha)}{\rho \tan(\theta - \psi_c)} = \frac{2\pi p}{\lambda} \frac{b_\perp}{\rho \tan(\theta - \psi_c)}$$

$(\phi \Leftrightarrow \Delta\phi)$

- Note that the fringe rate depends on the local slope and the perpendicular baseline length.
- The fringe rate in the azimuth or along track direction is zero unless there is an azimuth slope. It also depends on the magnitude of the local slope and the perpendicular baseline length

$$\frac{\partial \phi}{\partial s} = \frac{2\pi p}{\lambda} \frac{b\cos(\theta - \alpha)}{\rho} \sin\theta \tan\psi_s = \frac{2\pi p}{\lambda} \frac{b_\perp}{\rho} \sin\theta \tan\psi_s$$

Flattened Phase

- In creating an image, ISCE performs a "motion compensation" step, recalculating positions and phases as though from a reference orbit. This step removes the flat earth fringes the resulting fringes will follow the local topography, the so-called "flattened" phase.
- The flattened phase is given by

$$\Delta\phi_{flat} = -\frac{4\pi}{\lambda}\left(\langle\hat{\ell},\vec{b}\rangle - \langle\hat{\ell}_o,\vec{b}\rangle\right)$$

where $\hat{\ell}$ is the look vector to a point and $\hat{\ell}_o$ is the corresponding look vector to the flat surface at the same range.

- Making the usual 2 dimensional simplifications

$$\begin{aligned}\Delta\phi_{flat} &= \frac{4\pi}{\lambda}b(\sin(\theta-\alpha)-\sin(\theta_o-\alpha)) \\ &\approx \frac{4\pi}{\lambda}b\cos(\theta-\alpha)\delta\theta\end{aligned}$$

Flattened Phase II

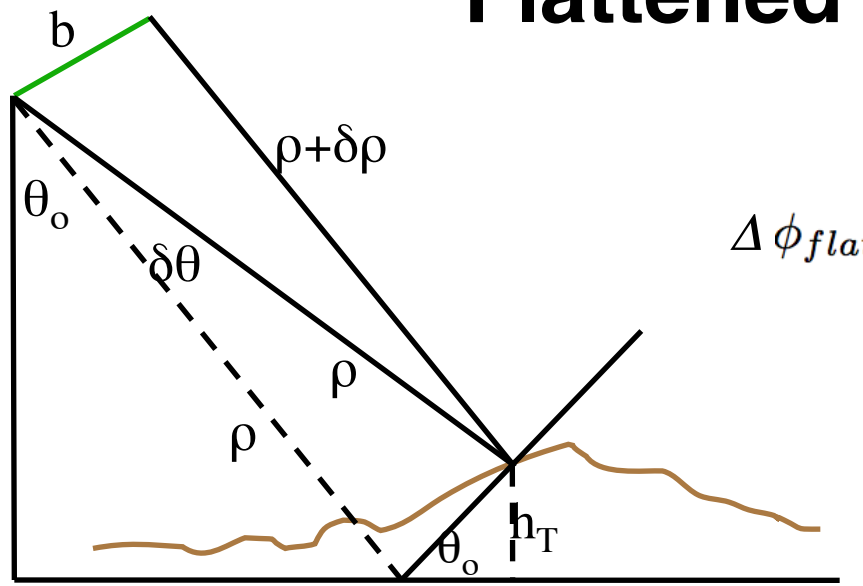

$$\Delta\phi_{flat} = \frac{4\pi}{\lambda} b(\sin(\theta-\alpha) - \sin(\theta_o - \alpha))$$
$$\approx \frac{4\pi}{\lambda} b\cos(\theta-\alpha)\delta\theta$$

From the figure we have

$$\delta\theta \approx \frac{h_T}{\rho \sin\theta_o}$$

which gives

$$\Delta\phi_{flat} = \frac{4\pi}{\lambda} b_\perp \delta\theta$$
$$= \frac{4\pi}{\lambda} b_\perp \frac{h_T}{\rho\sin\theta_o}$$

Thus the topographic portion of the interferometric phase is a function of the perpendicular baseline length.

Sensitivity of Height with Respect to Phase

Sensitivity to Phase

$$\frac{\partial \vec{T}}{\partial \phi} = \frac{-\lambda\rho}{2\pi p b \cos(\theta - \alpha)} \begin{bmatrix} 0 \\ \cos\theta \\ \sin\theta \end{bmatrix}$$

Ambiguity Height

$$h_a = 2\pi \frac{\partial T_z}{\partial \phi} = \frac{-\lambda\rho \sin(\theta)}{p b \cos(\theta - \alpha)}$$

$p=1,2$

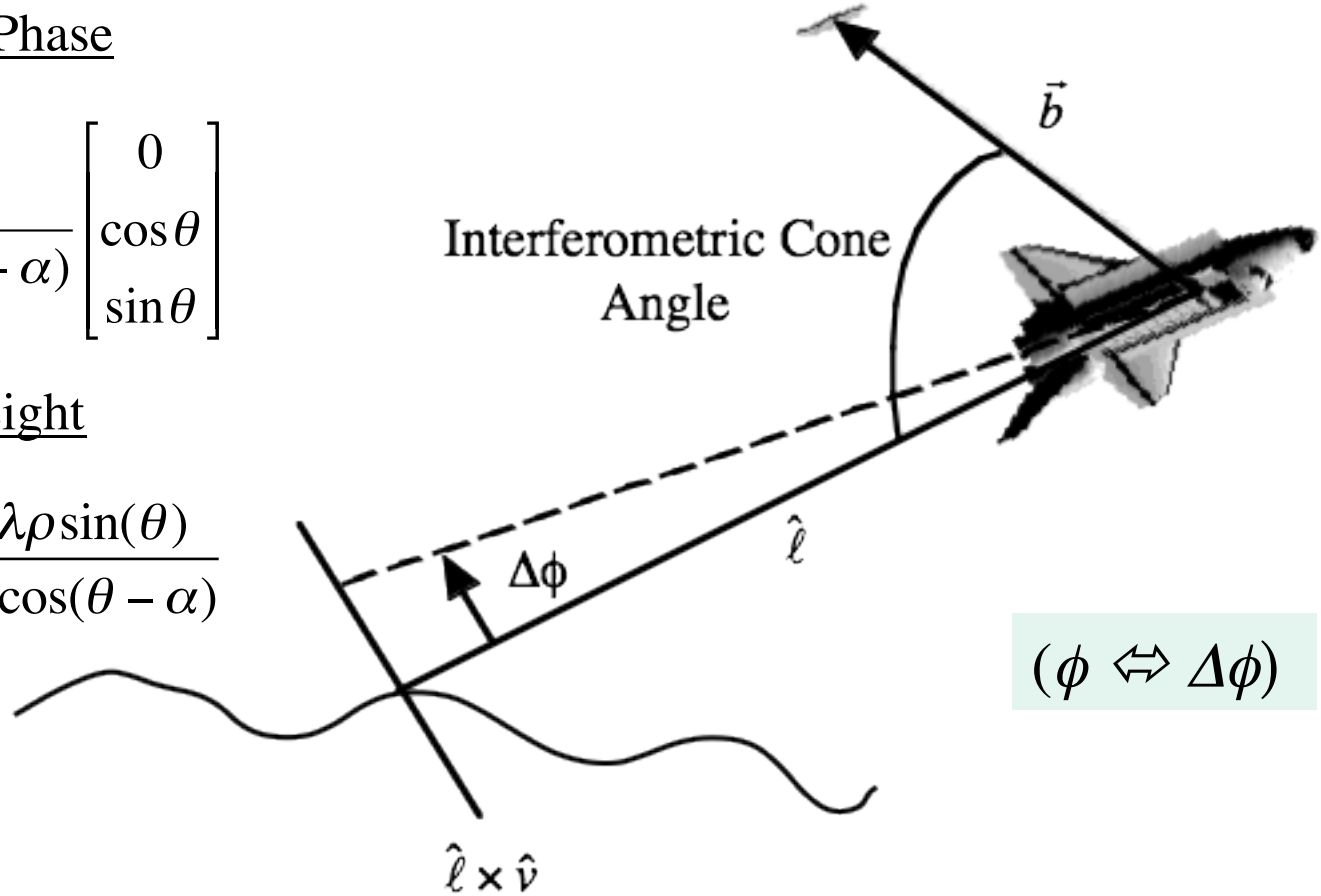

$(\phi \Leftrightarrow \Delta\phi)$

- Observe that $\frac{\partial \vec{T}}{\partial \phi}$ is parallel to $\hat{\ell} \times \hat{v}$.

Data Collection Options II

Interferometric data can also be collected in the repeat pass mode (RPI). In this mode two spatially close radar observations of the same scene are made separated in time. The time interval may range from seconds to years. The two observations may be made different sensors provided they have nearly identical radar system parameters.

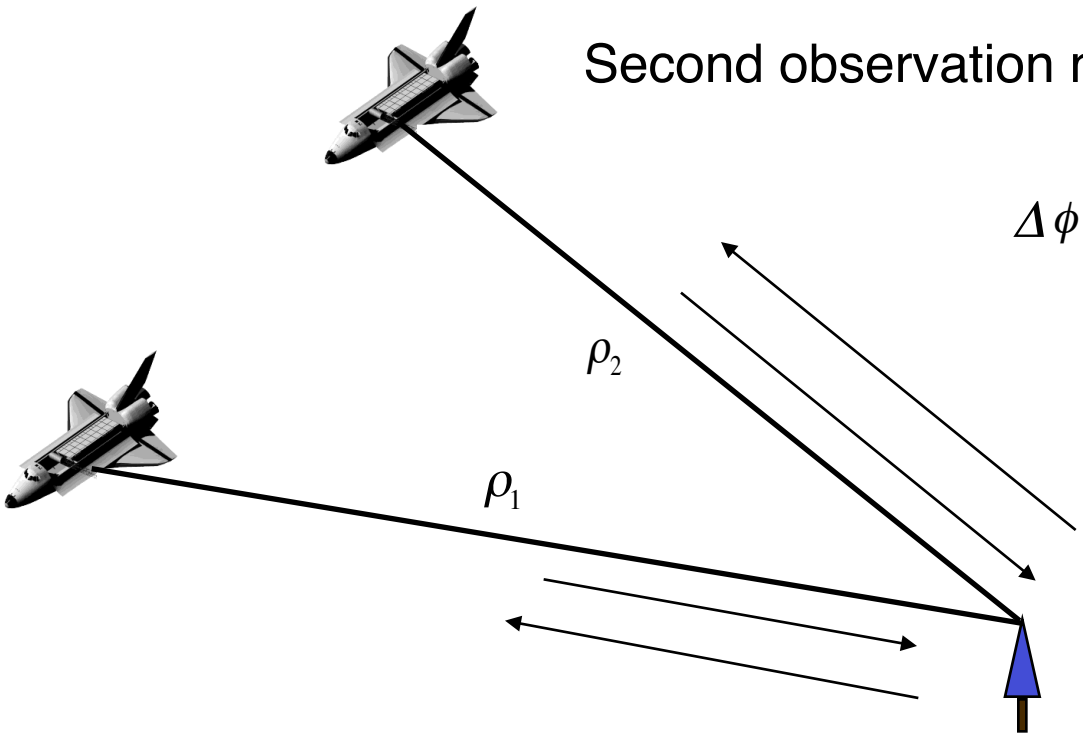

Second observation made at some later time.

$$\Delta\phi = \frac{2\pi}{\lambda}(\rho_2 + \rho_2) - \frac{2\pi}{\lambda}(\rho_1 + \rho_1)$$

$$= \frac{4\pi}{\lambda}(\rho_2 - \rho_1)$$

$$\Delta\phi = \frac{2\pi p}{\lambda}\delta\rho,$$

$$p = 2$$

Differential Interferometry

When two observations are made from the same location in space but at different times, the interferometric phase is proportional to any change in the range of a surface feature directly.

$$\Delta\phi = \frac{4\pi}{\lambda}(\rho(t_1) - \rho(t_2)) = \frac{4\pi}{\lambda}\Delta\rho_{\text{change}}$$

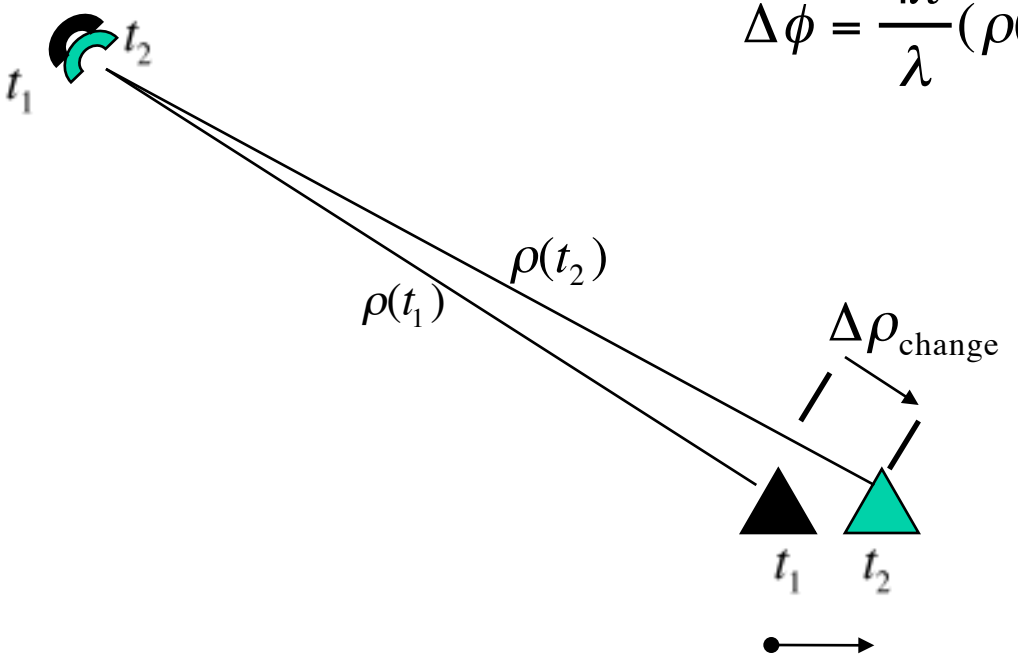

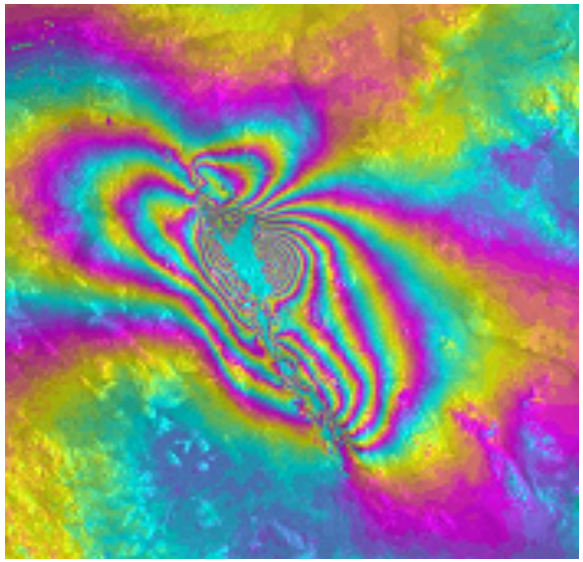

Differential Interferometric Phase

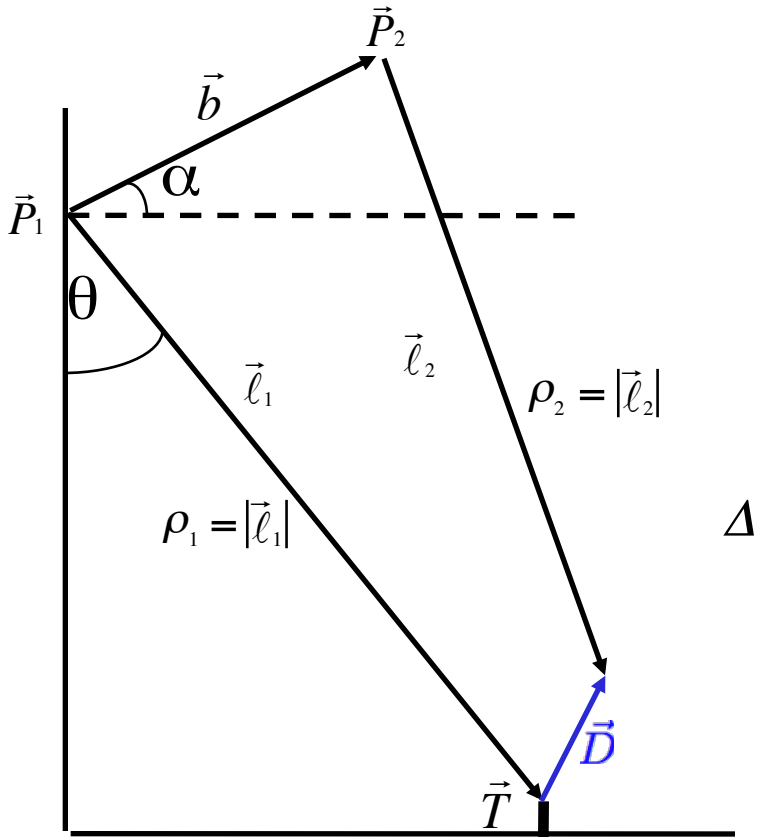

$$\vec{b} = \vec{P}_2 - \vec{P}_1 = \vec{\ell}_1 - \vec{\ell}_2$$

$$\vec{\ell}_2 = \vec{T} + \vec{D} - \vec{P}_2 = \vec{\ell}_1 + \vec{D} - \vec{b}$$

$$b = |\vec{b}| = \langle \vec{b}, \vec{b} \rangle^{\frac{1}{2}} \quad , \quad \hat{\ell}_1 = \frac{\vec{\ell}_1}{|\vec{\ell}_1|} = \frac{\vec{\ell}_1}{\rho_1}$$

$$\Delta\phi = \frac{2\pi p}{\lambda}(\rho_2 - \rho_1) = \frac{2\pi p}{\lambda}\left(|\vec{\ell}_2| - |\vec{\ell}_1|\right)$$

$$= \frac{2\pi p}{\lambda}\left(\langle \vec{\ell}_2, \vec{\ell}_2 \rangle^{\frac{1}{2}} - \rho_1\right)$$

$$\Delta\phi = \frac{4\pi}{\lambda}\left(\langle \vec{\ell}_1 + \vec{D} - \vec{b}, \vec{\ell}_1 + \vec{D} - \vec{b} \rangle^{\frac{1}{2}} - \rho_1\right)$$

Assuming that

$$\begin{aligned} |\vec{b}| &\leq \rho \\ |\vec{D}| &\leq \rho \\ |\langle \vec{b}, \vec{D} \rangle| &\leq \rho \end{aligned}$$

yields

$$\Delta\phi = \frac{4\pi}{\lambda}\left(-\langle \hat{\ell}, \vec{b} \rangle + \langle \hat{\ell}, \vec{D} \rangle\right)$$

Differential Interferometry and Topography

- Generally two observations are made from different locations in space and at different times, so the interferometric phase is proportional to topography and topographic change.

$$\Delta\phi = \frac{4\pi}{\lambda}\left(-\langle\hat{\ell},\vec{b}\rangle + \langle\hat{\ell},\vec{D}\rangle\right)$$

Topography Term **Change Term**

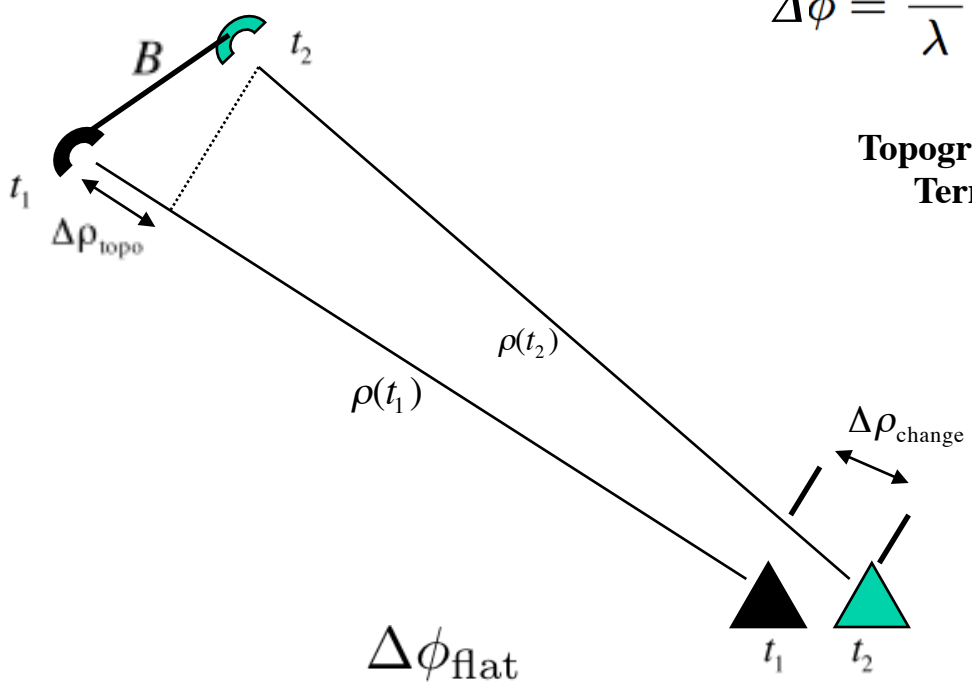

$$\Delta\phi = \frac{4\pi}{\lambda}(\Delta\rho_{change} - \Delta\rho_{topo})$$

$$\Delta\phi = \frac{4\pi}{\lambda}(\Delta\rho_{change} - b\sin(\theta-\alpha))$$

$$\Delta\phi_{flat} = \frac{4\pi}{\lambda}\left(\Delta\rho_{change} - \frac{b_\perp h_T}{\rho\sin\theta}\right)$$

Note: Sensitivity of phase with respect to change is much greater than with respect to topographic relief

If topography is known, then second term can be eliminated to reveal surface change

Extracting the Deformation Term - Pre-Existing DEM

$$\Delta\phi_{b_1} = \frac{4\pi}{\lambda}\left(-\langle\hat{\ell},\vec{b}_1\rangle + \langle\hat{\ell},\vec{D}\rangle\right)$$

Phase Simulated from DEM

$$\phi_{topo} = -\frac{4\pi}{\lambda}\langle\hat{\ell},\vec{b}_1\rangle$$

<u>Using Unflattened Phases</u>

$$\begin{aligned}\Delta\rho_{disp} &= \langle\hat{\ell},\vec{D}\rangle \\ &= \frac{\lambda}{4\pi}\left(\Delta\phi_{b_1} - \phi_{topo}\right)\end{aligned}$$

<u>Using Flattened Phases</u>

$$\begin{aligned}\Delta\phi_{flat_1} &= \frac{4\pi}{\lambda}b_{\perp_1}\frac{h_T}{\rho\sin\theta_o} + \frac{4\pi}{\lambda}\Delta\rho_{disp} \\ \Delta\phi_{flat_2} &= \frac{4\pi}{\lambda}b_{\perp_1}\frac{h_T}{\rho\sin\theta_o}\end{aligned}$$

$$\Delta\rho_{disp} = \frac{\lambda}{4\pi}\left(\Delta\phi_{flat_1} - \Delta\phi_{flat_2}\right)$$

Extracting the Deformation - Three Passes

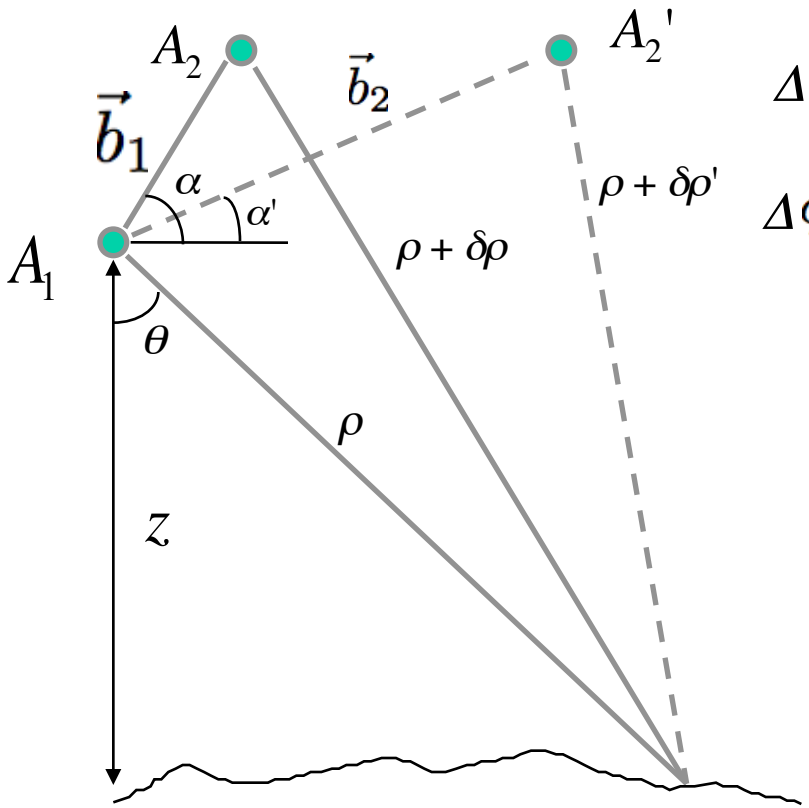

$$\Delta\phi_{b_1} = \frac{4\pi}{\lambda}\left(-\langle\hat{\ell},\vec{b}_1\rangle + \langle\hat{\ell},\vec{D}\rangle\right)$$ Change Pair

$$\Delta\phi_{b_2} = -\frac{4\pi}{\lambda}\langle\hat{\ell},\vec{b}_2\rangle$$ Topo Pair

Using Unflattened Phases

$$\begin{aligned}\Delta\rho_{disp} &= \langle\hat{\ell},\vec{D}\rangle \\ &= \frac{\lambda}{4\pi}\left(\Delta\phi_{b_1} - \frac{\langle\hat{\ell},\vec{b}_1\rangle}{\langle\hat{\ell},\vec{b}_2\rangle}\Delta\phi_{b_2}\right) \\ &= \frac{\lambda}{4\pi}\left(\Delta\phi_{b_1} - \frac{b_{||_1}}{b_{||_2}}\Delta\phi_{b_2}\right)\end{aligned}$$

Using Flattened Phases

$$\begin{aligned}\Delta\phi_{flat_1} &= \frac{4\pi}{\lambda}b_{\perp_1}\frac{h_T}{\rho\sin\theta_o} + \frac{4\pi}{\lambda}\Delta\rho_{disp} \\ \Delta\phi_{flat_2} &= \frac{4\pi}{\lambda}b_{\perp_2}\frac{h_T}{\rho\sin\theta_o}\end{aligned}$$

$$\Delta\rho_{disp} = \frac{\lambda}{4\pi}\left(\Delta\phi_{flat_1} - \frac{b_{\perp_1}}{b_{\perp_2}}\Delta\phi_{flat_2}\right)$$

Differential Interferometry Sensitivities

- The reason differential interferometry can detect millimeter level surface deformation is that the differential phase is much more sensitive to displacements than to topography.

$$\frac{\partial \phi}{\partial h} = \frac{2\pi p b \cos(\theta - \alpha)}{\lambda \rho \sin\theta} = \frac{2\pi p b_{\perp}}{\lambda \rho \sin\theta}$$ Topographic Sensitivity

$(\phi \Leftrightarrow \Delta\phi)$

$$\frac{\partial \phi}{\partial \Delta\rho} = \frac{4\pi}{\lambda}$$ Displacement Sensitivity

$$\sigma_{\phi_{topo}} = \frac{\partial \phi}{\partial h}\sigma_h = \frac{4\pi}{\lambda}\frac{b_{\perp}}{\rho \sin\theta}\sigma_h$$ Topographic Sensitivity Term

$$\sigma_{\phi_{disp}} = \frac{\partial \phi}{\partial \Delta\rho}\sigma_{\Delta\rho} = \frac{4\pi}{\lambda}\sigma_{\Delta\rho}$$ Displacement Sensitivity Term

Since $\frac{b}{\rho} << 1$ ==> $\frac{\sigma_{\phi_{disp}}}{\sigma_{\Delta\rho}} >> \frac{\sigma_{\phi_{topo}}}{\sigma_h}$

Meter Scale Topography Measurement - Millimeter Scale Topographic Change

Some Examples of Deformation

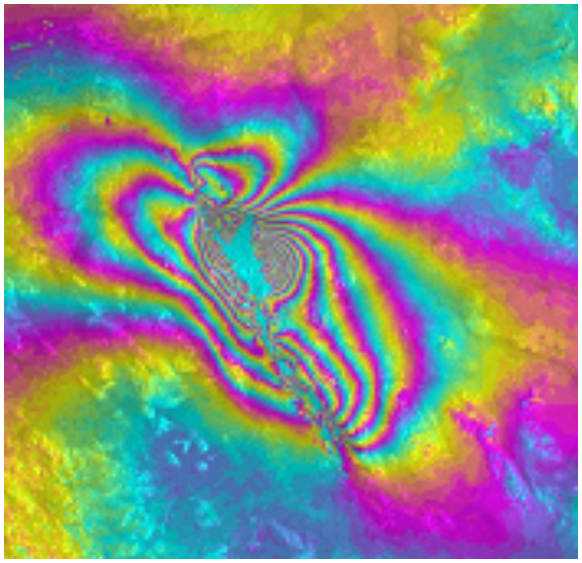

Hector Mine Earthquake

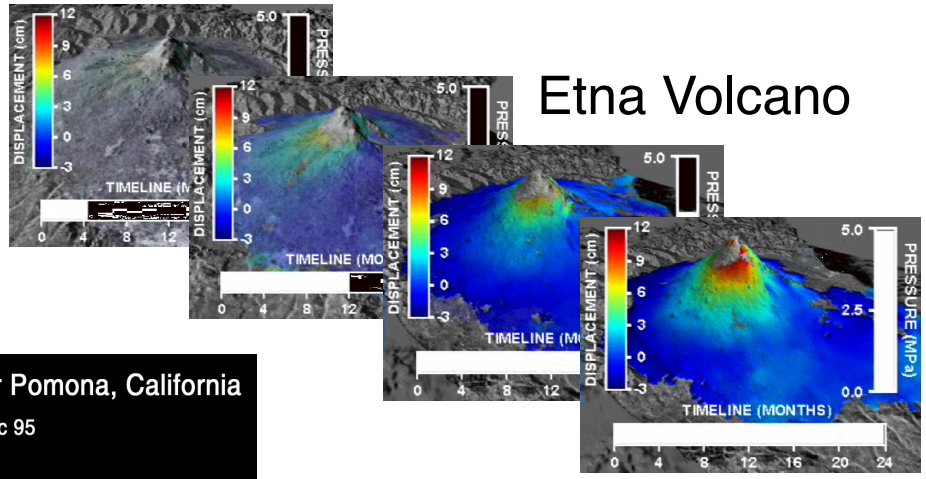

Etna Volcano

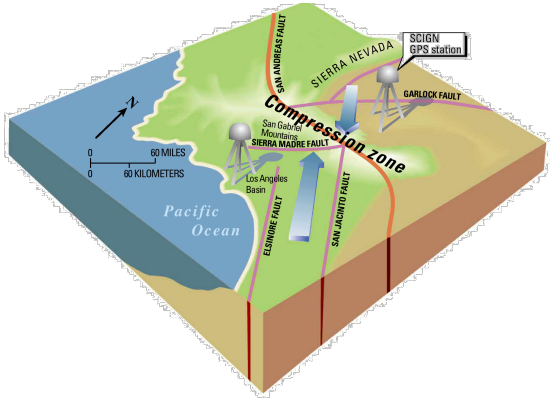

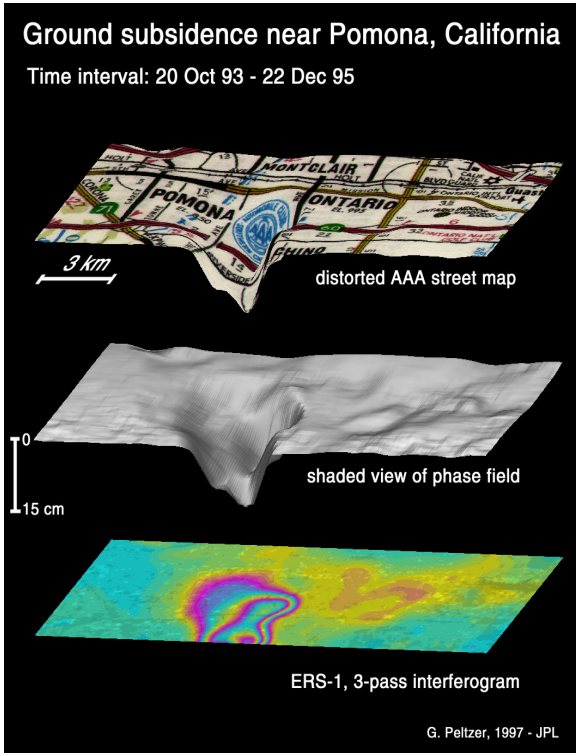

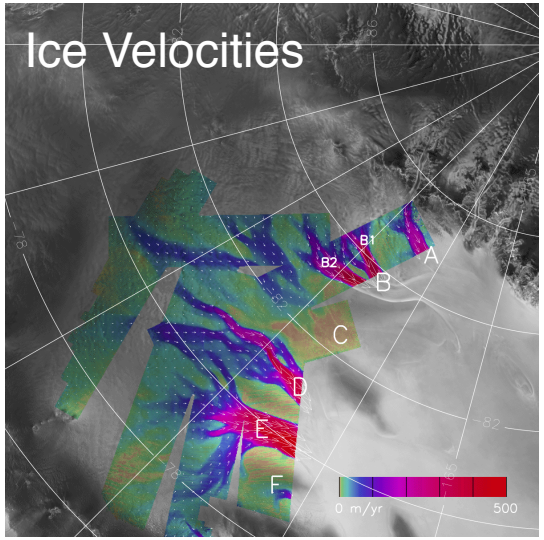

Joughin et al , 1999

Phase Unwrapping

From the measured, wrapped phase, unwrap the phase from some arbitrary starting location, then determine the proper 2π phase "ambiguity".

$$\Delta\phi_{topo} = \frac{2\pi p}{\lambda}\left(\rho_1 - \rho_2\right) = \frac{2\pi p}{\lambda}\vec{b} \bullet \vec{l}$$

$$\Delta\phi_{meas} = \mathrm{mod}\left(\Delta\phi_{topo}, 2\pi\right)$$

$$\Delta\phi_{unwrap}(s,\rho) = \Delta\phi_{topo}(s,\rho) + \Delta\phi_{const}$$

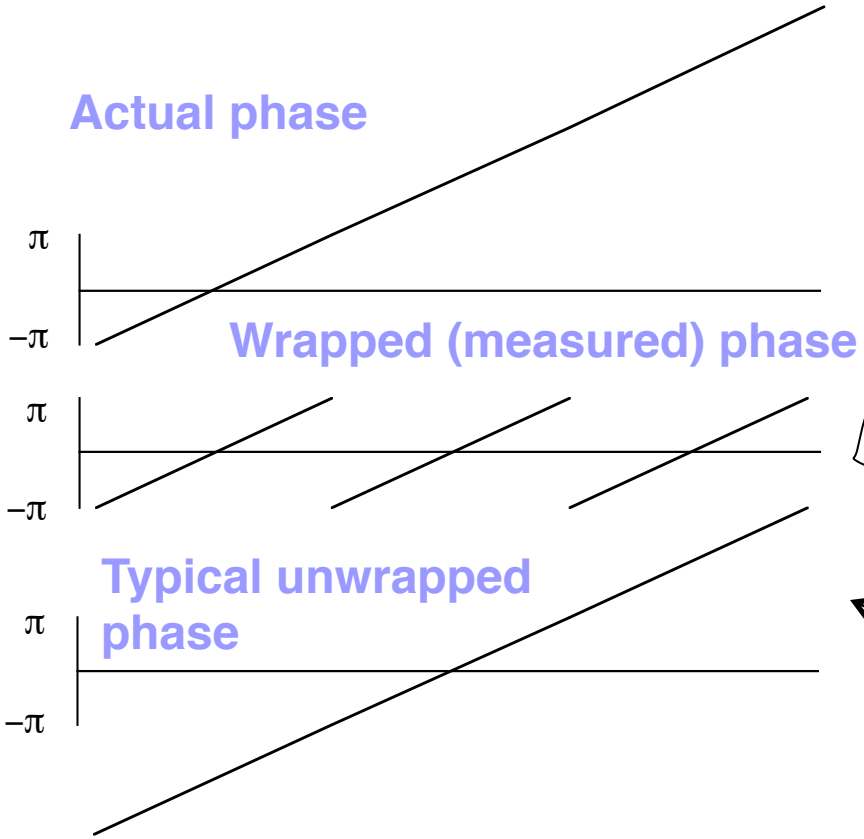

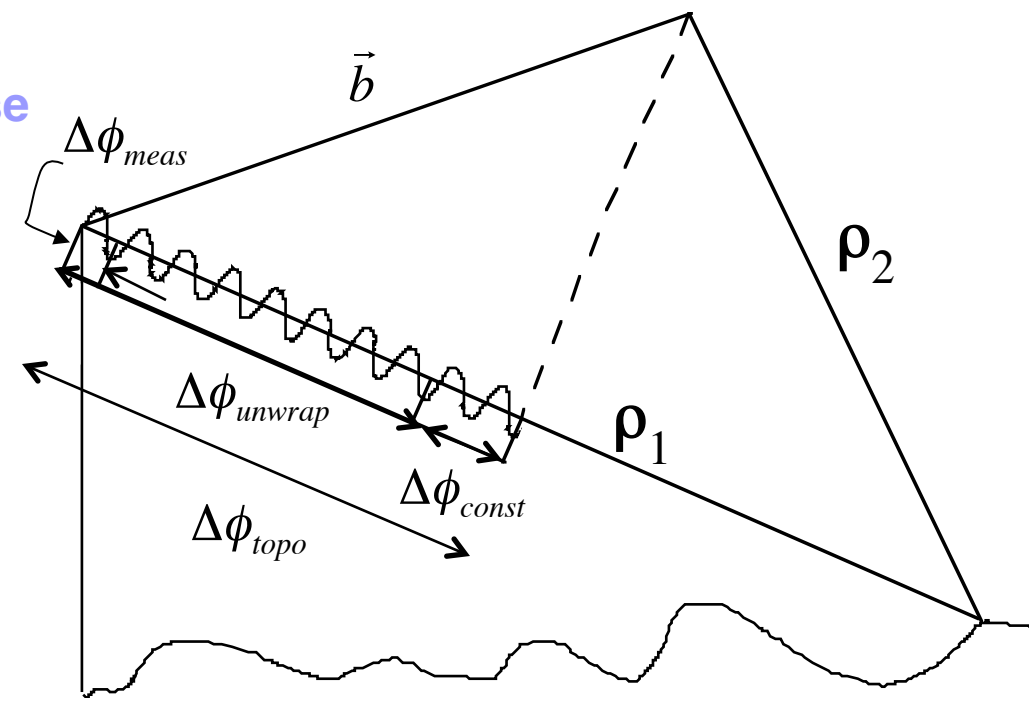

Phase Unwrapping Algorithm Options

- There are a number of approaches to unwrapping:
  - *Residue –or branch cut– methods* that use a simple mechanism to detect where phase consistencies in the phase field exist and generate cuts to avoid them
  - *Least squares methods* that pose the unwrapping problem as an estimation problem and try to efficiently solve the resulting series of equations. (mostly obsolete)
  - *Minimum cost flow algorithms* that pose the unwrapping problem as a network flow problem for which algorithms have been developed over the years

ISCE supports two residue methods and a version of minimum cost flow developed at Stanford (SNAPHU)

Real World Phase Behavior

- Benign topography resulting in a monotonous and well-behaving phase

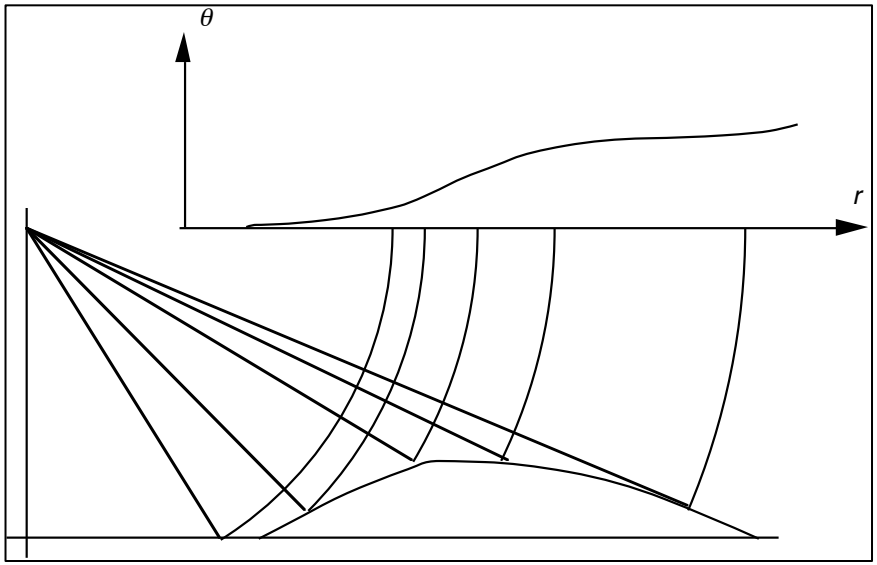

- Rough topography leading to lay-over and shadows and a generically non-monotonous and non-continuous phase

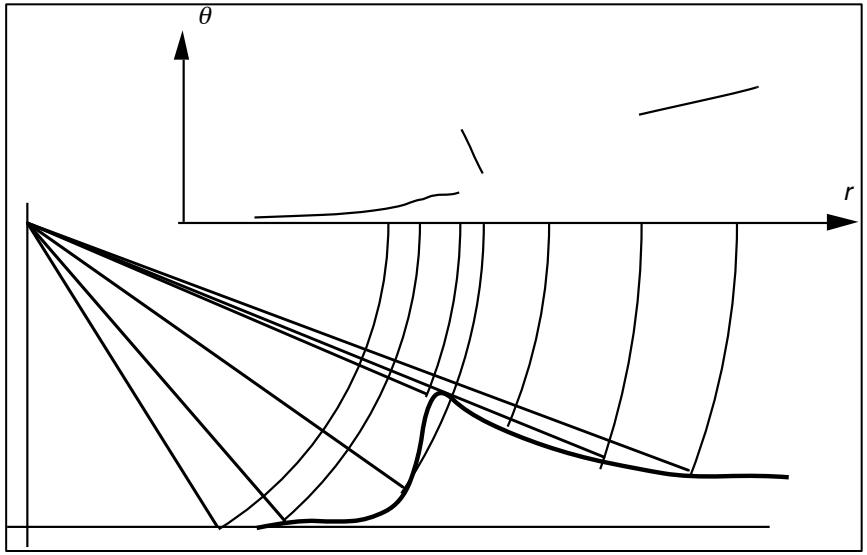

Two-Dimensional Phase Unwrapping

- Two dimensional phase field values below are in units of cycles
- One-dimensional unwrapping criterion of half-cycle proximity is inconsistent in two dimensions

0.0	0.0	0.3	0.0	0.0	0.3	0.0	0.0
0.0	0.3	0.6	0.3	0.3	0.6	0.3	0.0
0.0	0.0	0.9	0.6	0.6	0.9	0.0	0.0
0.0	0.0	1.2	0.9	0.9	1.2	0.0	0.0
0.0	0.0	1.2	0.9	0.9	1.2	0.0	0.0
0.0	0.0	0.9	0.6	0.6	0.9	0.0	0.0
0.0	0.3	0.6	0.3	0.3	0.6	0.3	0.0
0.0	0.0	0.3	0.0	0.0	0.3	0.0	0.0

0.0	0.0	0.3	0.0	0.0	0.3	0.0	0.0
0.0	0.3	0.6	0.3	0.3	0.6	0.3	0.0
0.0	0.0	-0.1	-0.4	-0.4	-0.1	0.0	0.0
0.0	0.0	0.2	-0.1	-0.1	0.2	0.0	0.0
0.0	0.0	0.2	-0.1	-0.1	0.2	0.0	0.0
0.0	0.0	-0.1	-0.4	-0.4	-0.1	0.0	0.0
0.0	0.3	0.6	0.3	0.3	0.6	0.3	0.0
0.0	0.0	0.3	0.0	0.0	0.3	0.0	0.0

- **Residues, marked with + and -, define ambiguous boundaries.**

Residues in Phase Unwrapping

- The wrapping operator delivers the true phase modulo 2 π, in the interval $-\pi < \phi < \pi$.
- The true phase gradient is conservative: $\nabla \times \nabla \phi = 0$
- The wrapped gradient of the measured, wrapped phase, however, may not be conservative: $\nabla \times W\{\nabla \phi_w\} \neq 0$
- When this function is non-conservative, its integration becomes path dependent.
- Residues occur at locations of high phase noise and/or phase shear such that the wrapped gradient of the measured, wrapped phase is no longer conservative.

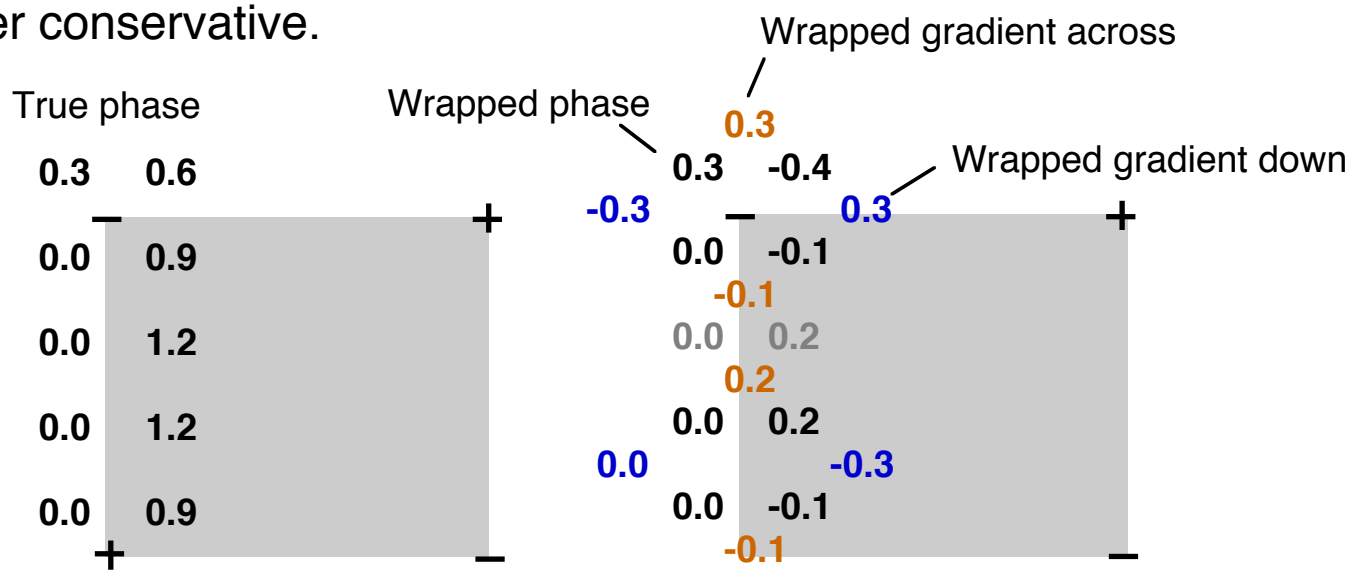

Branch Cuts in Phase Unwrapping

- Branch-cut algorithms (Goldstein, Zebker, and Werner 1986) seek to neutralize these regions of inconsistency by connecting residues of opposite solenoidal sense with cuts, across which integration may not take place.
- Branch cut connections force path independence in the integration of the wrapped phase gradient.
- If done properly, the integrated phase field will be correct. But which is correct?

0.0	0.0	0.3	0.0	0.0	0.3	0.0	0.0
0.0	0.3	0.6	0.3	0.3	0.6	0.3	0.0
0.0	0.0	0.9	0.6	0.6	0.9	0.0	0.0
0.0	0.0	1.2	0.9	0.9	1.2	0.0	0.0
0.0	0.0	1.2	0.9	0.9	1.2	0.0	0.0
0.0	0.0	0.9	0.6	0.6	0.9	0.0	0.0
0.0	0.3	0.6	0.3	0.3	0.6	0.3	0.0
0.0	0.0	0.3	0.0	0.0	0.3	0.0	0.0

0.0	0.0	0.3	0.0	0.0	0.3	0.0	0.0
0.0	0.3	0.6	0.3	0.3	0.6	0.3	0.0
0.0	0.0	-0.1	-0.4	-0.4	-0.1	0.0	0.0
0.0	0.0	0.2	-0.1	-0.1	0.2	0.0	0.0
0.0	0.0	0.2	-0.1	-0.1	0.2	0.0	0.0
0.0	0.0	-0.1	-0.4	-0.4	-0.1	0.0	0.0
0.0	0.3	0.6	0.3	0.3	0.6	0.3	0.0
0.0	0.0	0.3	0.0	0.0	0.3	0.0	0.0

Illustration of Branch Cut Algorithm

Connect all simple pairs

Expand search window and connect where possible

Initiate search from every residue encountered

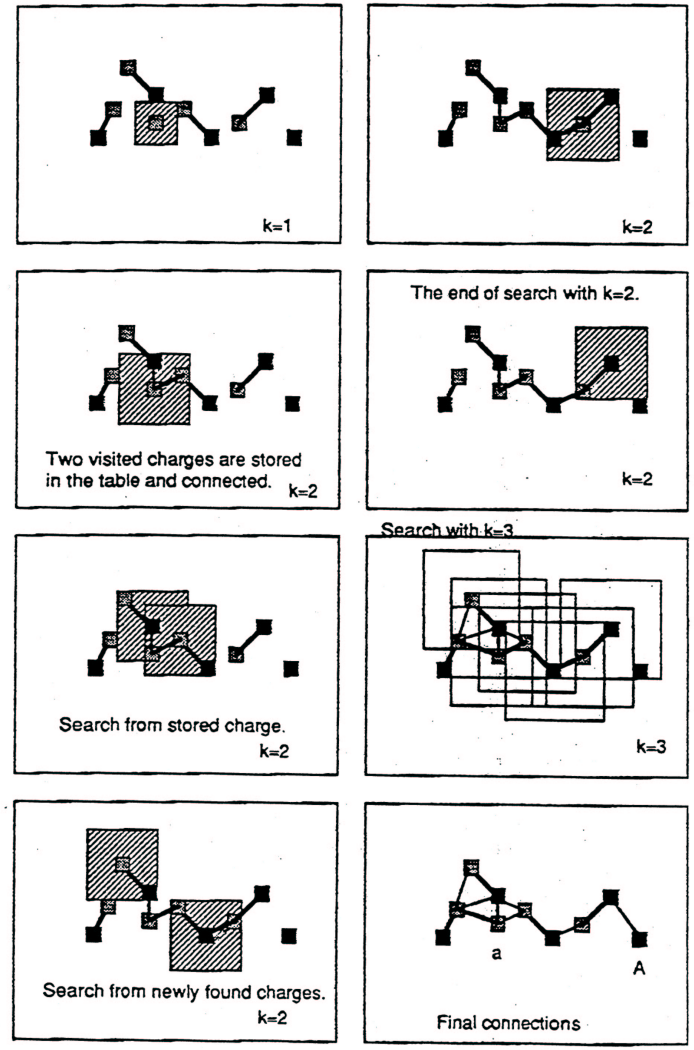

Could not connect last residue with this search window size

Repeat all steps with larger search window size

Branch Cut Strategies

- The standard GZW algorithm is designed to connect residues into a neutral network into the shortest possible connection tree, i.e. to minimize the length of the individual branch cuts comprising a tree
- This will not necessarily create the shortest possible tree, since GZW makes many unnecessary connections in its search for neutrality
- Various criteria have been devised to place guiding centers (unsigned residues) along expected paths to facilitate the right choice in branch cut connection

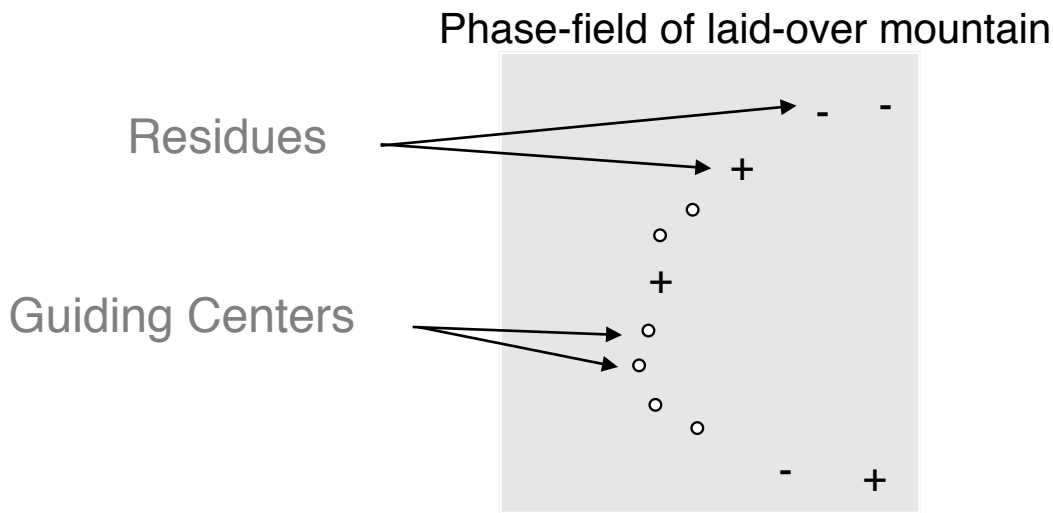

Guiding Center Criteria

- A number of criteria have been devised for selecting guiding centers, each more or less tailored to characteristics of SAR data:
  - when phase slope exceeds threshold (implies layover)
  - when derivative of phase slope exceeds threshold
  - when radar brightness exceeds threshold (implies layover)
  - when decorrelation estimator exceeds threshold (implies noise and/or layover
- Some guiding center selections help in some cases
- Difficult to assess performance in a quantitative way

Connected Components

- Connected component is a term borrowed from topology that denotes a set of points in a patch such that any two points in the set can be connected by a continuous path that does not cross a branch cut or a mask or patch boundary.
- Connected components arise during the unwrapping process when the trees or noise mask separate the patch into multiple regions.

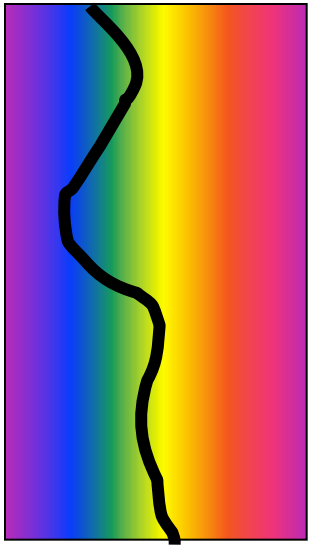

An example of this would be a river running down the middle of the patch with low correlation, hence noisy phase, in the river, effectively bissecting the phase into two distinct regions.

Absolute Phase Determination

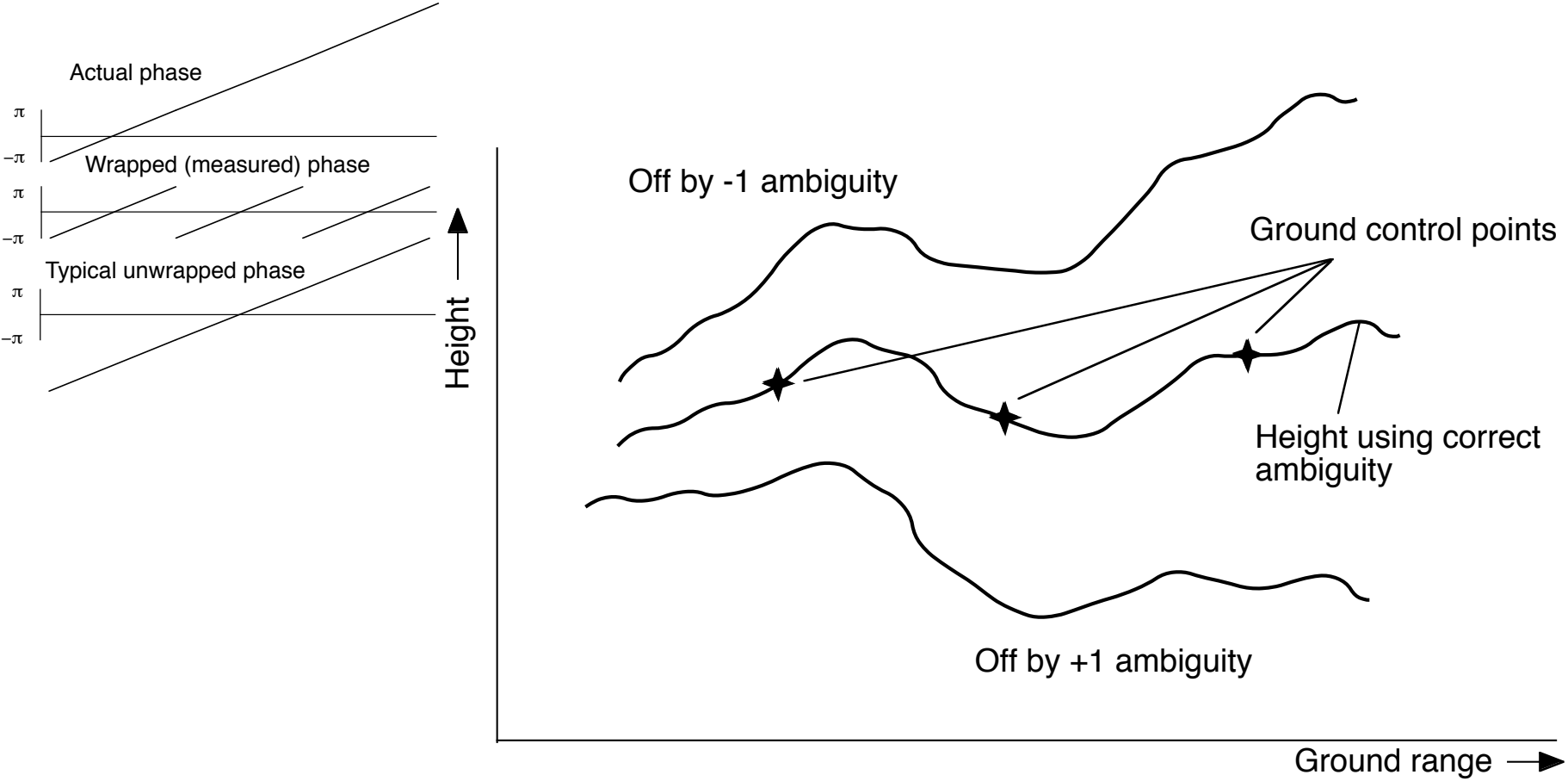

Ground control reference points can be used to determine the absolute phase ambiguity

Tropospheric Effects on InSAR

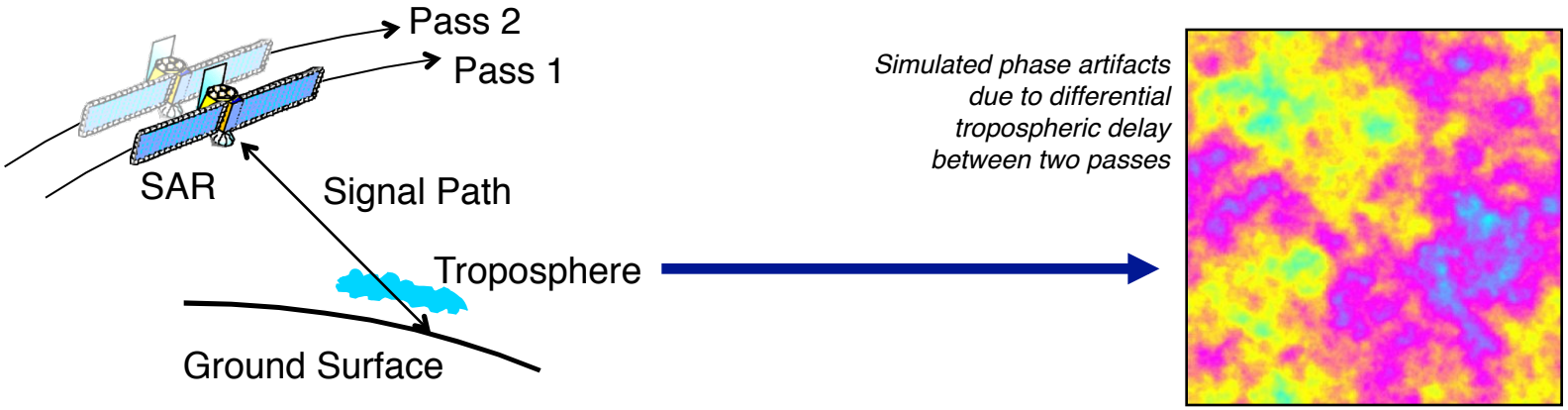

- Tropospheric path delays cause artifacts in repeat-pass interferometric synthetic aperture radar (InSAR) measurements of surface displacement
  - Rapidly varying tropospheric delays (both spatially and temporally) are most problematic
  - Such variations are primarily due to changes in water vapor content along signal propagation path

Effects on InSAR Phase

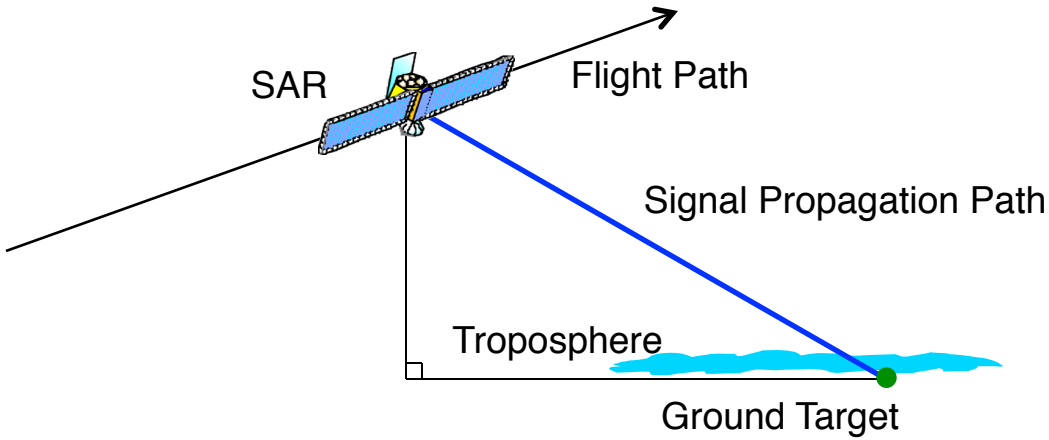

- Observed InSAR phase for broadside acquisition:

$$\phi_{\text{obs}} = -\frac{4\pi}{\lambda}\left(\delta_{LOS} + \delta_{atm}\right) + \phi_{\text{noise}}$$

- Have two unknown parameters (δ_{atm}, δ_{LOS}), but only one equation
- Tropospheric delays δ_{atm} are indistinguishable from line-of-sight (LOS) surface displacements δ_{LOS}

Hawaii SIR-C One Day Repeat Pass Data Showing Tropospheric Distortion

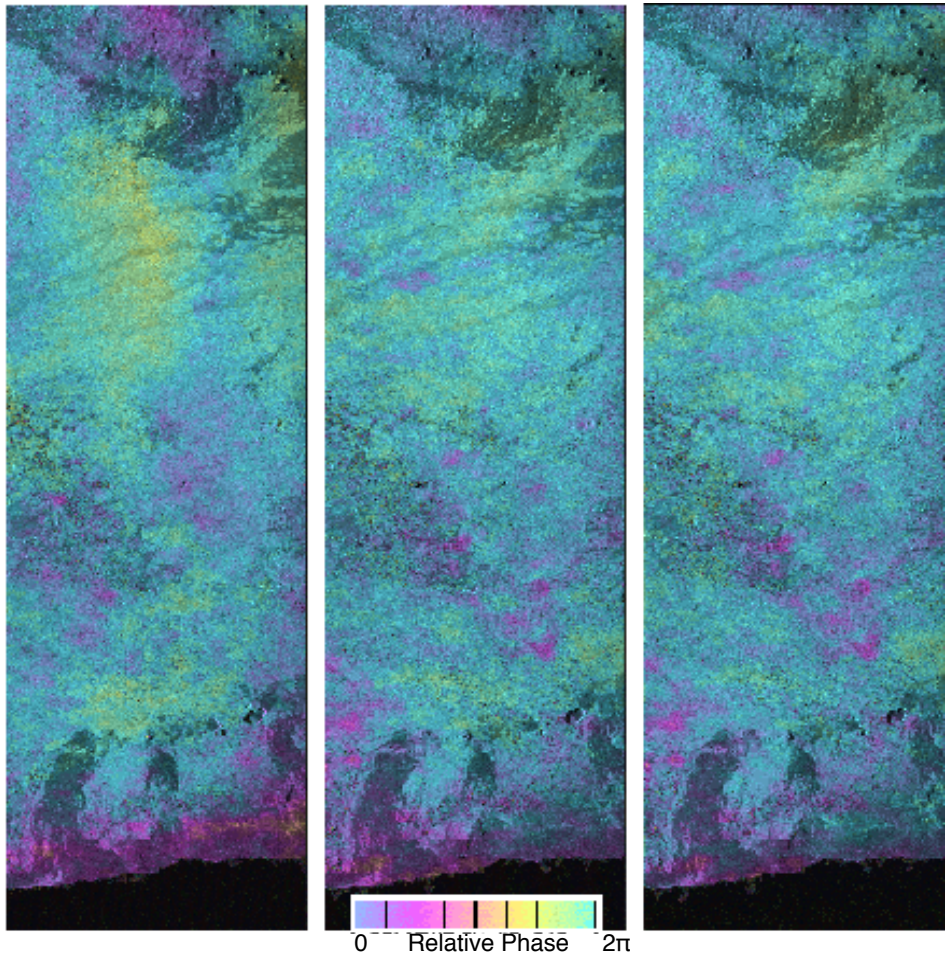

DAYS 7-8 TWO-PASS

DAYS 7-10 TWO-PASS

DAYS 7-8-10 THREE-PASS

Landslide Motion Detection

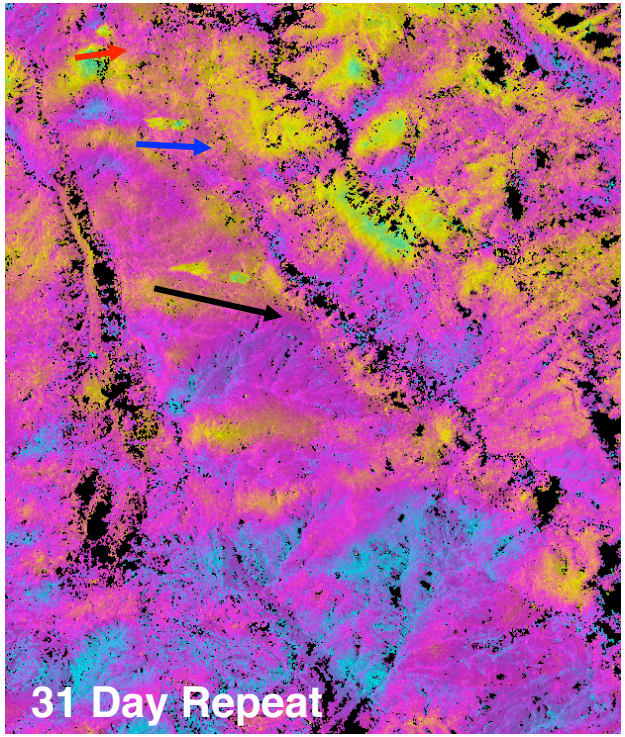

- Creeping landslides detected in 31 and 80 day repeat pass interferograms
- The amount of deformation increased for the larger pair with the larger temporal baseline indicating continued creep from May to July

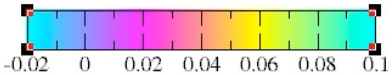

LOS Displacement (m)

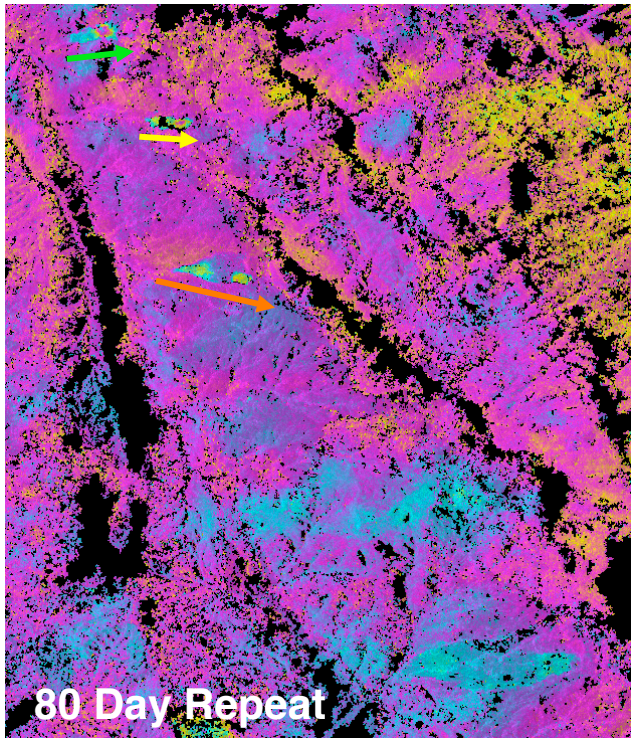

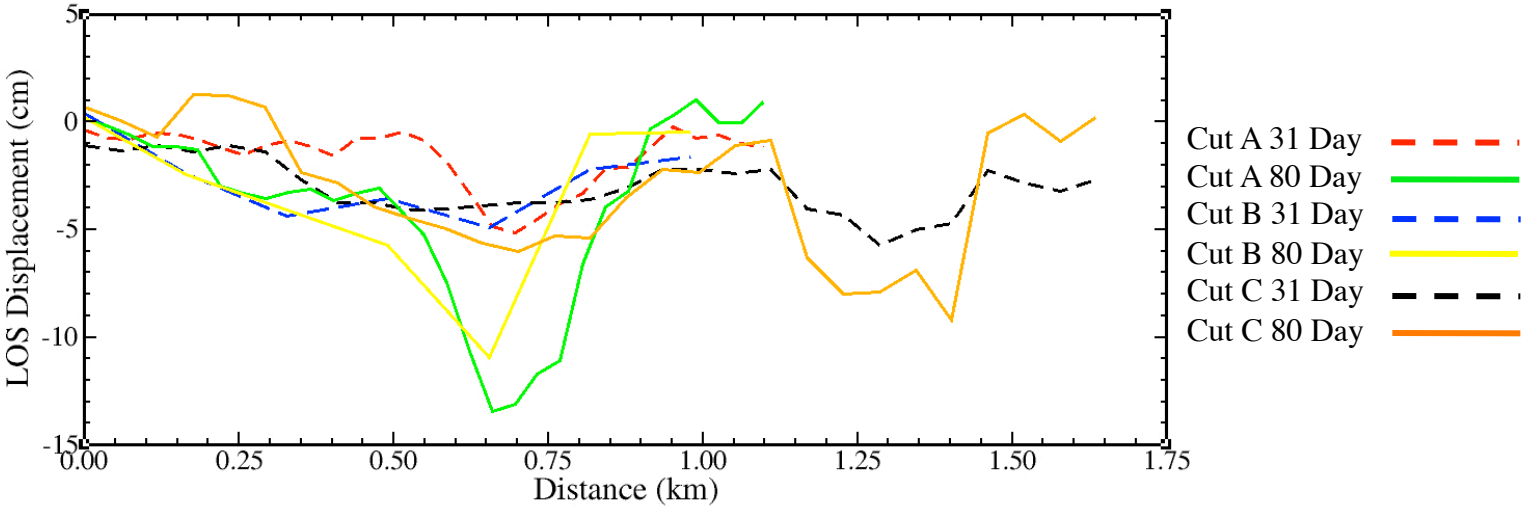

Basic Interferometric Flow

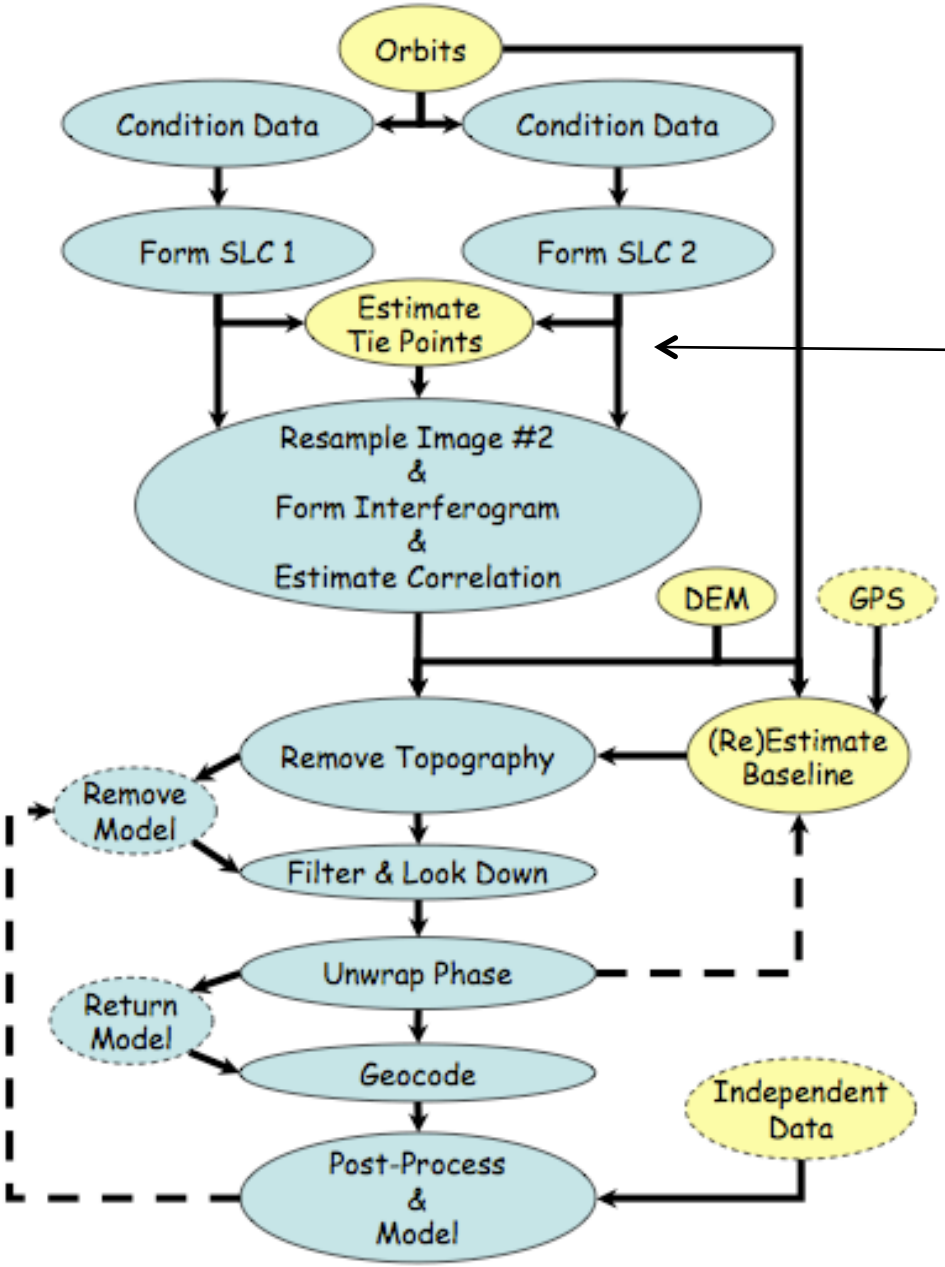

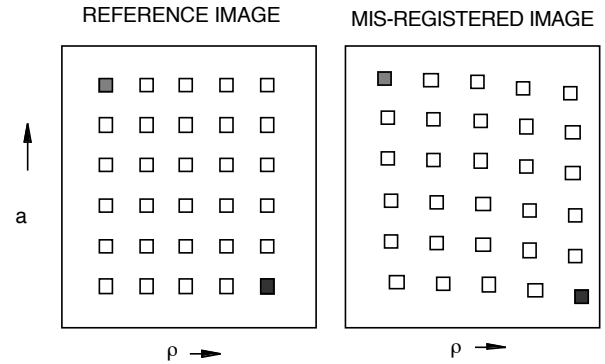

(ISCE does not have baseline re-estimation capability)

Interferometric Error Sources

- *Interferometric decorrelation*
- *Propagation delay errors from atmosphere and ionosphere*
- Phase unwrapping errors
- Range and azimuth ambiguities due to design constraints

- Layover and shadow in radar imagery from slant range geometry
- Multiple scattering within and among resolution cells
- Range and azimuth sidelobes due to bandwidth/resolution constraints
- Multipath and channel cross-talk noise as low-level interference
- Calibration errors

Radar Coherent Backscatter

Pixels in a radar image are a complex phasor representation of the coherent backscatter from the resolution element on the ground and the propagation phase delay

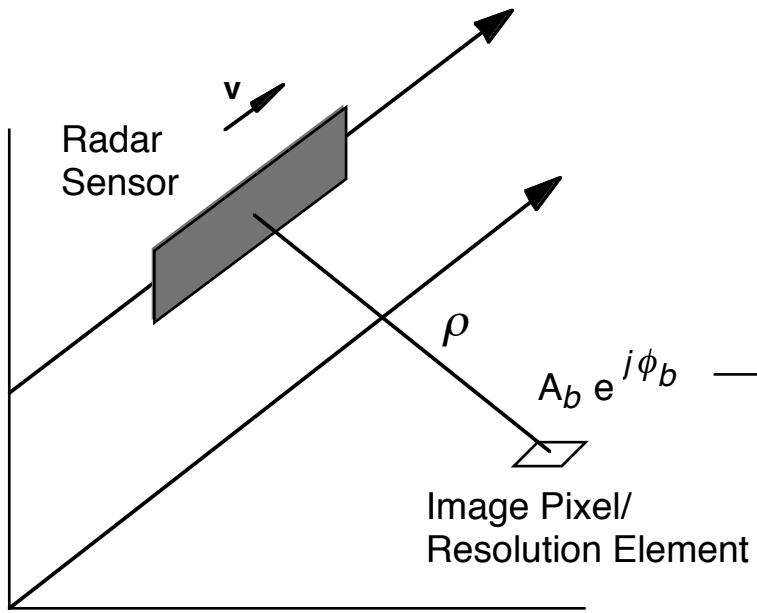

$$\sum_i A_{\varepsilon i} e^{j\phi_{\varepsilon i}} e^{-j\frac{4\pi}{\lambda}\rho_{\varepsilon i}}$$

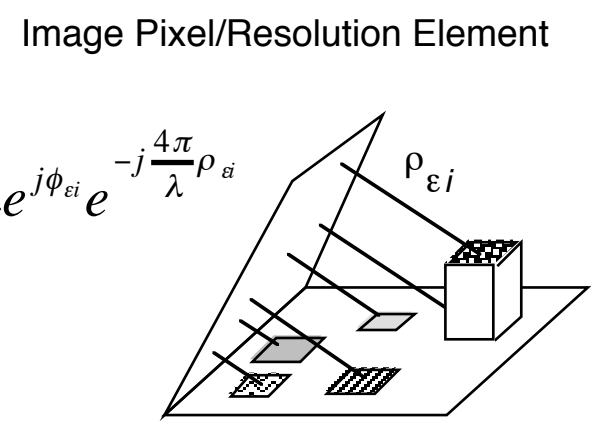

Propagation Phase Delay $\phi = -j\frac{4\pi}{\lambda}\rho$

Backscatter phase delay is coherent sum of contributions from all elemental scatterers in the resolution element with backscatter $A_{\varepsilon i} e^{j\phi_{\varepsilon i}}$ and their differential path delays $\rho_{\varepsilon i}$

Interferometric Phase Characteristics

Pixels in two radar images observed from nearby vantage points have nearly the same complex phasor representation of the coherent backscatter from a resolution element on the ground but a different propagation phase delay

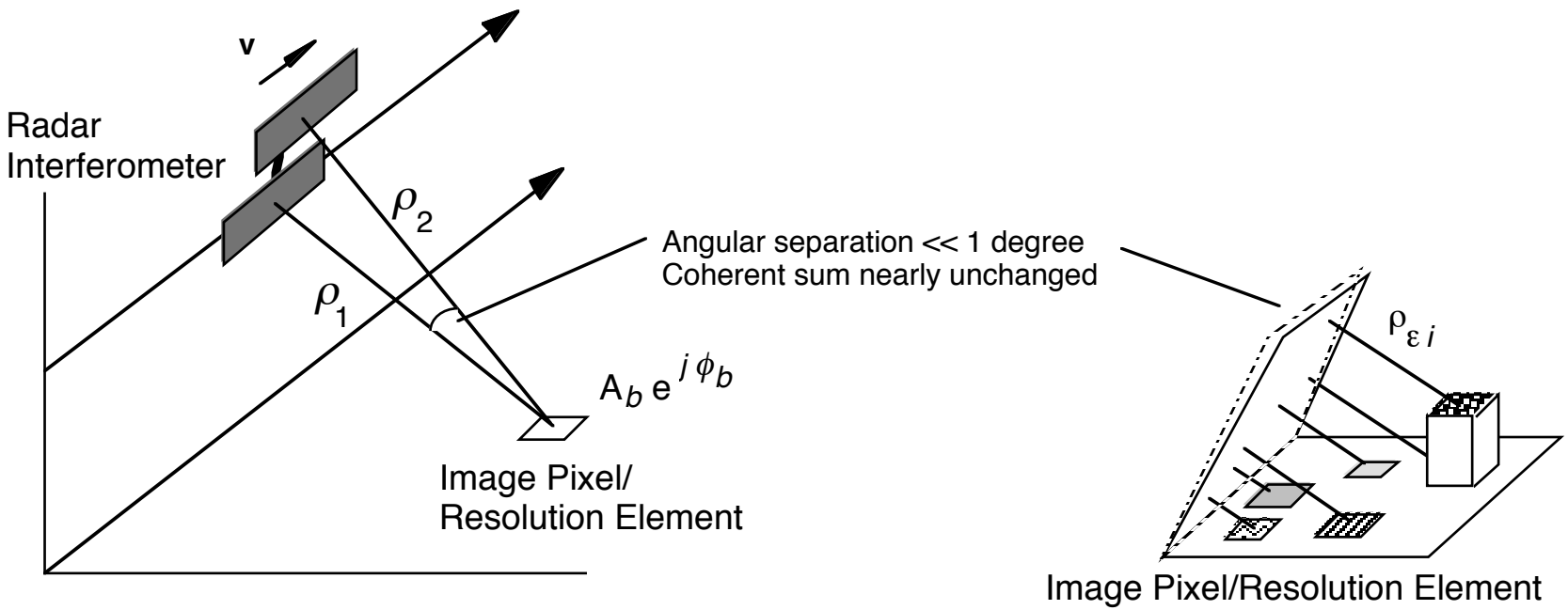

$$s_1 = A_b e^{j\phi_b} e^{-j\frac{4\pi}{\lambda}\rho_1} \qquad s_2 = A_b e^{j\phi_b} e^{-j\frac{4\pi}{\lambda}\rho_2}$$

Correlation* Theory

- Signals decorrelate due to
  - Thermal and Processor Noise
  - Differential Geometric and Volumetric Scattering
  - Rotation of Viewing Geometry
  - Random Motions Over Time
- Decorrelation relates to the phase standard deviation of the interferogram
  - Affects height and displacement accuracy
  - Affects ability to unwrap phase

*"Correlation" and "Coherence" are often used synonymously

Correlation Definition

For signals s_1 and s_2 observed at interferometer apertures 1 and 2, the correlation γ is given by

$$\gamma \equiv \frac{\left|\left\langle s_1 s_2^* \right\rangle\right|}{\sqrt{\left\langle s_1 s_1^* \right\rangle \left\langle s_2 s_2^* \right\rangle}}$$

Deterministic signals or combinations have perfect correlation

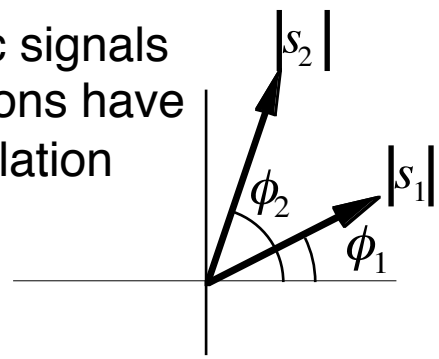

$$\gamma = \frac{\left|\left|s_1\right| e^{i\phi_1} \left|s_2\right| e^{-i\phi_2}\right|}{\sqrt{\left|s_1\right|^2 \left|s_2\right|^2}} = 1$$

Signals with random components have imperfect correlation

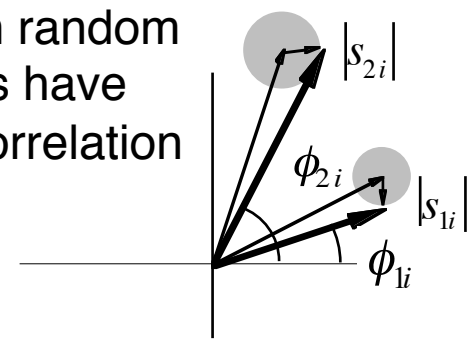

$$\gamma = \frac{\left|\left\langle \left|s_{1i}\right| e^{i\phi_{1i}} \left|s_{2i}\right| e^{-i\phi_{2i}} \right\rangle_i\right|}{\sqrt{\left\langle \left|s_{1i}\right|^2 \right\rangle_i \left\langle \left|s_{2i}\right|^2 \right\rangle_i}} \neq 1$$

Expectation Estimator

Expectation over the ensemble of realizations s_{1i} and s_{2i} cannot be calculated from a specific realization, that is, the observations s_1 and s_2. In general, an estimator derived from the image data must be devised.

The maximum likelihood estimator (MLE) of the interferometric *phase difference* between images forming an interferogram that have homogeneous backscatter and constant phase difference is

$$\hat{\phi} = \arg \sum_{l,m}^{N,M} s_{1l,m} s_{2l,m}^{*}$$

where *l* and *m* are image indices relative to some reference location and the sum is computed over a *N* x *M* box. *N* and *M* are known as the number of looks in their respective image dimensions.

Correlation Estimator

The standard estimator of the interferometric correlation between images forming an interferogram that have homogeneous backscatter and constant phase difference is

$$\hat{\gamma} = \frac{\left| \sum_{l.m}^{N,M} s_{1l,m} s_{2l,m}^{*} \right|}{\sqrt{\left| \sum_{l.m}^{N,M} s_{1l,m} s_{1l,m}^{*} \right| \left| \sum_{l.m}^{N,M} s_{2l,m} s_{2l,m}^{*} \right|}}$$

This estimator is biased. As an example, consider *N* = 1, *M* = 1. Then

$$\hat{\gamma} = \frac{\left| s_{1x,y} s_{2x,y}^{*} \right|}{\sqrt{\left| s_{1x,y} s_{1x,y}^{*} \right| \left| s_{2x,y} s_{2x,y}^{*} \right|}} = 1$$

where *x* and *y* are the coordinates of a particular image pixel. Other biases arise when backscatter homogeneity and phase constancy are violated.

Correlation Estimator Characteristics

A general set of curves of reveals the nature of the estimator bias when backscatter is homogeneous and phase is constant.

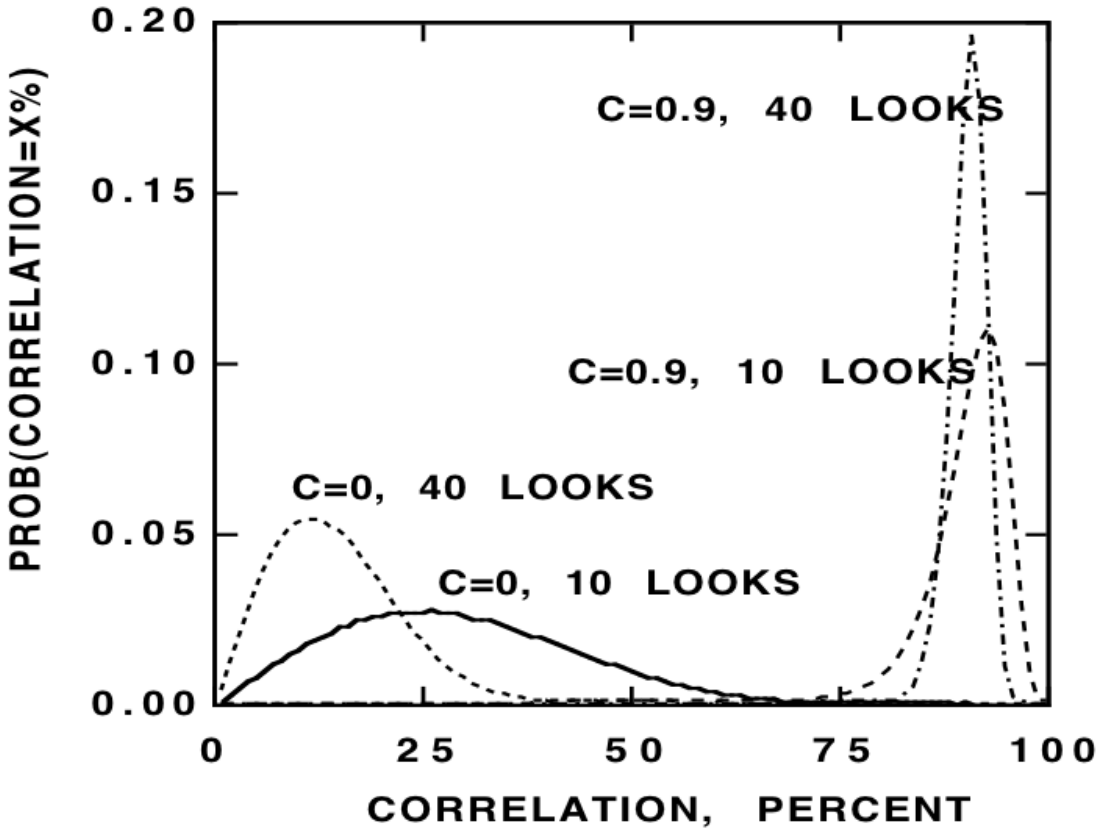

Relationship of Phase Noise and Decorrelation

- Increased decorrelation is associated with an increase in the interferometric phase noise variance
- If averaging $N > 4$ samples, the phase standard deviation approaches the Cramer-Rao bound on the phase estimator:

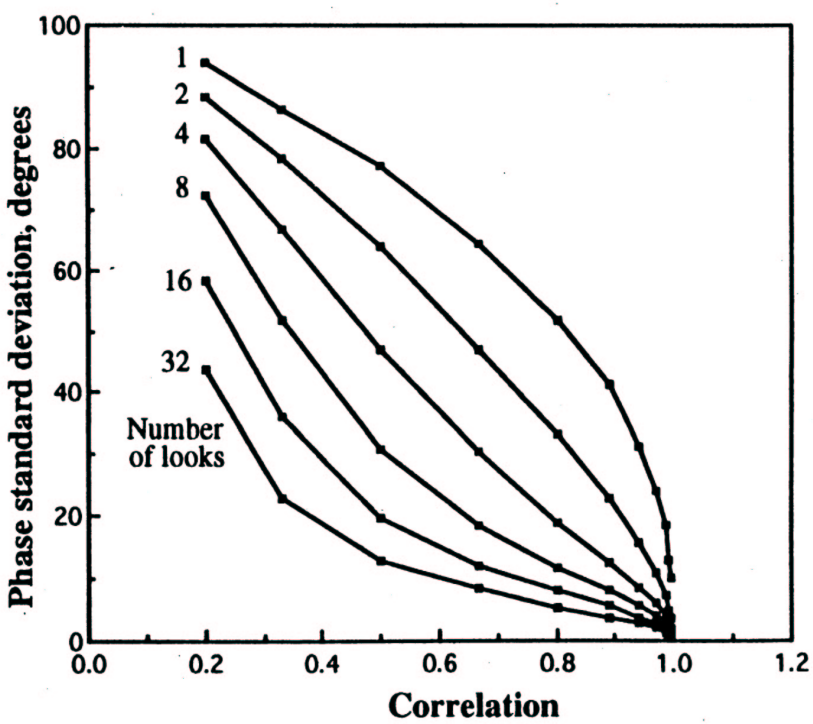

$$\sigma_\phi = \frac{1}{\sqrt{2N}} \frac{\sqrt{1-\gamma^2}}{\gamma}$$

Phase noise contributes to height errors in interferometry as demonstrated in the sensitivity equations

Thermal Noise Decorrelation

Radar receiver electronics will add thermally generated noise to the image observations.

$$s_1^{'} = A_b e^{j\phi_b} e^{-j\frac{4\pi}{\lambda}\rho_1} + n_1 \; ; \; s_2^{'} = A_b e^{j\phi_b} e^{-j\frac{4\pi}{\lambda}\rho_2} + n_2$$

The added noise contributes randomly to the interferometric phase from pixel to pixel, causing thermal noise decorrelation. Assuming uncorrelated noise, the correlation between $s_1^{'}$ and $s_2^{'}$ is

$$\gamma = \frac{\left|\left\langle (s_1 + n_1)(s_2 + n_2)^* \right\rangle\right|}{\sqrt{\left\langle (s_1 + n_1)(s_1 + n_1)^* \right\rangle \left\langle (s_2 + n_2)(s_2 + n_2)^* \right\rangle}}$$

$$= \frac{\left|s_1 s_2\right|}{\sqrt{\left\langle \left(s_1^{\,2} + n_1^{\,2}\right)\right\rangle \left\langle \left(s_2^{\,2} + n_2^{\,2}\right)\right\rangle}}$$

$$= \frac{\sqrt{P_1}\sqrt{P_2}}{\sqrt{P_1 + N_1}\sqrt{P_{21} + N_2}} = \frac{1}{\sqrt{1 + N_1 / P_1}} \frac{1}{\sqrt{1 + N_2 / P_2}}$$

Thermal Noise Decorrelation

The correlation is related in a simple way to the reciprocal of the Signal-to-Noise Ratio (SNR). For observations with identical backscatter and equal noise power,

$$\gamma = \frac{1}{1 + N/P} = \frac{1}{1 + \mathrm{SNR}^{-1}}$$

Decorrelation is defined as

$$\delta = 1 - \gamma$$

The decorrelation due to thermal noise can vary greatly in a scene, not from thermal noise variations, but from variations in backscatter brightness. Extreme cases are:

- **Radar shadow, where no signal is returns; correlation is zero.**
- **Bright specular target, where signal dominates return; correlation is 1**

Baseline Decorrelation

Pixels in two radar images observed from nearby vantage points have *nearly* the same complex phasor representation of the coherent backscatter from a resolution element on the ground

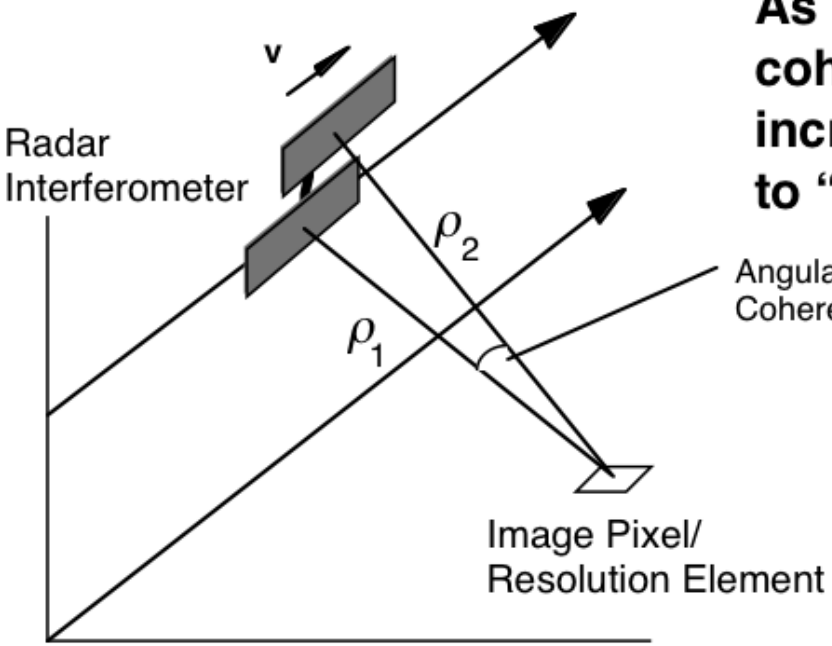

As interferometric baseline increases, the coherent backscatter phase becomes increasingly different randomly, leading to "baseline" or "speckle" decorrelation.

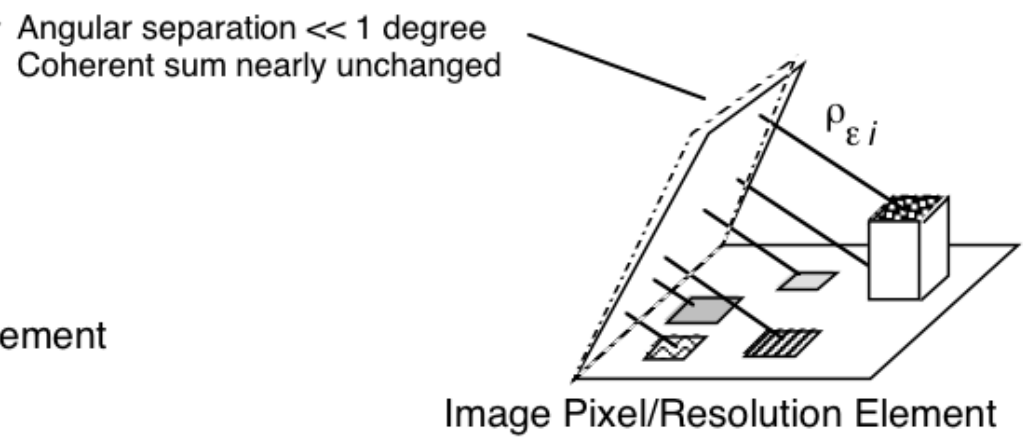

$$s_1 = A_{b1} e^{j\phi_{b1}} e^{-j\frac{4\pi}{\lambda}\rho_1} \qquad s_2 = A_{b2} e^{j\phi_{b2}} e^{-j\frac{4\pi}{\lambda}\rho_2}$$

Form of Baseline Correlation Function

If $W(x,y)$ is assumed to be a sinc function, then the integral can be done in closed form (for ping-pong mode)

$$\gamma_B = 1 - \frac{2(B\cos\theta)(\Delta\rho_y \cos\theta)}{\lambda\rho}$$

$$\boxed{= 1 - \frac{2B_\perp \Delta\rho_\perp}{\lambda\rho}}$$

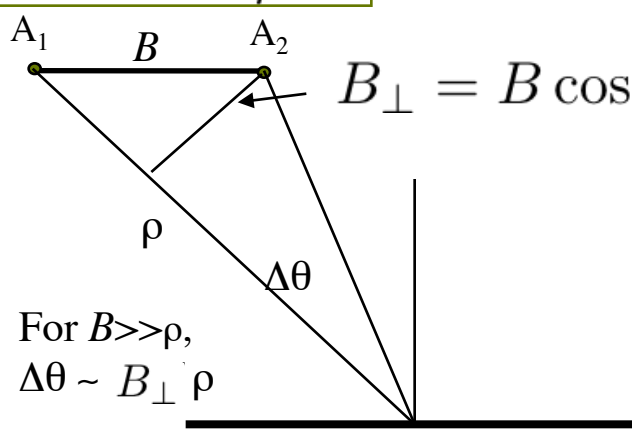

$$B_\perp = B\cos\theta$$

For B>>ρ,
$\Delta\theta \sim B_\perp \rho$

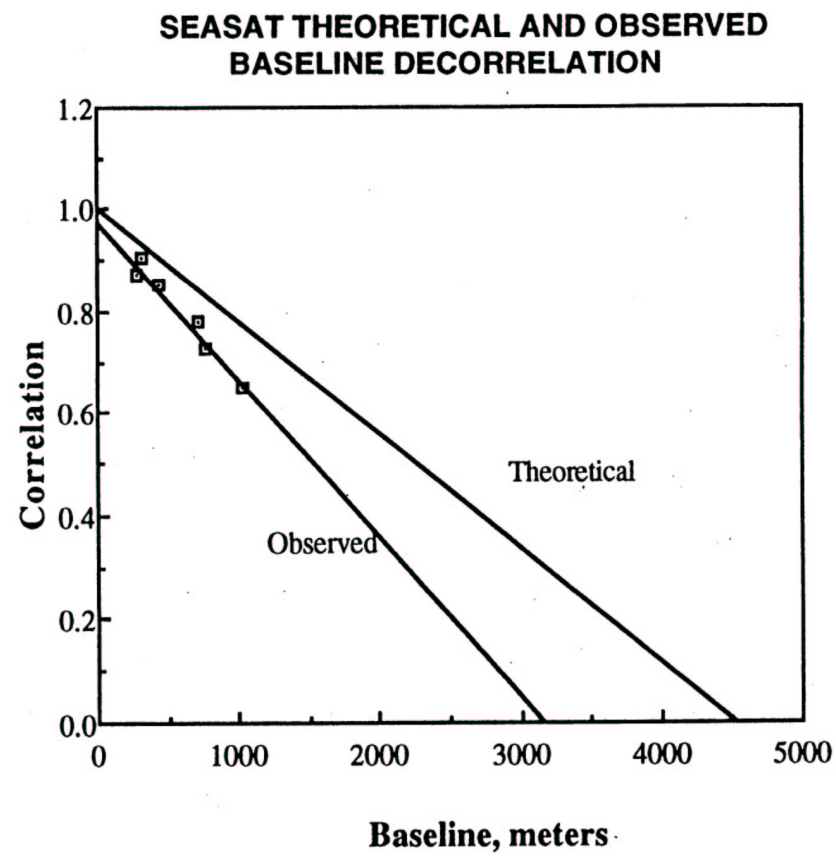

This function goes to zero at the *critical baseline*

$$\boxed{B_{\perp,\mathrm{crit}} = \frac{\lambda\rho}{n\Delta\rho_\perp}} \qquad n = 1, 2$$

The "Pixel Antenna" View of Baseline Decorrelation

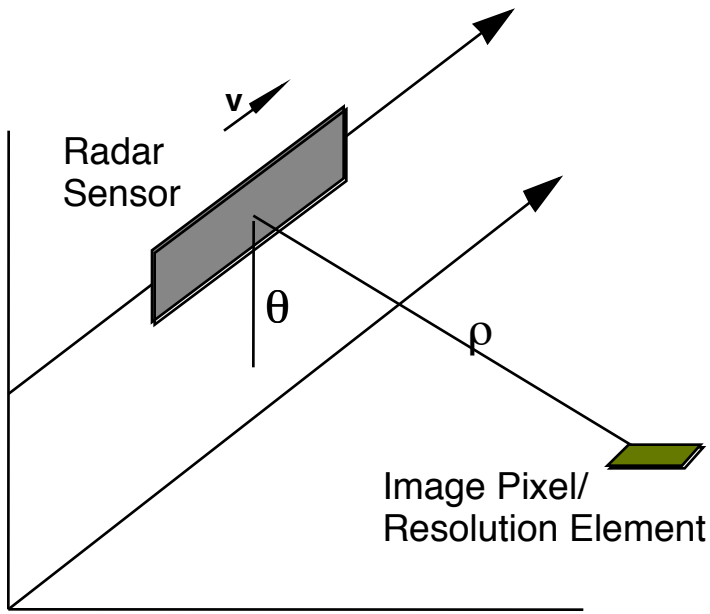

Each resolution element can be considered a radiating antenna with beamwidth of $\Delta\theta_{\Delta\rho_\perp}$, which depends on the range and local angle of incidence.

$$\Delta\theta = \frac{\lambda}{n\,\Delta\rho_\perp} \qquad n=1,2$$

$$\Delta\rho = \frac{c}{2\Delta f_{\mathrm{BW}}}$$

$$\Delta\rho_\perp = \Delta\rho / \tan\theta$$

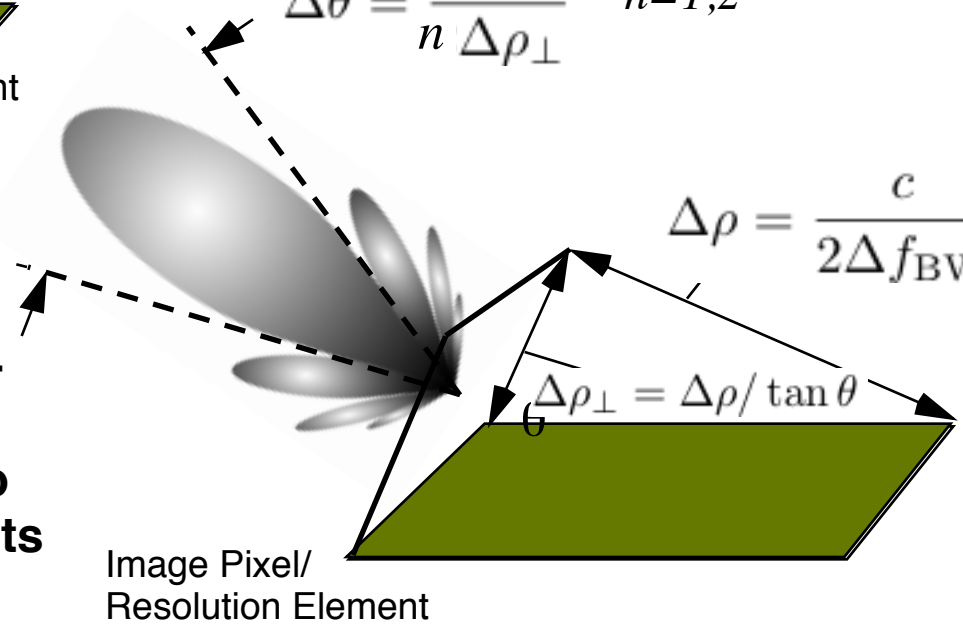

When the two apertures of the interferometer are within this beamwidth, coherence is maintained. Beyond this critical baseline separation, there is no coherence for distributed targets

Overcoming Baseline Decorrelation

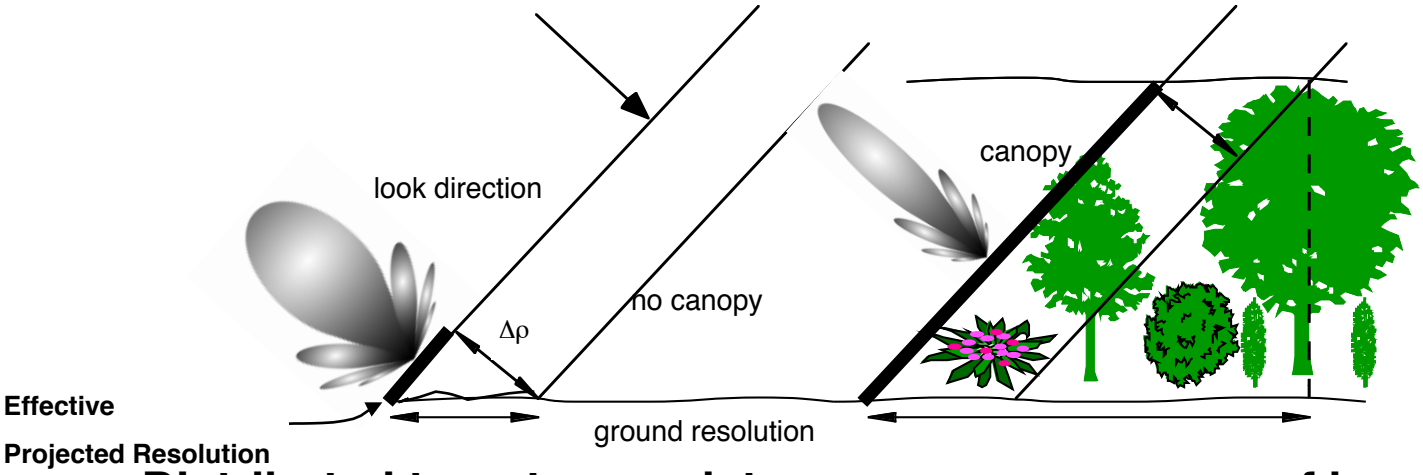

Distributed targets correlate over a narrow range of baselines

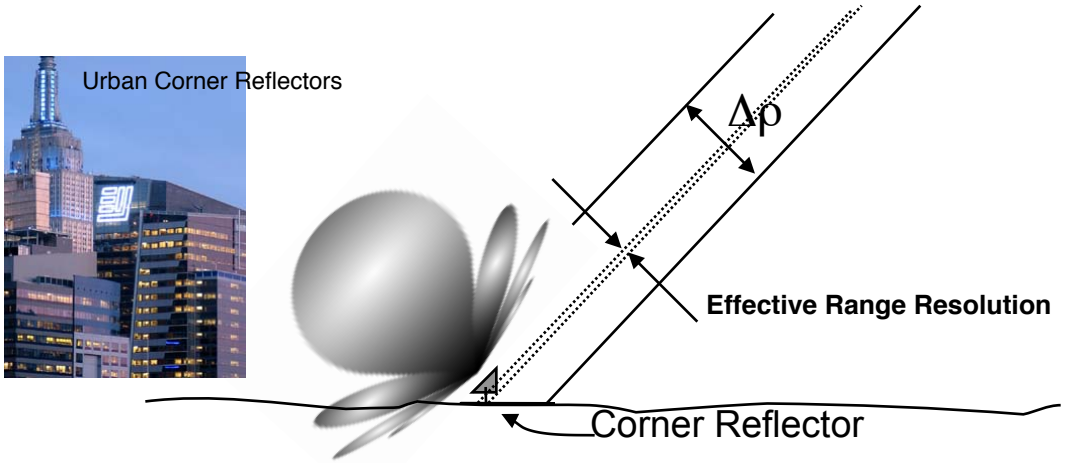

JPL Corner Reflector

Pixels dominated by single scatterers generally behave though imaged at much finer resolution

Critical Baseline

The critical baseline is the aperture separation perpendicular to the look direction at which the interferometric correlation becomes zero.

$$B_{\text{crit}} = \rho\Delta\theta_{\Delta\rho_\perp} = \frac{\lambda\rho\tan\theta}{n\Delta\rho} \qquad n=1,2$$

Interferometers with longer wavelengths and finer resolution are less sensitive to baseline decorrelation. When the critical baseline is reached, the interferometric phase varies as

$$\frac{\partial\phi_{\text{crit}}}{\partial\rho} = \frac{\partial\phi_{\text{crit}}}{\partial\theta}\frac{\partial\theta}{\partial\rho}$$

$$= \frac{2n\pi}{\lambda}B_{\text{crit}}\frac{1}{\rho\tan\theta} = \frac{2\pi}{\Delta\rho}$$

The relative phase of scatterers across a resolution element changes by a full cycle, leading to destructive coherent summation

Rotational Decorrelation

Rotation of scatterers in a resolution element can be thought of as observing from a slightly different azimuthal vantage point. As with baseline decorrelation, the change in differential path delay from individual scatterers to the reference plane produces rotational decorrelation.

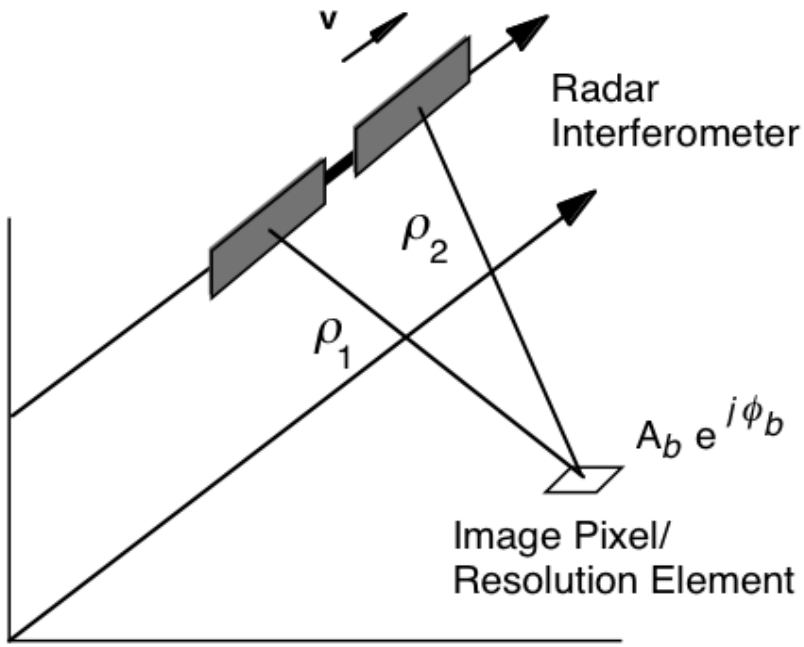

The critical rotational baseline is the extent of the synthetic aperture used to achieve the along track resolution.

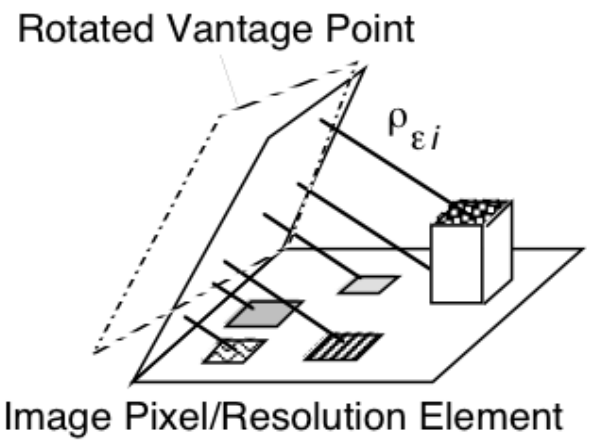

$$s_1 = A_{b1} e^{j\phi_{b1}} e^{-j\frac{4\pi}{\lambda}\rho_1} \qquad s_2 = A_{b2} e^{j\phi_{b2}} e^{-j\frac{4\pi}{\lambda}\rho_2}$$

Form of Rotational Correlation Function

A similar Fourier Transform relation as found in the baseline decorrelation formulation exists

$$\gamma_\phi = 1 - \frac{n \sin\theta B_\phi R_x}{\lambda\rho} \quad n = 1, 2$$

where R_x is the azimuth resolution and B_ϕ is the distance along track corresponding to the rotation angle of the look vector

This function goes to zero at the *critical rotational baseline*

$$B_{\phi,\mathrm{crit}} = \frac{\lambda\rho}{n\Delta\rho_\phi}, \Delta\rho_\phi \equiv R_x \sin\theta$$

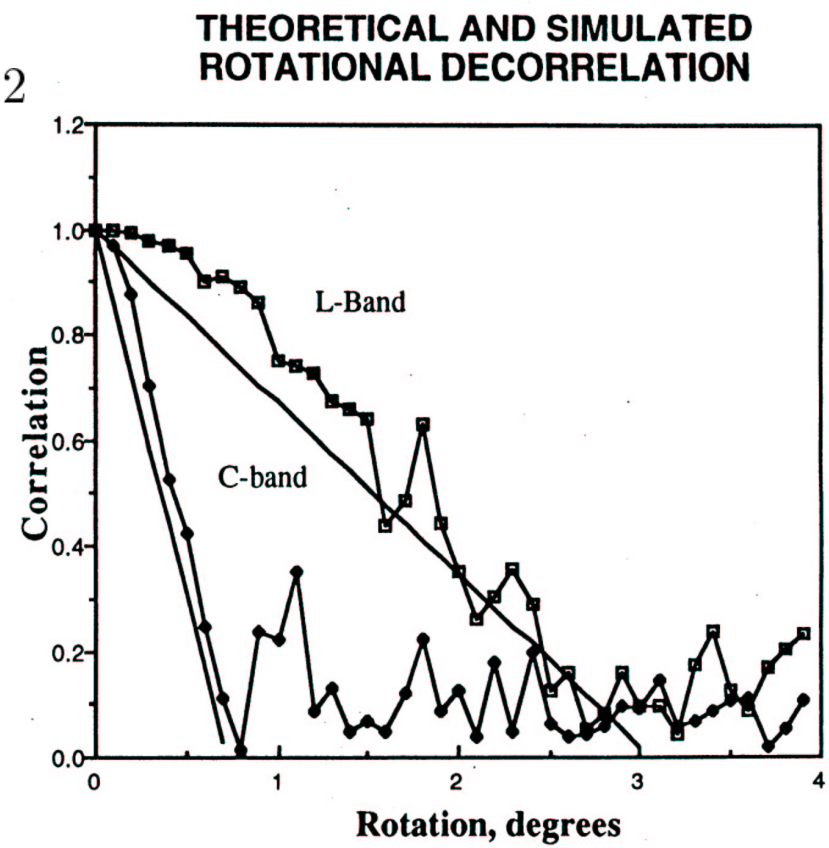

Scatterer Motion

Motion of scatterers within the resolution cell from one observation to the next will lead to randomly different coherent backscatter phase from one image to another, i.e. "temporal" decorrelation.

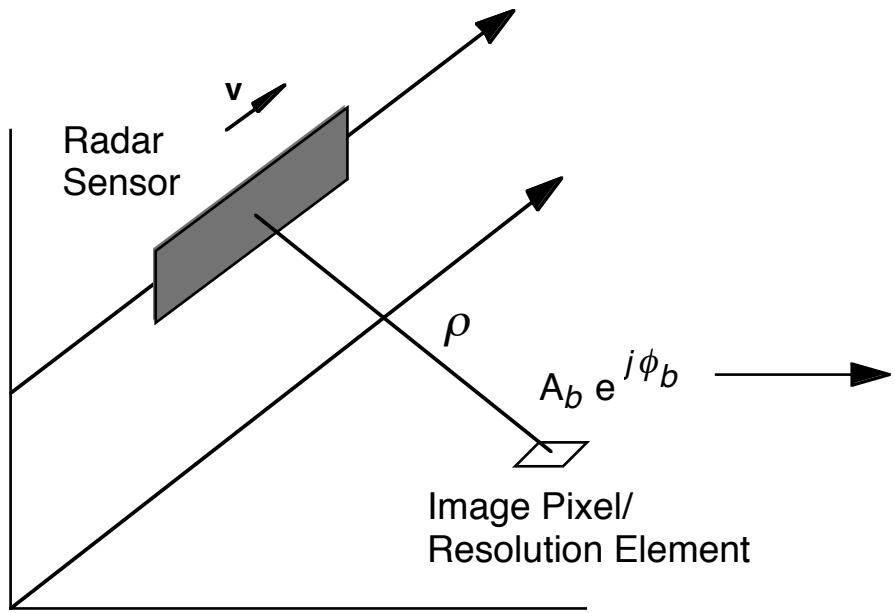

Propagation Phase Delay $\phi = -j\frac{4\pi}{\lambda}\rho$

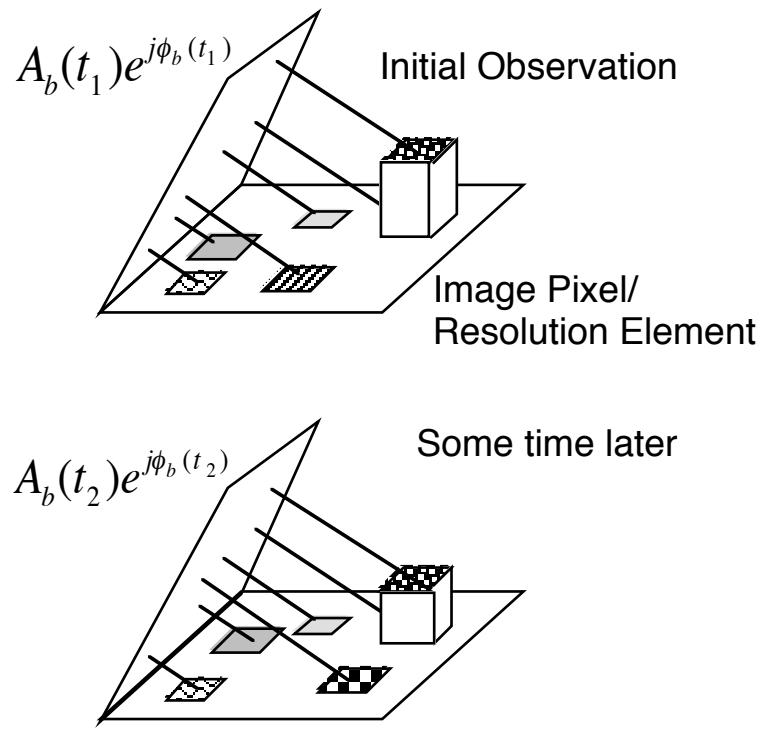

Form of Motion Correlation Function

The Fourier Transform relation can be evaluated if Gaussian probability distributions for the motions are assumed

$$\gamma_t = e^{-\frac{1}{2}\left(\frac{4\pi}{\lambda}\right)^2(\sigma_y^2 \sin^2\theta + \sigma_z^2 \cos^2\theta)}$$

where $\sigma_{y,z}$ is the standard deviation of the scatterer displacements cross-track and vertically

Note correlation goes to 50% at about 1/4 wavelength displacements

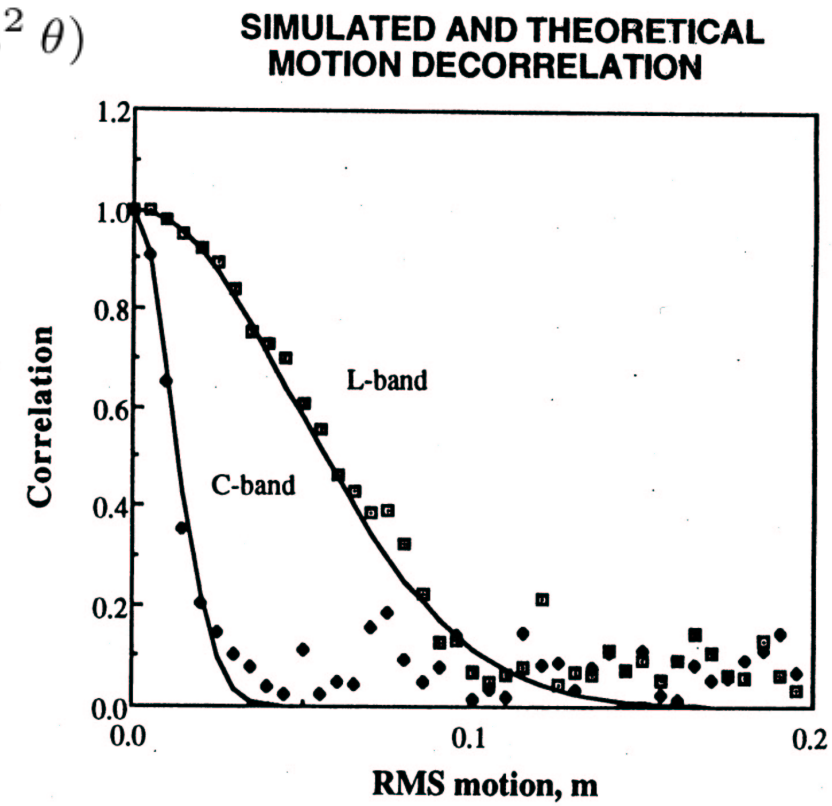

Repeat-pass Interferometry and Coherent Change Detection

L-Band low frequency improves correlation in vegetated areas

Most radars do well in areas of sparse vegetation

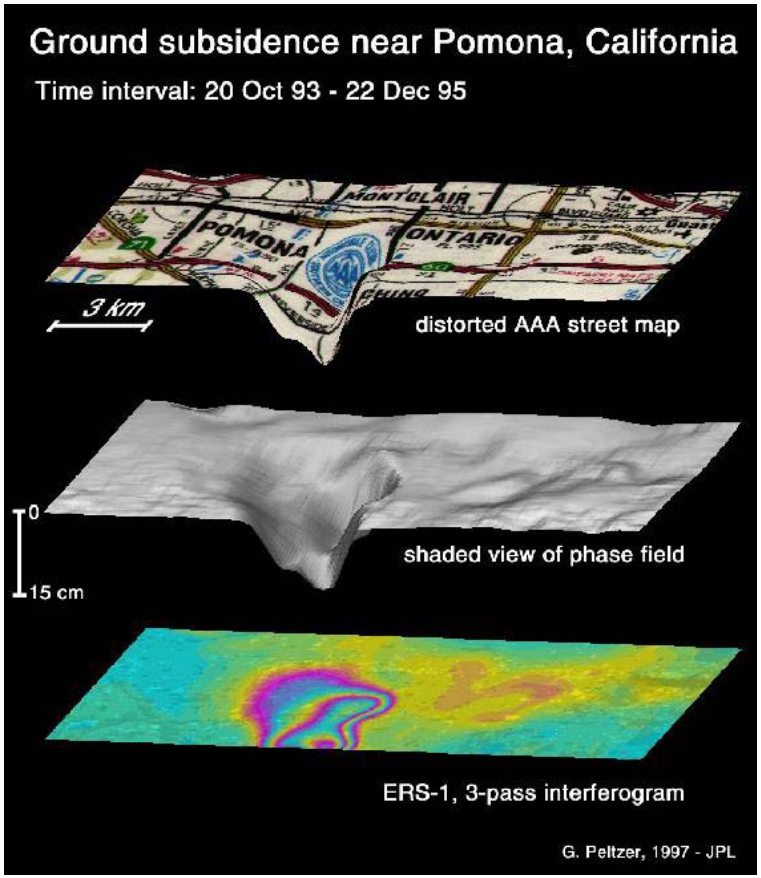

But maintaining correlation in dense vegetation requires longer wavelengths

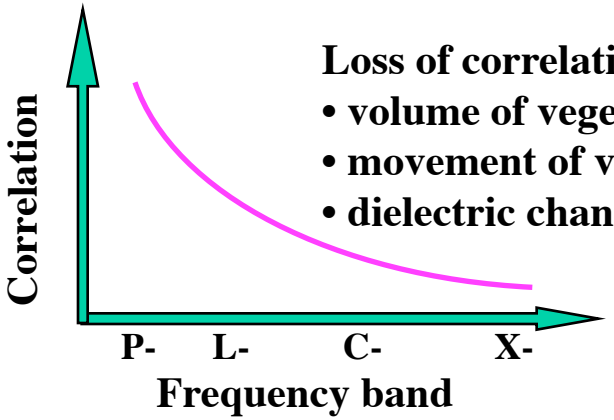

Loss of correlation is due to:

- volume of vegetation
- movement of vegetation
- dielectric change (moisture)

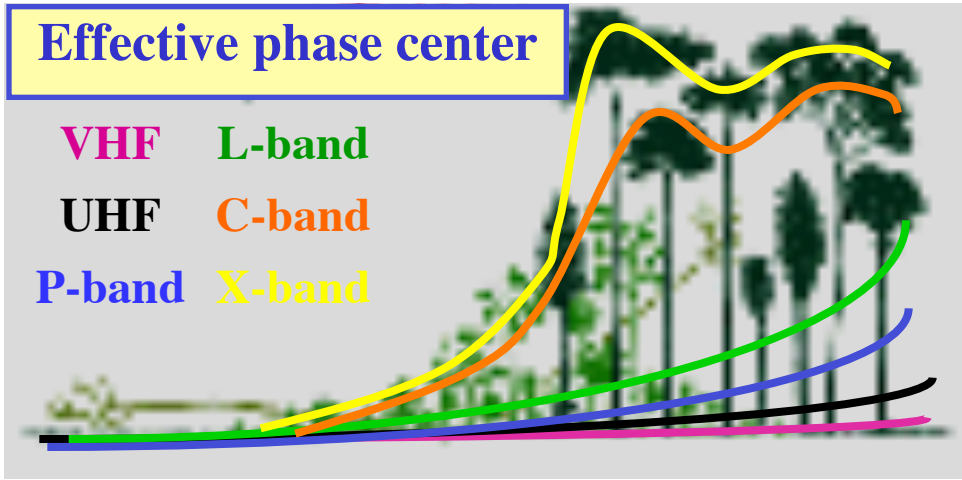

Coherent Change Detection
SIR-C L and C-band Interferometry

6 month time separated observations to form interferograms
Simultaneous C and L band

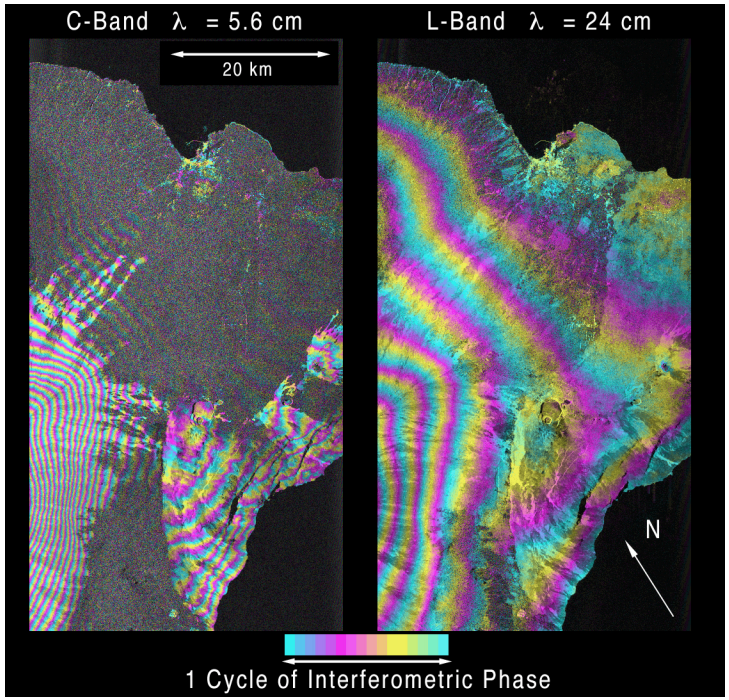

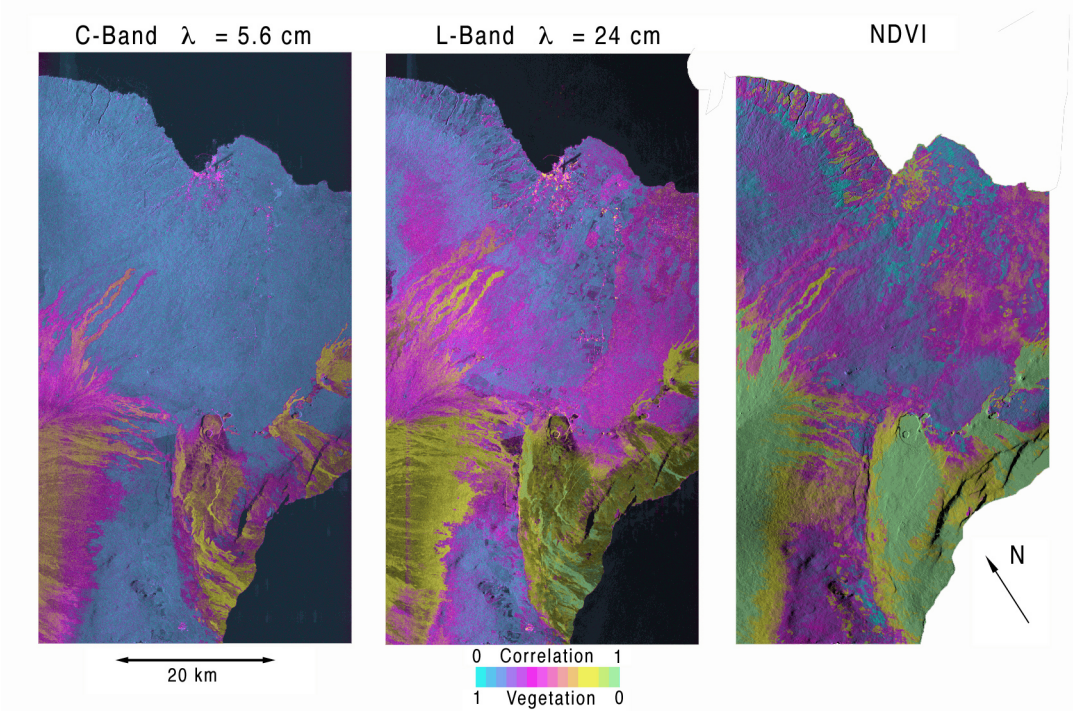

InSAR experiments have shown good correlation at L-band

AIRSAR Coherent Change Detection

Interferograms

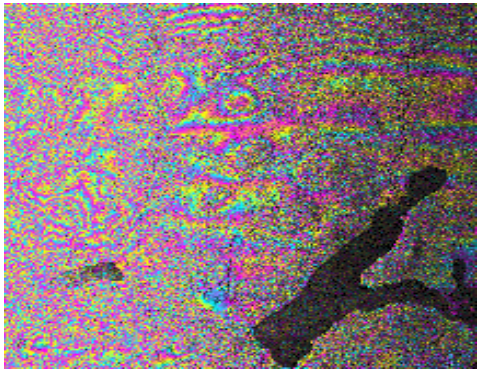

C-band

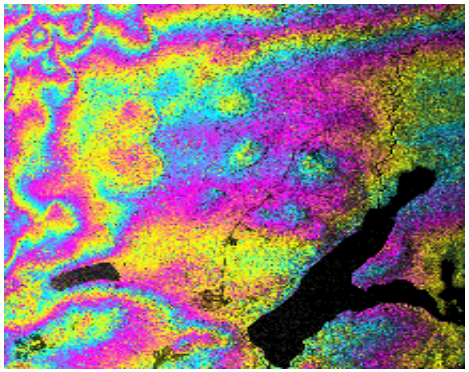

L-band

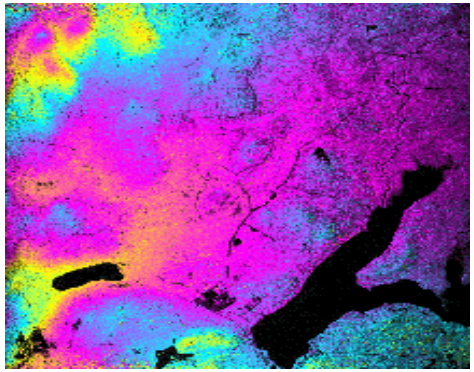

P-band

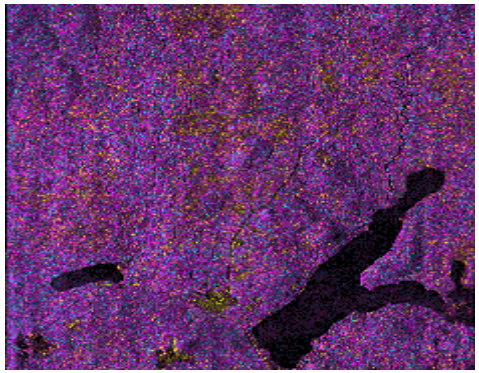

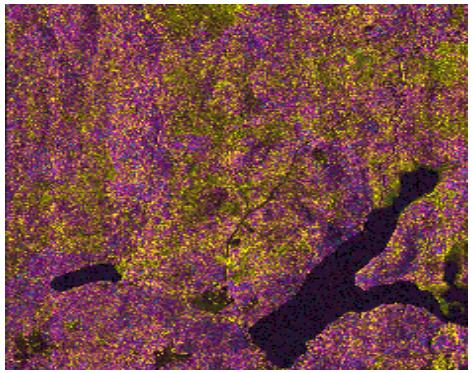

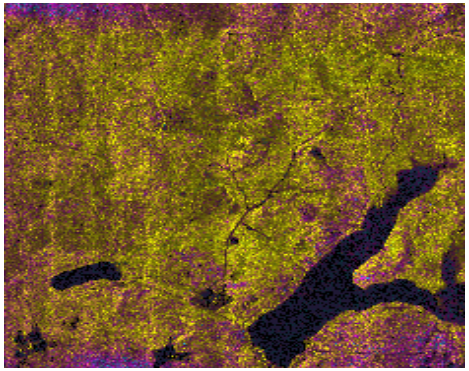

Correlation

Airborne InSAR experiments have shown good correlation at L-band

A Correlation Test:
What were the interferometric observation conditions?

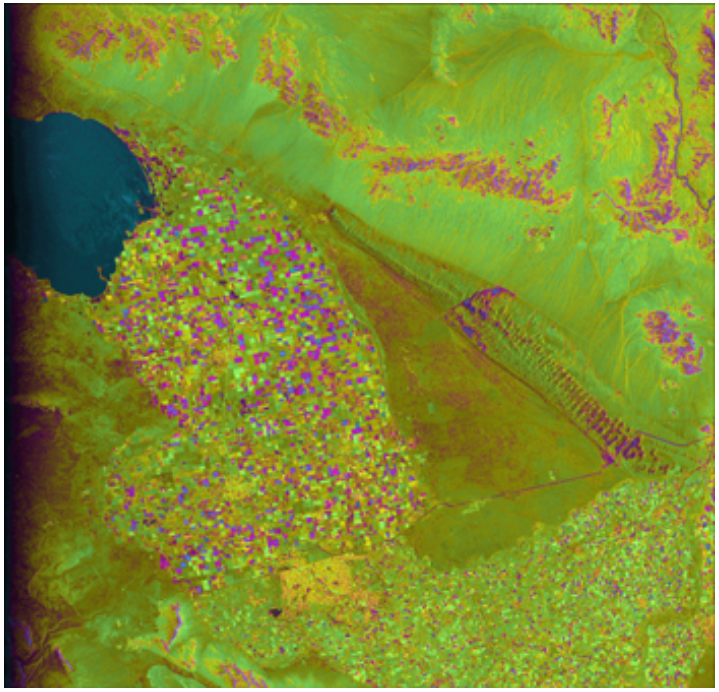

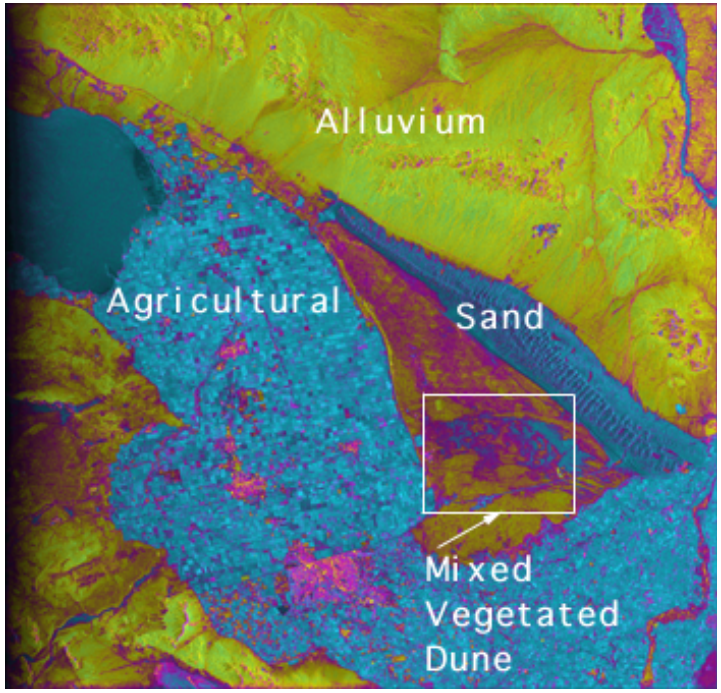

Other Resources

M. Simons and P. Rosen,
Interferometric Synthetic Aperture Radar Geodesy
Treatise on Geophysics, Schubert, G. (ed.), Volume 3- Geodesy, Elsevier Press, pp. 391-446, 2007
http://www.gps.caltech.edu/~simons/pdfs/Simons_Treatise.pdf

Rosen, P. A.; Hensley, S.; Joughin, I. R.; Li, F. K.; Madsen, S. N.; Rodriquez, E. & Goldstein, R. M.
Synthetic Aperture Radar Interferometry
Proc. IEEE, 2000***, 88*, 333-382**

Burgmann, R.; Rosen, P. & Fielding, E.
Synthetic Aperture Radar Interferometry to measure Earth's surface topography and its deformation
Ann.~Rev.~Earth Planet.~Sci., 2000***, 28*, 169-209**

Madsen, S. N. & Zebker, H. A.
Synthetic Aperture Radar Interferometry: Principles and Applications
Manual of Remote Sensing, Artech House, **1999***, 3*

Massonnet, D. & Feigl, K. L.
Radar interferometry and its application to changes in the earth's surface
Reviews of Geophysics, **1998***, 36*, 441-500

Bamler, R. & Hartl, P.
Synthetic Aperture Radar Interferometry
Inverse Problems, 1998***, 14*, 1-54**

Richards, J.A.
***Remote Sensing with Imaging Radar*, 2009, Springer.**